4-18-2013 12:00 AM

Detection, Receivers, and Performance of CPFSK and CPCK

Mohammed Zourob, *The University of Western Ontario*

Supervisor: Dr. Raveendra K. Rao, *The University of Western Ontario*

A thesis submitted in partial fulfillment of the requirements for the Master of Science degree in Electrical and Computer Engineering

Detection, Receivers, and Performance of CPFSK and CPCK

(Thesis format: Monograph)

by

Mohammed O. M. Zourob

Graduate Program
in
Engineering Science
Electrical and Computer Engineering Department

A thesis submitted in partial fulfillment
of the requirements for the degree of
Master of Engineering Science

The School of Graduate and Postdoctoral Studies
The University of Western Ontario
London, Ontario, Canada

Abstract

Continuous Phase Modulation (CPM) is a power/bandwidth efficient signaling technique for data transmission. In this thesis, two subclasses of this modulation called Continuous Phase Frequency Shift Keying (CPFSK) and Continuous Phase Chirp Keying (CPCK) are considered and their descriptions and properties are discussed in detail and several illustrations are given. Bayesian Maximum Likelihood Ratio Test (MLRT) is designed for detection of CPFSK and CPCK in AWGN channel. Based on this test, an optimum receiver structure, that minimizes the total probability of error, is obtained. Using high- and low-*SNR* approximations in the Bayesian test, two receivers, whose performances are analytically easy-to-evaluate relative to the optimum receiver, are identified. Next, a Maximum Likelihood Sequence Detection (MLSD) technique for CPFSK and CPCK is considered and a simplified and easy-to-understand structure of the receiver is presented. Finally, a novel Decision Aided Receiver (DAR) for detection of CPFSK and CPCK is presented and closed-form expressions for its Bits Error Rate (*BER*) performance are derived.

Throughout the thesis, performances of the receivers are presented in terms of probability of error as a function of Signal-to-Noise Ratio (*SNR*), modulation parameters and number of observation intervals of the received waveform. Analytical results wherever possible and, in general, simulation results are presented. An analysis of numerical results is given from the viewpoint of the ability of CPFSK and CPCK to operate over AWGN Channel.

Keywords: Continuous phase modulation, Frequency shift keying, Chirp modulation, Optimum receivers, Sub-optimum receivers, Viterbi receiver, Decision Aided receiver.

Acknowledgments

All praise be to Allah for bestowing upon me His countless blessings.

Words cannot help me in describing my sincere appreciation and gratitude to my supervisor and mentor Dr. Raveendra K. Rao for giving me the opportunity of working under his guidance, for his time, unwavering support and imparting not only scientific knowledge, but also his life experience and wisdom, which have been a priceless inspiration for me. Only by his enthusiasm, analytical outlook and constructive criticism that this work can be presented here today.

I am extremely grateful and indebted to my parents for their sacrifice and support in every possible means and doing their best in pushing me to attain further heights, whether through helping me through tough times or letting me fight my way through hardships. Without their hard work and dedication in my upbringing, I would not have been the person who I am today.

I wish to thank my best friend Saleem Yaghi for all his invaluable encouragement motivations and support, though far away, throughout the course of my Master's thesis. I would like also to thank my dear friend, Abdulafou Kabbani and colleagues, Muhammad Ajmal Khan, Basil Tarek and Monir Al Hadid. In particular, I appreciate valuable suggestions and help given by Muhammad Ajmal Khan during the time of difficulties.

Last but not least, I would like to thank the members of the faculty and staff of the Department of Electrical and Computer Engineering for their support and help, especially Melissa Harris and Christopher Marriott. It gives me great pleasure in thanking Hydro one for contributing to my Queen Elizabeth II Graduate Scholarship for pursuing my Master's program.

Table of Contents

List of Tables

List of Figures

Abbreviations

AWGN	Additive White Gaussian Noise
BER	Bit Error Rate
BPSK	Binary Phase Shift Keying
CDMA	Code Division Multiple Access
CPM	Continuous Phase Modulation
CPFSK	Continuous Phase Frequency Shift Keying
CPCK	Continuous Phase Chirp Keying
WCS	Wireless Communications Systems
DCS	Digital Communications Systems
FM	Frequency Modulation
HF	High Frequency
MLD	Maximum Likelihood Detector
MLSE	Maximum Likelihood Sequence Estimation
MLSD	Maximum Likelihood Sequence Detection
MLRT	Maximum Likelihood Ratio Test
RF	Radio Frequency
SNR	Signal-to-Noise Ratio
REC	Rectangular Pulse
PSK	Phase Shift Keying
PSD	Power Spectral Density
PDF	Probability Distribution Function
MIMO	Multiple-Input-Multiple-Output
VA	Viterbi Algorithm
DAR	Decision Aided Receiver
AMF	Average Matched Filter
MSK	Minimum Shift Keying

Chapter 1

Introduction

In this Chapter, an overview of the functional block diagram of a Digital Communication System (DCS) is presented with emphasis on digital modulation and demodulation sub-blocks. Digital modulation techniques and parameters that are used to describe the performance of the DCS are also given. Transmission and detection strategies, particularly, those associated with CPFSK and CPCK, are discussed. All in all the emphasis in this Chapter is mainly on the literature review, problem statements, their justifications, approaches for their solutions, and organization of the thesis.

1.1 Digital Communication System (DCS) Overview

Digital Communication has become one of the most rapidly growing industries in the world, and its products cover a wide array of applications and they are exerting a direct impact on our daily lives. Basically, communication involves implicitly the transmission of information from one point to another through a succession of processes. The first step is the generation of a message signal, either analogue (voice, music or picture) or digital

(computer data). The second step is to describe that message signal with a certain measure of precision by using a set of electrical, aural or visual symbols. These symbols are encoded in a form that is suitable for transmission over the available physical medium. The encoded symbols are transmitted using a transmission device to a specific destination. The encoded symbols are received on the other side using a receiver device. Then, the encoded symbols are decoded to produce an estimate of the original symbols. Thus, the message signal is re-created with a definable degradation in quality due to signal fading, system imperfections and the different types of noise (Thermal noise, Additive White Gaussian Noise (AWGN)…). A typical digital communication system is shown in Figure 1.1.

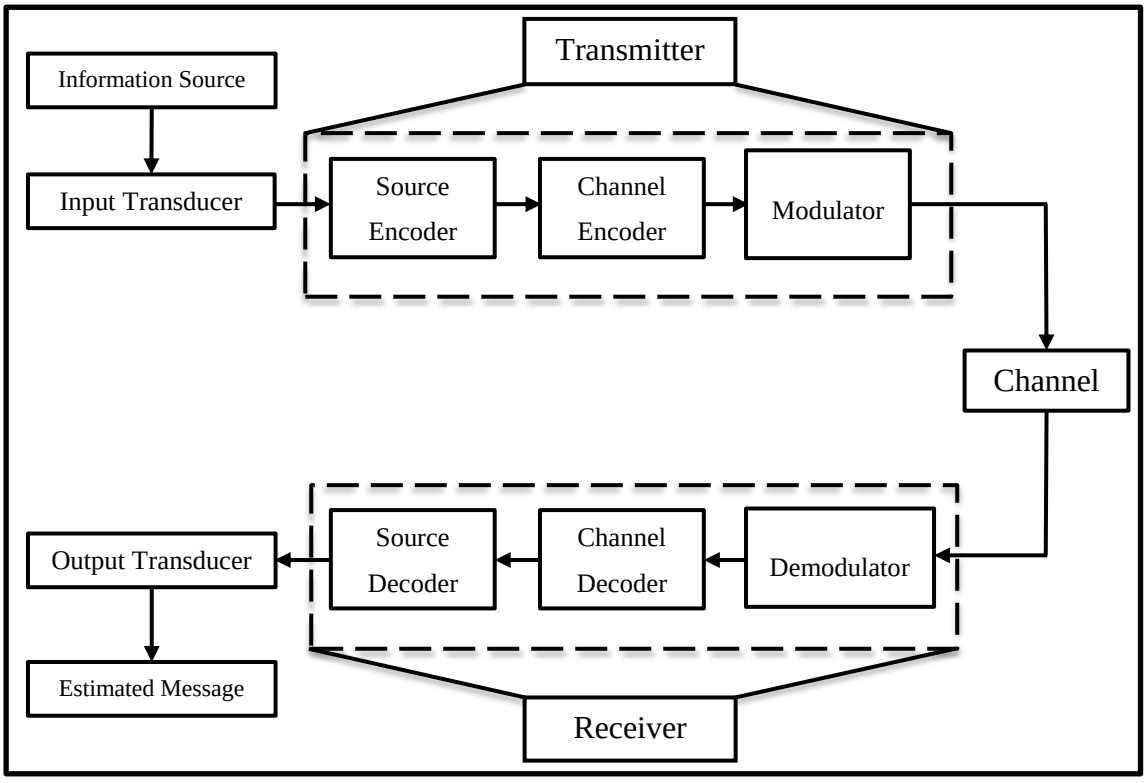

Figure 1.1: Block Diagram of General Digital Communication System

Information source may be either analog (audio or video) or digital (computer output) signal. In a Digital Communication System, messages produced by source are always converted to a sequence of binary digits (010110…). If source output is analog, Analogue to Digital conversion (Sampling, Quantization and Encoding) is employed using Analogue to Digital convertor (ADC).

The second stage is the source encoder. Ideally, we would like to represent the source output by as few binary digits as possible. Thus, the objective of the Source Encoder is to provide an efficient representation of the source output. The process of efficiently converting the source output into a sequence of binary digits is called Source Encoding or Data Compression. Examples of source encoding are Huffman Coding and Lempel-Ziv Coding [50]. These use information theoretic concepts to remove redundancies present in the source output.

The third stage is the channel encoder block. The purpose of the channel encoder is to introduce, in a controlled manner, some redundancy in the binary sequence at its input; primarily to combat the effects of noise and interference over the channel. The added redundancy improves the fidelity of the received signal and increases the signal's immunity to noise. It provides the message with error detection and correction capabilities. Examples of channel encoding are single-parity check codes, convolutional coding and cyclic redundancy check codes. Typically, channel encoding involves taking k-information bits at a time as input and in response producing a unique n-bit sequence, called the code word, as output. The amount of redundancy introduced by the channel encoder in this manner is measured by the ratio n/k. The code rate is the ratio k/n.

The fourth stage is the Modulator. Modulation is a fundamental process in any communication system and especially so in a radio system. In Digital Communication Systems (DCS), the modulator's function is the translation between digital data and the electrical signal required at the input to the Radio Frequency (RF) section. The modulator can be considered as a signal sub-system that maps input data, usually binary 0 and 1, on to a modulated RF carrier for later processing, transmissions and amplification by the RF section. First, the modulator maps the binary information sequence into a set of values suitable for the modulation scheme that will be used at the Radio Frequency (RF) transmission stage. Second, each value in the set is assigned to its corresponding RF signal that will be used over the channel. Suppose that the coded information sequence will be transmitted one bit at a time at some uniform rate R bits/sec. The coded bits will be assigned to two values, +1 or -1.Next, each value is assigned to two signals, $S_1(t)$ or $S_2(t)$. An illustration is shown in Figure 1.2.

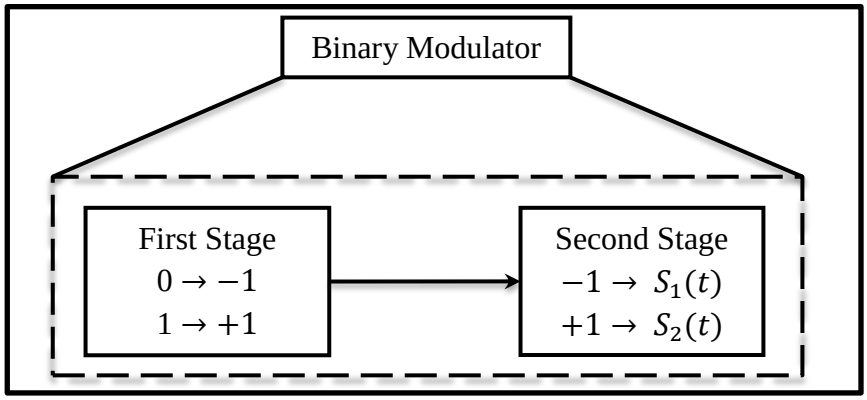

Figure 1.2: Block Diagram of Binary Modulator

The block diagram of a binary modulator is shown in Figure 1.2. In Binary Modulation, two values, $+1$ or -1, are used to map to $S_1(t)$ or $S_2(t)$. Alternatively, the modulator may transmit n coded information bits at a time by using $M = 2^n$ values, where each one of the 2^n possible n-bit sequences has its own distinct waveform $S_i(t),\ i = 1,2,\dots,M$. M is called the modulation order and the modulation scheme is called M-ary modulation. Various types of waveforms can be used at the RF stage, such as phase shift keying and frequency shift keying. Thus, the modulator is characterized by the modulation order and the type of waveforms used in the process along with other modulation parameters specific to each scheme. The modulation stage decides the bandwidth occupied by the transmitted signal. Furthermore, modulation controls the robustness of the communication system to channel impairments, due both to the RF sub-systems (such as phase distortion and amplifiers nonlinearity) and the RF channel (such as additive noise, multipath fading and dispersion). Thus, a suitable choice of modulation scheme is important for the efficient operation of DCS.

The communication channel represents the physical medium that is used to send the signal from the transmitter to the receiver. Different channels can be used such as wireless/free space channels, telephone/wire-line channels, fiber-optic channels, underwater channels, storage channels, etc. The essential feature of the physical medium is that the transmitted signal is corrupted in a random manner by a variety of mechanisms- additive thermal noise (AWGN), fading or signal attenuation, amplitude and phase distortion and multipath distortion especially in wireless communication.

The Source encoder, channel encoder and modulator form the integral parts of the transmitter. The reverse of all these processes is taken care of on the destination side by the receiver, which will typically contain a demodulator, channel decoder and source decoder. When an analog output is desired, the output of the source decoder is fed to the Digital to Analogue converter (DAC) to reconstruct the estimated message. Because of channel conditions and distortions, the message at the destination output is an approximation to the original source message. Each one of the blocks shown in Figure 1.1 is a research field on its own. In this thesis, our focus is on the modulation/demodulation sub-blocks of DCS.

1.2 Modulation Scheme Parameters

Radio systems are always strictly limited by the regulating authorities to certain frequency bands. Usually, each one of those bands is shared among multiple users of the system by means of Frequency Division Multiple Access (FDMA) and, therefore, the bandwidth occupied by each user is narrower, and more users can be accommodated. Moreover, communication system bandwidth requirement is determined by the spectrum of the modulated signal, which is typically presented as a plot of Power Spectral Density (PSD) as a function of frequency. Theoretically speaking, the PSD should be zero outside the occupied band, where in practice, however, this is never the case, and the spectrum extends to infinity beyond the band's limit. This is either due to the specific characteristics associated with the different modulation schemes or due to the imperfectness of the practical implementation of filters. Therefore, it is essential to set the bandwidth, W, of the modulated signal such that the signal's power portion falling beyond the band's limit is less than a certain threshold. In practical implementation, this threshold is determined by the system's tolerance to Adjacent Channel Interference (ACI), which is also another feature of the modulation scheme. In addition, the bandwidth or spectral efficiency of a modulation scheme is defined as the channel data rate r per unit bandwidth occupied ($r/W\ bits/s/Hz$).

Another parameter used in characterizing a modulation scheme is the Bit-Error-Rate (BER) performance. BER is defined as the ratio of bits received in *error* to the *total*

number of bits received. Moreover, BER is also referred to as the probability of bit error, $P(\varepsilon)$, and is frequently plotted logarithmically against Signal-to-Noise-Ratio (SNR) in dB. For a more system-independent measure, the coordinate of this graph is normally the bit-energy-to-noise density ratio E_b/N_o. This is due to the fact that noise power spectral density N_o is a primary feature of a channel and independent of the bandwidth of the system, unlike the noise power. E_b/N_o is dimensionless, since N_o has dimension of $Watts/Hz$, which is equivalent to $Joules$.

In addition, modulator and demodulator complexity is another parameter that plays a major role in determining the choice of a specific modulation scheme for any DCS. The number of correlators required in the implementation of the demodulator is normally used as a complexity measure for each modulation scheme. Moreover, all DCS require a particular degree of synchronization with incoming signals by the receivers, which further increases the complexity of receivers especially in coherent detection.

Hence, the ultimate choice of one modulation scheme over the others in a DCS depends on spectral efficiency, BER performance and receiver complexity. In general, these parameters can be viewed as a set of basis-functions that can be used to pinpoint DCS as a point in a three-dimensional space. Following this analogy, trade-offs in the design of a DCS exist among these three main resources. In practice, two types of modulation schemes are found, one that is optimized for bandwidth efficiency and the other that is optimized for power efficiency. The choice of which one to go with depends on the DCS in question, if it is either power-limited or bandwidth limited. Consequently, different modulation schemes are referred to as either power-efficient or bandwidth-efficient.

While efficient power and bandwidth utilization is considered an important criteria in the design of DCS, there are situations where this efficiency is sacrificed in order for other design objectives to be met, such as providing secure communication in a hostile environment. A major advantage of such systems is their ability to reject intentional or unintentional interference. The class of signals that provide this requirement is referred to as spread-spectrum modulation. In a spread-spectrum system, the transmitted signal is

spread over a wide frequency band, usually much wider than the minimum bandwidth required for information to be conveyed.

Nowadays, indoor wireless communication is of great importance and its market share has been growing rapidly due to its advantages over cable networks such as users' mobility, wiring cutoffs and flexibility. Classical applications are cordless phone systems, Wireless Local Area Networks (WLANs) for office and home applications and flexible mobile data transmission links between robots, actuators, sensors, and controller units in industrial environments. Because of the hostile electromagnetic (EM) environment, which includes severe EM emissions from other devices as well as multipath propagation distortions [1], communication link robustness is an extremely important feature for wireless communication system, and here comes in spread-spectrum technology.

Spread-spectrum's most important ability is its robust data transmission even in very noisy radio environments [2]. The critical processes in spread spectrum systems are the spreading and de-spreading functions in the transmitter and receiver. In Frequency Hopping (FH) and Direct Sequence (DS) systems, the synchronization of the de-spreading code needs high computational effort and it is difficult. Chirp modulation and Linear Frequency Modulation (FM) are spread spectrum signaling techniques in which the carrier frequency is swept over a wideband during a given data pulse interval. In such systems, the spreading is accomplished solely for combating multi-path distortions, whereas in Code Division Multiple Access (CDMA), this objective is achieved by using additional coding [3]. Spreading and de-spreading with chirp signals can be easily implemented using Surface Acoustic Wave (SAW) technology [4], which offers a rapid close-to-optimum method for both generation and correlation of wideband chirp pulses [5]. Moreover, these devices are very compact and can be realized at low cost, due to the analog correlation process involved in the complex synchronization circuits.

While a variety of modulation techniques exist in the literature, the emphasis in this thesis is on phase modulations. In particular, two subclasses of phase-continuous signals referred to as Continuous Phase Frequency Shift Keying (CPFSK) and Continuous Phase Chirp Keying (CPCK) are considered, in an attempt to arrive at power efficient

modulations. In the next Section, an overview of the relevant development in the area of CPM is provided with particular references to CPFSK and CPCK modulations, detection techniques, receivers and their performance.

1.3 Review of Continuous Phase Modulation (CPM)

Over the past twenty years or so, research has been intensely focused on finding *efficient* Digital Communication Systems, especially modulation techniques that can meet high bit rate transmissions. Generally speaking, one modulation scheme is chosen over another based on which one requires the least value of SNR for a specific error rate threshold and still satisfies the various system constraints [6].

In this context, constant-envelope CPM has emerged as an excellent modulation technique for applications in satellite communication and global digital radio channels. CPM offers excellent bandwidth and power efficiency [7]. Moreover, CPM designs are fairly immune to nonlinear channel effects because of their constant-envelope characteristic. Although there are many CPM classes with diverse properties and applications, they are all based on the usage of inherent memory, which is introduced by the continuous phase. This continuous phase constraint offers enhanced bit error probability performance [8], sharper spectral roll-off [9], and permits multi-symbol detection rather than the conventional symbol-by-symbol detection. In general, BER performance is improved by increasing the number of observation intervals. However, the implementation of the corresponding optimal receiver becomes much more complex. Thus, it is important to examine the class of constant envelope CPM for its ability to offer tradeoffs among receiver complexity, bandwidth and power.

Osborne and Luntz [10] considered a bandwidth efficient modulation technique, Continuous Phase Frequency Shift Keying (CPFSK), and showed that Binary CPFSK with a modulation index of $h = 0.715$ and optimum 3-bit observation receiver can outperform Binary Phase Shift Keying (BPSK). Later, these results were extended to the more general case of M-ary CPFSK by Schonhoff [11]. In these works, the focus was on finding optimum modulation parameters that provide least BER. However, it is important to examine the loss in performance relative to the optimum if one were to use non-

optimum modulation parameters due to bandwidth and receiver complexity constraints. It is noted that [10, 11] in order to arrive at BER performance of the optimum receiver, high-and low-SNR approximations have been employed. Nevertheless, it is not clear as to the value of SNR that distinguishes high-SNR from that of low-SNR. Thus, an investigation to answer this question is important.

Moreover, Aulin *et. al.* have studied CPM using minimum Euclidean distance notion in the signal space, and have suggested schemes that are efficient in terms of bandwidth and power compared to PSK [8, 12]. Optimum signaling schemes have been determined based on maximizing the minimum Euclidean distance in signal-space. Again, it is noted that an examination of distance properties as a function of modulation parameters is important to understand the ability of CPM to operate over practical communication channels.

In addition, Miyakawa's *et. al.* have suggested the use of time-varying modulation indices from one bit interval to the next and have demonstrated that multi-*h* CPFSK can outperform single-*h* CPFSK [13]. Anderson and Taylor [14] generalized Miyakawa's work by imposing certain constraints on the modulation indexes employed and have confirmed that multi-*h* phase codes can achieve up to 4 dB BER performance improvement in approximately the same bandwidth relative to PSK. In another work, Aulin and Suridberg [15] have thoroughly worked on the distance properties of multi-*h* signals. In addition, Raveendra and Srinivasan [16] have arrived at optimum multi-*h* CPM schemes, which minimize the bit-error-probability. Moreover, they have arrived at closed-form expressions describing bit error rates of an easy-to-implement multi-*h* CPM Average Matched Filter (AMF) receiver.

Later on, Hwang *et. al.* have introduced the concept of asymmetric modulation indices [17]. In this technique, the modulation indices were set as a function of the data symbols and it was demonstrated that performance improvements can be achieved over conventional multi-*h* schemes in essentially the same bandwidth. Fonseka and Mao [18] considered a class of nonlinear asymmetrical multi-*h* CPFSK with the ability to achieve higher distance properties relative to other multi-*h* schemes. By adaptively changing

modulation indices in a time-varying manner, it is also possible to obtain an adaptive multi-*h* CPFSK signaling [19]. This signaling scheme realizes higher coding gains compared to the well-known Minimum Shift Keying (MSK) scheme. Further important works in nonlinear CPFSK has been carried out [20, 21, 22]. Also, Raveendra and Srinivasan [23] considered a Decision Directed Receiver for coherent demodulation of a subclass of CPM over AWGN.

Chirp modulation or Linear FM represents a class of spread-spectrum signals. It is useful in certain communication systems for its abilities such as anti-eavesdrop, low-Doppler sensitivity and anti-interference [24]. Moreover, there are several applications of chirp signals in communication such as cordless systems, radio telephony, data communication in High Frequency (HF) band, air-ground communication via satellite repeaters and WLANs. Recently, Institute of Electrical and Electronics Engineers (IEEE) introduced Chirp Spread Spectrum (CSS) physical layer in the new wireless standard 802.15.4a [25], which uses chirp modulation with no additional coding. The new standard, 802.15.4a, targets applications in sensor actuator networking, industrial and safety control, medical and private communication devices.

A combination of chirp modulation [26] with some kind of pseudo-random coding has been shown to produce significant improvement in anti-jam performance. Among several applications of chirp signals in communication are cordless systems, data communication in High Frequency (HF) [27], radiotelephony, WLANs [28] and air-ground communication via satellite repeaters [29][30].

While majority of chirp signals are employed in radar applications [31], Winkler [32] first proposed them for data communication, due to their noise immunity property to intentional interference. Hirt and Pasupathy studied the performance of coherent and non-coherent binary chirp signals over AWGN channel [33, 34]. Since the optimum receivers were required to make independent bit-by-bit decisions, it was concluded that chirp systems did not compare favorably with conventional PSK and FSK systems. By introducing phase continuity into chirp signals at bit transitions, the use of multiple-bit detection techniques became possible, which offered power advantages [35]. Thus, Hirt

and Pasupathy considered a class of CPM referred to as Continuous Phase Chirp (CPC) binary signals [33] and showed that an advantage of 1.66 dB at most can be achieved over conventional PSK. Raveendra extended this work to the more general case of M-ary signaling [36]. It was shown that 4-ary chirp system with five bit observation interval, when coherently detected, offers an SNR gain that is nearly equal to 3.2 dB compared to that of the conventional 4-PSK system. Also, Raveendra introduced a class of multi-mode binary CPC signals [37] that used the concept of time-varying modulation parameters. He showed that dual-mode phase-continuous chirp signals, with two different sets of modulation parameters, outperform conventional CPC signals by nearly 0.8 dB. Fonseka extended these results [38] to include partial response CPC signals. More recently, Bhumi and Raveendra [39] considered digital asymmetric phase continuous chirp signals. They showed that it can outperform dual-mode chirp modulation that was considered before [37]. Wang, Fei, and Li [40] proposed a structure for chirp Binary Orthogonal Keying (BOK) system. They obtained an expression for the probability of bit error and showed that chirp BOK performs better than traditional BOK modulation in Additive White Gaussian Noise (AWGN) channel.

Several other works in this area clearly exhibit the choice of chirp modulation in a variety of digital communication systems [41, 42, 43, 44, 45 and 46]. In all these works, binary chirp systems with receivers that are required to make independent bit-by-bit decisions have been considered.

In the literature, there are several other notable papers, which address the advancement in CPM over the past 20-30 years [12, 13, 17, 18, 33 and 37].

1.4 Problem Statement and Justification

The optimum coherent receiver which minimizes the bit error probability observes the received CPM signal contaminated with AWGN, over several bit intervals and makes a decision on the first bit in this interval. The optimum receiver is complex and its precise analysis is too complicated to attempt analytically. The complexity of the receiver grows exponentially as the number of observed symbol intervals. Also, the performance of the

optimum receiver is determined in terms of the performance of the sub-optimum receivers.

These sub-optimum receivers have been arrived at based on high- and low-SNR approximations. It is not obvious as to the value of SNR that defines the boundary between high- and low-SNR. Also, most performance analyses have focused on determining the optimum modulation parameters that achieve minimum BER. Thus, our first objective in the thesis is to derive from first principles, the structure of the optimum receiver and subject it to high- and low-SNR performance analysis. Closed-form expressions for BER are then derived and used to find the boundary between high- and low-SNRs; first using analytical results and then using simulations. Moreover, we provide a thorough investigation of the effect of modulation parameters on BER performance for the subclasses of CPM namely CPFSK and CPCK. This study is carried out using exhaustive computer search and backed with mathematical analysis, wherever possible.

It is well-known that the Viterbi Algorithm (VA), a Maximum Likelihood Sequence Estimation (MLSE) technique, is widely used for estimation and detection problems in digital communications. In this thesis, we are particularly interested in the application of VA for detection of CPFSK and CPCK signals. The main issue is to develop VA in software to examine the performance of specific CPFSK and CPCK signaling.

The problem of finding low-complexity receivers for CPM has received wide spread attention by researchers. One is particularly interested in arriving at reduced complexity receivers whose performances are comparable to that of the optimum receiver. In fact, in all these works, four different types of receivers are considered, of which two are generally receivers that work for all CPM schemes and the other two work for binary schemes with a modulation index of 0.5. In this thesis, quite different to the approaches available in the literature, we introduce a low-complexity receiver, for both CPFSK and CPCK, which we have called Decision Aided Receiver (DAR). The detection strategy involves first obtaining coarse estimates and then using these to refine the estimate in a specific bit in the observation interval. Not only we provide the decision aided detection

strategy, but also we obtain closed-form expression for estimating the BER of such a receiver.

1.5 Thesis Contributions

The major contributions of the thesis are summarized below:

- Two subclasses of constant-envelope phase-continuous signals called CPFSK and CPCK signals are presented. Mathematical descriptions and properties of these signals are given and illustrated.
- Optimum and sub-optimum receivers are derived based on Bayesian Maximum Likelihood Ratio Test (MLRT). Performance of these receivers is analyzed and the effect of the different modulation parameters on BER is examined in detail for CPFSK and CPCK modulations.
- Minimum Distance Criteria for both CPFSK and CPCK signaling techniques are provided, and optimum parameters that maximize the minimum distance are determined through extensive computer search.
- Performance of the Maximum Likelihood sequence Estimation (MLSE) receiver, which is referred to as Viterbi Algorithm (VA) is provided for specific CPFSK and CPCK modulations.
- A *novel* Decision Aided Receiver (DAR) for CPFSK and CPCK modulations is presented and closed-form expressions for BER of the receiver are derived. Best CPFSK and CPCK systems for DAR have been determined and illustrated.

1.6 Thesis Organization

Chapter 2 provides the concept, mathematical descriptions and properties of CPM signals. A mathematical frame work required for the understanding of Continuous Phase Chirp Keying (CPCK) and Continuous Phase Frequency Shift Keying (CPFSK) signaling techniques is described. We demonstrate the fundamental difference between CPFSK and CPCK signaling techniques. Illustrations of phase functions, frequency functions, phase trees and trellises, baseband and passband waveforms for CPFSK and CPCK as a function of modulation parameters are all provided.

In Chapter 3, the problem of detection of CPM in AWGN channel is considered. Using Maximum Likelihood Ratio Test (MLRT), an optimum receiver is derived for detection of arbitrary CPM signals in AWGN channel. Also, we discuss the computational complexity of this optimum receiver for CPFSK and CPCK. Two sub-optimum receivers for high- and low-SNR values are derived. The low-SNR, sub-optimum, also known as Average Matched Filter (AMF), receiver is examined thoroughly for CPFSK and CPCK. At high-SNR, another sub-optimum receiver is provided. A thorough examination of the relationship among BER, Signal-to-Noise Ratio (SNR), modulation parameters and detection observation length are provided using number of illustrations. An attempt is made to answer the question, "What value of SNR separates high-SNR from low-SNR when studying the effect of the modulation parameters on BER ?" A composite bound is provided using the performance of sub-optimum receivers that represents the performance of the optimum receiver.

In Chapter 4, we present the distance properties of both signaling schemes, CPFSK and CPCK. This lays the ground work for introducing the MLSE receiver for CPFSK and CPCK signals, also known as the Viterbi Algorithm (VA) receiver. Advantages of Viterbi receiver over the MLRT-based receiver are demonstrated and performance of Viterbi receiver for specific CPFSK and CPCK schemes is illustrated.

In Chapter 5, a Decision Aided Receiver (DAR) for CPFSK and CPCK as an alternative for the AMF receiver is presented. Decision aided detection strategy is presented and explicit expressions for computation of BER are developed for AWGN environment. Numerical results are reported, and a discussion of the performance of DAR is given.

The thesis is concluded in Chapter 6 by summarizing the work carried out, contributions made and conclusions from the results obtained. Also, we outline areas for further research in the light of the needs of modern reliable DCS and the work done in the thesis.

Chapter 2

Continuous Phase Modulation (CPM)

Continuous Phase Modulation (CPM) is a memory-type, constant-envelope, nonlinear modulation, which allows the use of power efficient low cost, nonlinear power amplifiers without introducing distortion. Digital transmission using constant-envelope CPM has become important because of its attractive properties. The constant-envelope designs are fairly immune to nonlinear channel effects. Although constructions of CPM are diverse in their properties and applications, they all rely upon the use of inherent memory introduced by the continuous phase. This constraint of continuous phase not only provides faster spectral roll-off, but also permits multiple symbol detection rather than the more conventional symbol-by-symbol detection. In this Chapter, two subclasses of CPM called Continuous Phase Frequency Shift Keying (CPFSK) and Continuous Phase Chirp Keying (CPCK) are described, although the treatment provided applies, in general, to any CPM. Concepts, mathematical descriptions and properties of CPM signals are presented with primary focus on CPFSK and CPCK signaling techniques, which will be used all through the thesis.

2.1 Description of CPM Signals

The general form of a CPM signal is given by

$$s(t,\boldsymbol{a}) = \sqrt{\frac{2E_b}{T}}\cos(2\pi f_c t + \phi(t,\boldsymbol{a}) + \phi_0), \quad 0 \le t \le nT, \tag{2.1}$$

where E_b is the symbol energy, T is the symbol duration, f_c is the carrier frequency, ϕ_0 is the initial phase offset which is assumed to be zero for coherent detection without any loss of generality. $\boldsymbol{a}$ is a sequence of independent and identically distributed M-ary information symbols each taking one of the $\pm 1, \pm 3 \ldots \pm (M - 1)$ values with an equal probability of $1/M$ such that

$$\boldsymbol{a} = (a_1, a_2, \ldots a_n), \quad a_k \in \{\pm 1, \pm 3, \ldots, \pm(M-1)\}, \quad 1 \le k \le n, \tag{2.2}$$

In this work, the focus is binary case, $M = 2$. The information carrying phase, $\phi(t,\boldsymbol{a})$, during the i^{th} symbol interval is given by

$$\phi(t,\boldsymbol{a}) = \sum_{k=1}^{i-L+1} a_k g(t-(k-1)T), \quad (i-1)T \le t \le iT, \tag{2.3}$$

where $1 \le i \le n$ and the phase function $g(t)$ is defined as the integral of an instantaneous frequency pulse and is given by:

$$g(t) = 2\pi \int_0^t f(\tau)d\tau \tag{2.4}$$

The derivative of $g(t)$ is the frequency pulse shape $f(t)$. That is

$$\begin{cases} f(t) \neq 0 & 0 \le t \le LT \\ f(t) = 0 & Otherwise \end{cases} \tag{2.5}$$

where L is the frequency response pulse length. The frequency pulse length dictates the time interval over which a single input data symbol can affect the instantaneous

frequency. Depending on the value of L, two different schemes of CPM can be defined. When $L = 1$, the entire pulse extends over one full symbol interval. This type of CPM is known as full response CPM. When $L > 1$, only a part of the pulse shape extends over a symbol and is known as partial response CPM signaling. In this work, we are only interested in full response CPM.

2.2 Frequency Pulse Shapes

One of the reasons for CPM to be a bandwidth efficient scheme is that it uses pulse shaping. Using various frequency pulse shapes such as Rectangular (REC), Raised Cosine (RC), Chirp, and Half-Cycle Sinusoid (HCS), various subclasses of CPM have been constructed. Table 2.1 lists the frequency pulse shaping functions used to describe CPFSK and CPCK modulations.

Table 2.1: Rectangular and Chirp Frequency Pulse Shapes with $L = 1$

CPFSK (REC)	$f(t) = \begin{cases} \frac{h}{2T}, & 0 \le t \le T \\ 0, & Otherwise \end{cases}$
CPCK (Chirp)	$f(t) = \begin{cases} \frac{h}{2T} - \frac{w}{T^2}t, & 0 \le t \le T \\ 0, & Otherwise \end{cases}$

In CPM, the information carrying phase is continuous all the time for all the combinations of data symbols. Therefore, memory is introduced into the CPM signal by means of its continuous phase. The quantity *h*, in Table 2.1 is the *modulation index* and represents the ratio of peak-to-peak frequency deviation and the symbol rate. Ideally, *h* can take any real value, but in order to limit the number of phase states, *h* is chosen a rational value between $0 < h < 1$ and ratio of two prime numbers v and p, i.e. $h = v/p$. In some cases, the modulation is described using more than one modulation parameter. Chirp is one such example, which will be explained later.

2.3 General Schematic of CPM Modulator

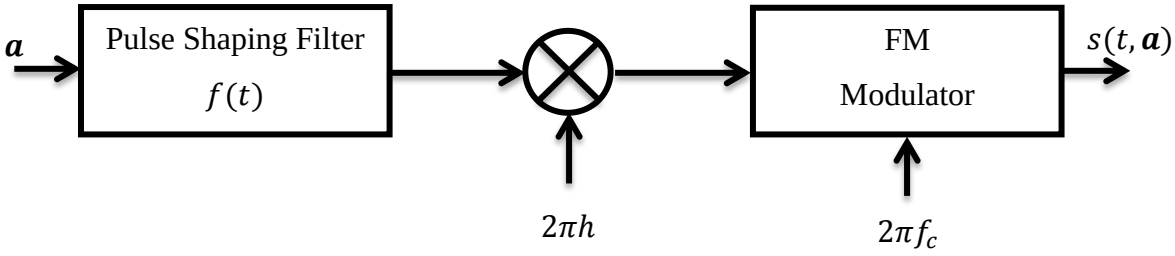

Figure 2.1: Basic structure of single-*h* CPM modulator

Figure 2.1 represents a conceptual block diagram of the single-*h* CPM, which is the focus of this thesis. Data sequence $\boldsymbol{a}$ passes through the pulse shaping filter and the multiplier to form frequency pulse sequence, which is then FM modulated to generate the CPM signal.

2.4 Phase States of CPM Signals

The phase of CPM can be represented by a tree structure. The tree structure is found by manipulating the information carrying phase of Equation 2.3. It can be viewed as the sum of two phase terms: instantaneous phase and accumulated phase. The phase of CPM signal during the i^{th} symbol interval to give

$$\begin{aligned}\phi(t, \boldsymbol{a}) &= \sum_{k=i-L+1}^{i} a_k g(t-(k-1)T) + g(t=T)\sum_{k=1}^{i-1} a_k \,, \\ &= \theta(t, a_i) + \theta_i \qquad\qquad (i-1)T \le t \le iT, \end{aligned} \tag{2.6}$$

where $\theta(t, a_i)$ is the *instantaneous* phase

$$\theta(t, a_i) = \sum_{k=i-L+1}^{i} a_k g(t-(k-1)T) \tag{2.7}$$

which represents the changing part of the total phase during $(i-1)T \le t \le iT$ and is determined by the current data symbols and previous $L-1$ symbols. The first term of Equation 2.6, is dependent on the sequence of $L-1$ past input data symbols and the current data input, $(a_{i-L+1}, \ldots, a_{i-1})$, and is called the *correlative state*. There are M^{L-1}

possible correlative states. Since we are only interested in full response CPM ($L = 1$), then

$$\theta(t, a_i) = a_i g(t - (i-1)T), \qquad (i-1)T \le t \le iT \tag{2.8}$$

and θ_i is the *accumulated* phase, the *phase state*, which represents the constant part of the total phase in the same interval is

$$\theta_i = g(t = T) \sum_{k=1}^{i-1} a_k \qquad (i-1)T \le t \le iT, \tag{2.9}$$

The *accumulated* phase can be interpreted as the sum of the maximum phase changes contributed by each symbol, accumulated along the time axis up to the $(i - 1)^{th}$ symbol interval. It can be computed recursively as:

$$\theta_{i+1} = \theta_i + g(t = T) a_i \tag{2.10}$$

The phase behavior of CPM signals can be best described by sketching the set of phase trajectories $\phi(t, \boldsymbol{a})$ generated by all possible values of the information sequence $\{a_i\}$. These phase diagrams are called *phase trees* and they are specific to each CPM scheme, based on the different modulation parameters, the M-ary points and most importantly the phase function $g(t)$.

A phase tree is a graphical representation of the phase of CPM signals and shows the amount of phase deviation as a function of time. For any random information sequence, the phases of CPM follow a unique continuous phase trajectory. Moreover, a phase tree can be interpreted as the set of all possible M^n phase trajectories associated with a data sequence of length n. Two examples are shown in Figures 2.2 and 2.3 for the two phase functions considered in this work. The joints represent the start of one bit interval and at each joint, we have two possibilities of input in the case of binary modulation, ± 1. The solid line represents a data input $+1$, and the dotted line represents a -1 data input. The joints themselves represent the accumulated phase at the end of that bit interval. Phase functions affect the shape of the path the CPM signal takes when changing from one phase to another. In Figure 2.2, it's seen that a REC phase function results in a straight

path between one phase and the other. In Figure 2.3, a Chirp phase function results in a curvy path between one phase and the other. Thus, it is intuitively concluded that different phase functions will have different performances.

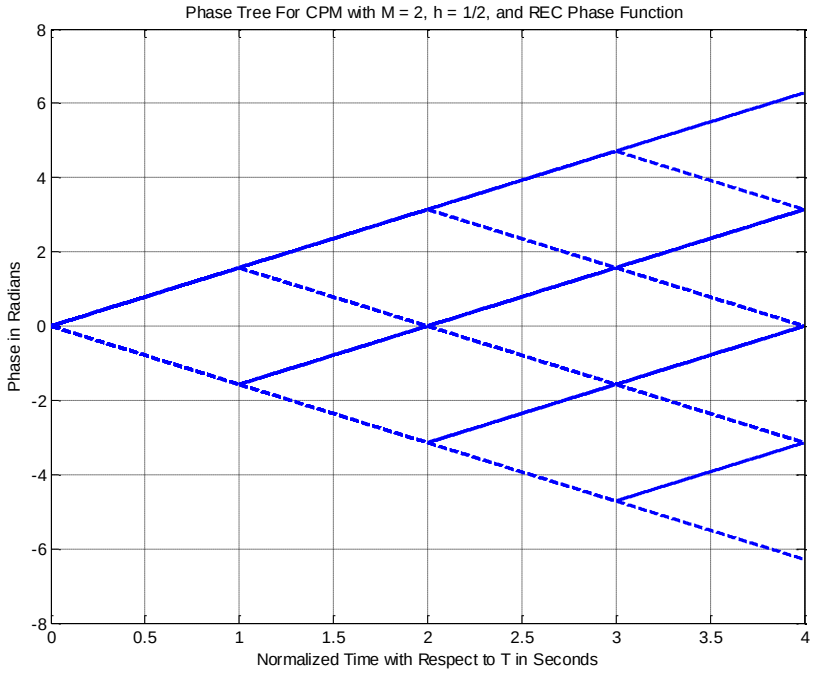

Figure 2.2: Phase Tree for REC Phase Function

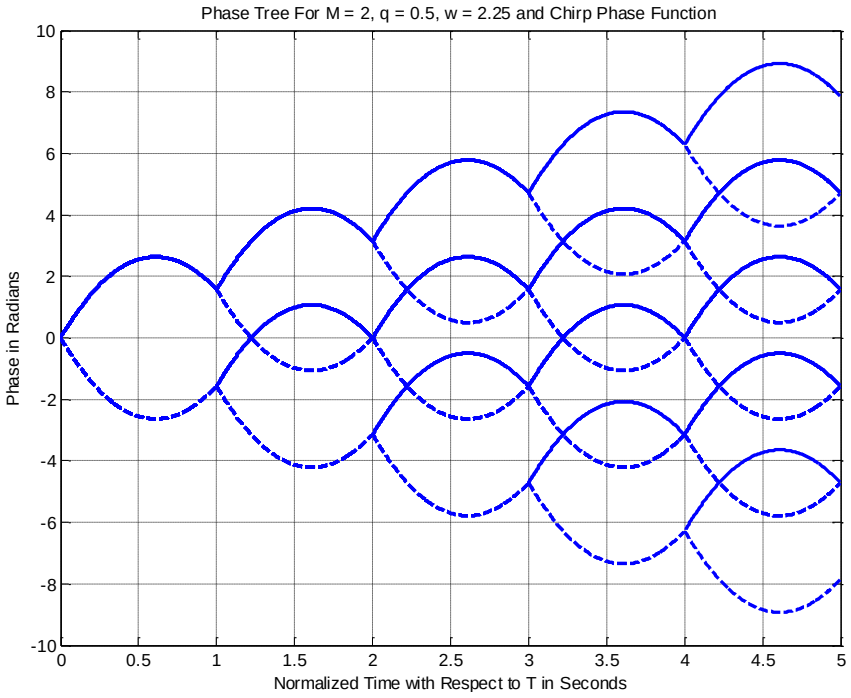

Figure 2.3: Phase Tree for Chirp Phase Function

Since phase is continuous, it repeats the same pattern over every i^{th} bit interval. Hence, the number of phase states increases with an increase in time and the tree becomes more complex. Thus, in order to reduce complexity in tracking, it is required to restrict this growth, which can be achieved by plotting the phase trajectory on modulo-2π scale i.e. between the range of $[-\pi, \pi]$ or $[0, 2\pi]$. The resultant plot is known as a *phase trellis*. In other words, the phase trellis is a modulo-2π version of the phase tree. The phase trellis is also a key concept when it comes to applying Maximum Likelihood Sequence Detection (MLSD) for CPM signals detection, referred to as the Viterbi Algorithm (VA).

The trellis structure is obtained by reducing the phase modulo-2π. The phase reduced modulo-2π is termed the *physical phase*, and we denote it as $\tilde{\phi}(t, \boldsymbol{a})$. It is impossible to distinguish between two phases that differ by 2π, and thus, the physical phase is the phase that is observable.

During the i^{th} symbol interval, $\tilde{\phi}(t, \boldsymbol{a})$ is given by

$$\begin{aligned}\tilde{\phi}(t, \boldsymbol{a}) &= [\phi(t, \boldsymbol{a})] \bmod 2\pi \\ &= \left[\sum_{k=i-L+1}^{i} a_k g(t-(k-1)T) + \theta_i \right] \bmod 2\pi \\ &= \left[\sum_{i=i-L+1}^{i} a_k g(t-(k-1)T) + [\theta_i] \bmod 2\pi \right] \bmod 2\pi \\ &= \left[\sum_{k=i-L+1}^{i} a_k g(t-(k-1)T) + \tilde{\theta}_i \right] \bmod 2\pi, \quad (i-1)T \le t \le iT, \end{aligned} \tag{2.11}$$

The $physical\ phase\ state$, $\tilde{\theta}_i$, is given by

$$\begin{aligned}\tilde{\theta}_i &= [\theta_i] \bmod 2\pi \\ &= \left[g(t=T) \sum_{k=1}^{i-L} a_k \right] \bmod 2\pi \end{aligned} \tag{2.12}$$

The tree will reduce to a trellis structure if the modulation index, h, is set to a ratio of two relatively prime integers, such that $h = v/p$, so a finite number of terminal phases is produced at the end of each bit interval. The modulation index, h determines the number of phase states in a CPM signal. That is for full-response CPM signal with $h = v/p$ where v and p have no common factors, the different values at the time instants $t = (i - 1)T$ will have the terminal/physical phase states θ_i, which is given by:

$$\theta_i = \left\{0, \frac{\pi v}{p}, \frac{2\pi v}{p}, \dots, \frac{(p-1)\pi v}{p}\right\} \tag{2.13}$$

when v is even and

$$\theta_i = \left\{0, \frac{\pi v}{p}, \frac{2\pi v}{p}, \dots, \frac{(2p-1)\pi v}{p}\right\} \tag{2.14}$$

when v is odd.

Hence, there are p terminal phase states when v is even and $2p$ states when v is odd. For example, for binary modulation, $M = 2$, with pulse length $L = 1$ with $h = 1/2 = 2/4$, the number of phase states is four. Going by another example, let $h = 1/4$, then according the to the Equations 2.13 & 2.14, binary CPFSK has 8 terminal states which are $\{0, \pi/4, 2\pi/4, 3\pi/4, \pi, 5\pi/4, 6\pi/4, 7\pi/4\}$ and with $h = 2/3$, 3 terminal states and corresponding phase states are $\{0, 2\pi/3, 4\pi/3\}$. A diagram illustration is shown in Figure 2.4.

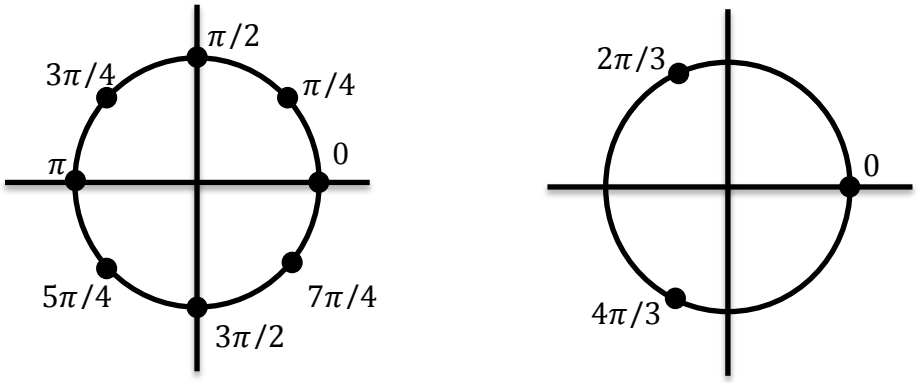

(a) $h = 1/4$ (b) $h = 2/3$

Figure 2.4: Signal Constellation Diagrams for CPFSK

An alternative representation to the state trellis is the state diagram, which also illustrates the state transitions at the time instants $t = (i-1)T$. This is an even more compact representation of the CPM signal characteristics. Only the possible (terminal) phase states and their transitions are displayed in the state diagram. Time does not appear explicitly as a variable. For example, the state diagram for the CPFSK signal with $h = 1/2$ is shown in Figure 2.5.

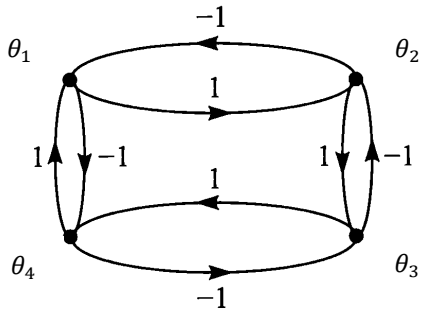

Figure 2.5: State diagram for binary CPFSK with $h = 1/2$.

However, for the real h, the number of states is huge and it becomes practically complex to implement receivers such as VA receiver. The *state vector* at the i^{th} bit interval is:

$$S_i = [\theta_i, a_i, a_{i-1}, a_{i-2}, \dots, a_{i-L+1}] \qquad (2.15)$$

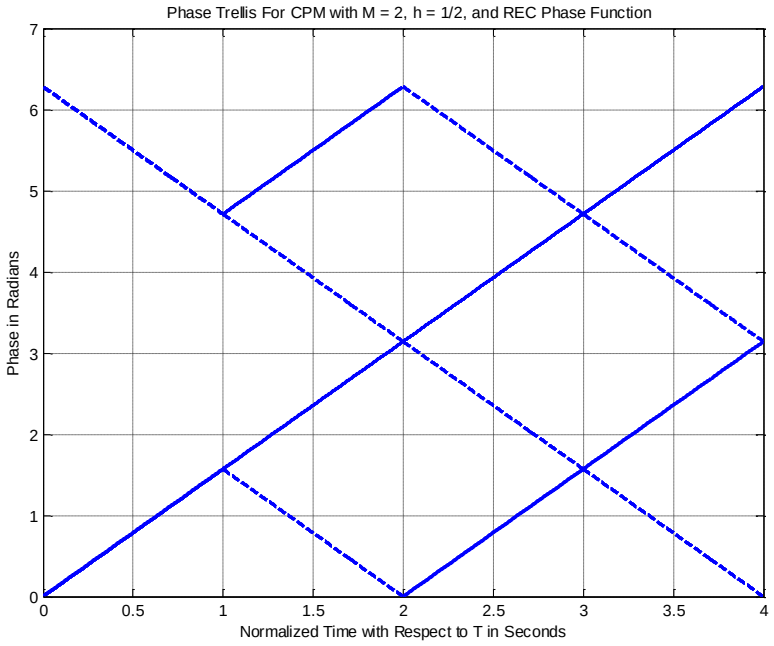

Figure 2.6: Phase Trellis for REC Phase Function

State vectors *pinpoint* the location of the signal at the at the i^{th} bit interval for a certain transmitted sequence. For full response CPM, $S_i = [\theta_i, a_i,]$, we only need the accumulated phase till that point and the current data point in order to identify the next phase. The concept of state vector is the key idea behind the operation of the Viterbi decoder, which will be discussed in Chapter 4. A phase trellis example is shown in Figure 2.6.

To properly view the phase trellis diagram, we may plot the two quadrature components $x_i(t;\boldsymbol{a}) = \cos\phi(t;\boldsymbol{a})$ and $x_q(t;\boldsymbol{a}) = \sin\phi(t;\boldsymbol{a})$ as functions of time. Thus, we generate a three-dimensional plot in which the quadrature components x_i and x_q appear on the surface of a cylinder of unit radius. For example, Figure 2.7 illustrates the phase trellis cylinder obtained with binary modulation, a modulation index $h = 1/2$, and a rectangular pulse with $L = 1$. The solid lines in Figure 2.7 represent a data input +1, and the dashed lines represent a -1 data input. The shape of the line changes based on the phase function in use. Specific examples for CPFSK and CPCK will be shown later.

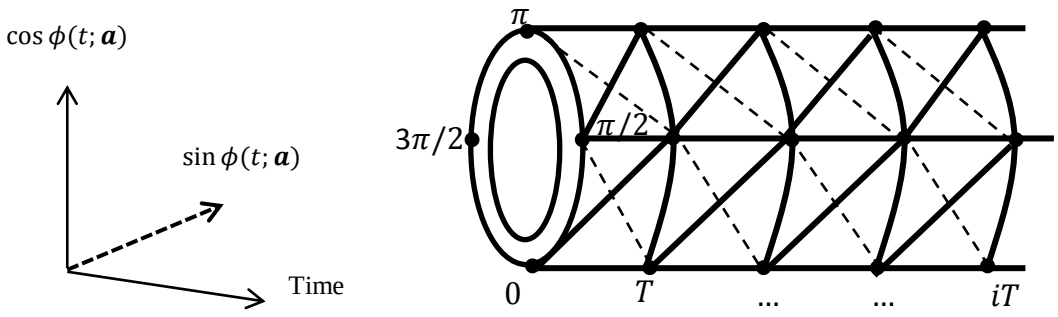

(a) 3D coordinates for Phase Cylinder (b) Phase Cylinder

Figure 2.7: Modulo 2π Phase Trajectory Wrapped Around a Cylinder

It is apparent now that infinite varieties of CPM signals can be generated by choosing different pulse shapes, the modulation index *h* and the data format. Among these, single-*h* and multi-*h* are major subclasses for power/bandwidth efficient CPM systems. We next describe two subclasses of CPM, CPFSK and CPCK, and discuss their phase properties and trellis structures.

2.5 Continuous Phase Frequency Shift Keying (CPFSK)

In rectangular pulse shaping (Linear Pulse Shaping), phase changes linearly with the time, and the frequency is held constant throughout the data interval. In general, frequency pulse of length *L* is denoted by LREC. With *L* = 1, 1REC-CPM signal is called Continuous Phase Frequency Shift Keying (CPFSK). Note that although the rectangular pulse-shaping function is discontinuous, the phase response function is continuous. Frequency function $f(t)$, of linear pulse shape with full response CPM (*L* = 1) signaling is given as:

$$f(t) = \begin{cases} \frac{h}{2T}, & 0 \le t \le T \\ 0, & Otherwise \end{cases} \tag{2.16}$$

and the corresponding phase function $g(t)$

$$g(t) = \begin{cases} 0, & t < 0 \\ \pi\frac{ht}{T}, & 0 \le t \le T \\ \pi h, & t > T \end{cases} \tag{2.17}$$

So, for full response CPFSK,

$$\phi(t, \boldsymbol{a}) = a_i g(t - (i-1)T) + \theta_i, \qquad (i-1)T \le t \le iT, \tag{2.18}$$

where $\theta(t, a_i)$, the *instantaneous* phase is

$$\theta(t, a_i) = a_i g(t - (i-1)T) = \frac{\pi h a_i (t - (i-1)T)}{T}, \qquad (i-1)T \le t \le iT \tag{2.19}$$

and θ_i, the *accumulated* phase or *phase state* is

$$\theta_i = \pi h \sum_{k=1}^{i-1} a_k \qquad (i-1)T \le t \le iT, \tag{2.20}$$

Figures 2.8, 2.9, 2.10 and 2.11 show CPFSK frequency and phase functions for data inputs ± 1. Figures 2.8 and 2.9 show the frequency functions associated with data inputs +1 and -1, respectively. These graphs describe the behavior of the frequency during a bit interval with a data input either +1 or -1. These figures show that the frequency of the

carrier signal is changed to a certain value in response to the incoming data a_i and held constant during the bit interval. Hence, the corresponding phase of the signal varies linearly as shown in Figures 2.10 and 2.11, having a positive slope for data input = +1, and a negative slope for data input = -1.

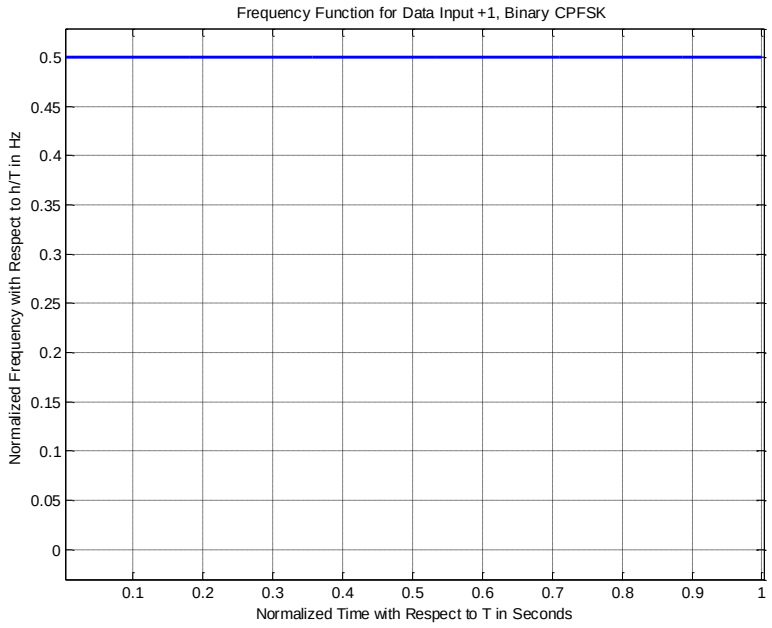

Figure 2.8: Frequency Function for CPFSK with Data Input +1

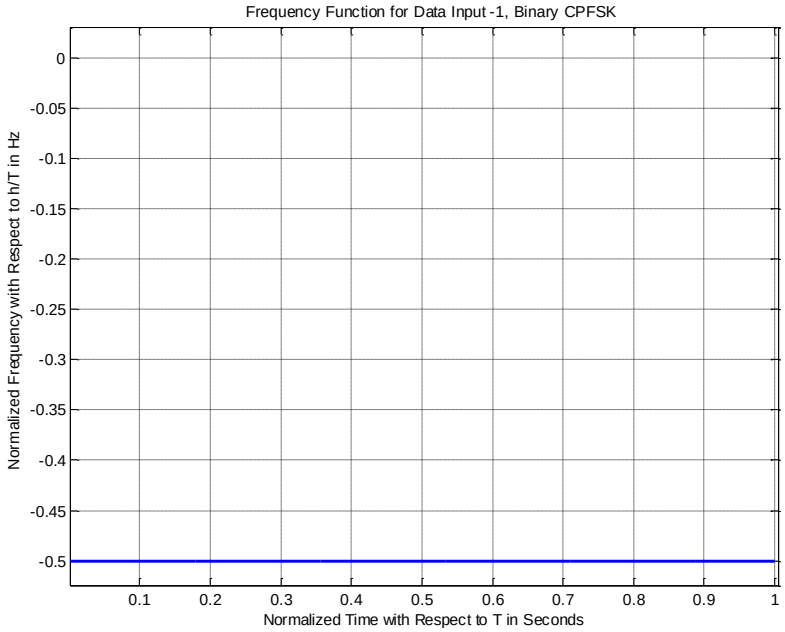

Figure 2.9: Frequency Function for CPFSK with Data Input -1

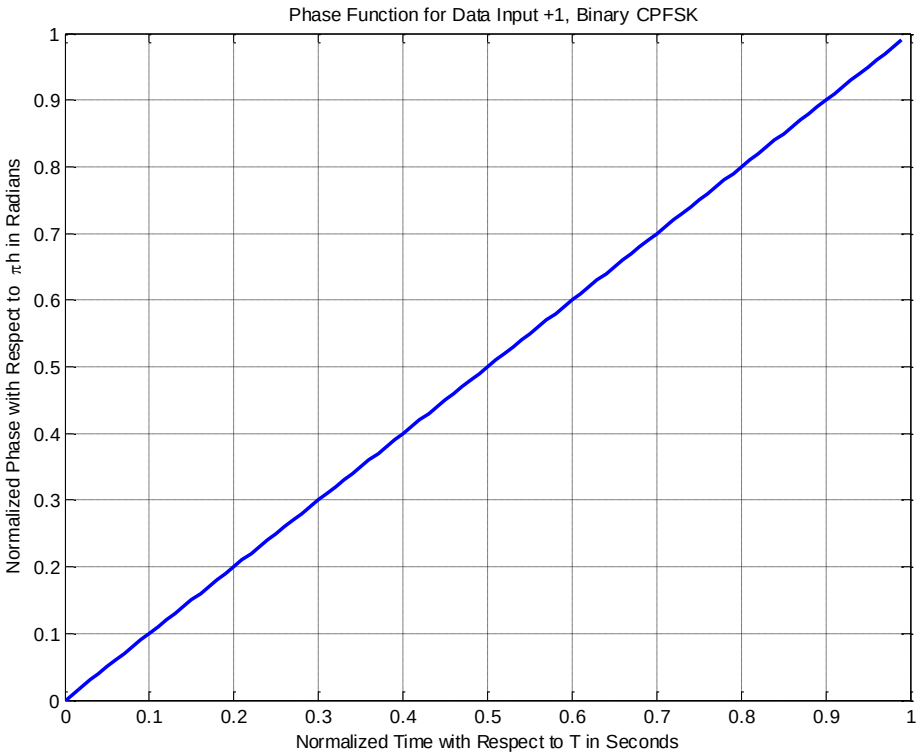

Figure 2.10: Phase Function for CPFSK with Data Input +1

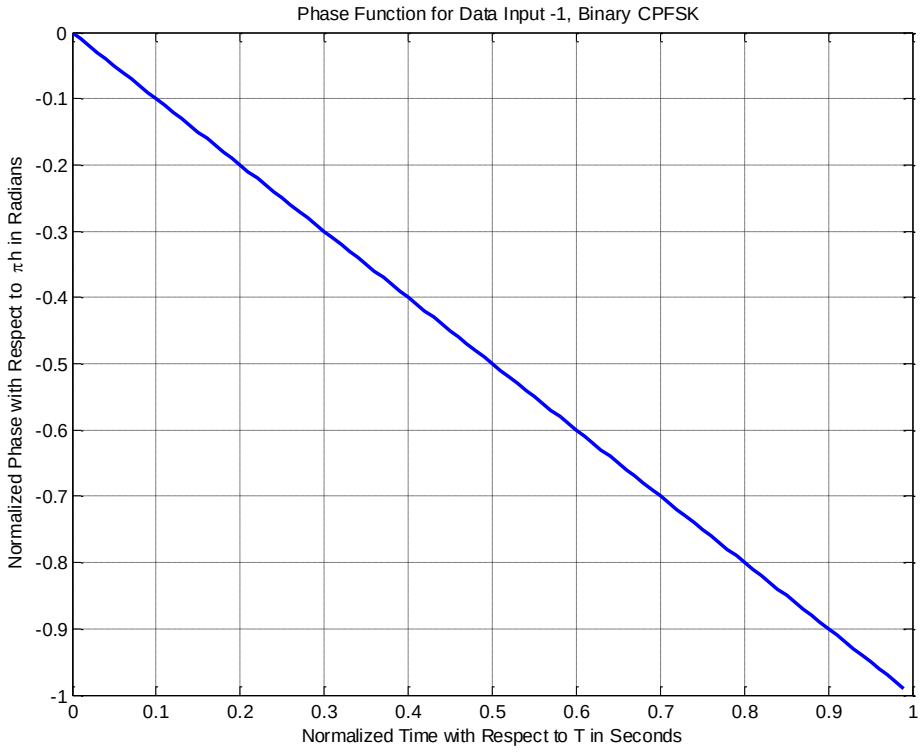

Figure 2.11: Phase Function for CPFSK with Data Input -1

In order to better understand CPFSK signals, we provide the following plots. Figure 2.12 shows the phase state plot for 2-CPFSK with $h = 1/2$. It can be inferred from the Figure that the transmitted sequence is [0 1 1 1 1 0 0], based on the direction the signal moves in, or the slope of the signal within the bit interval. Figure 2.13 shows the physical phase state, which is the observed phase. The jumps in the physical phase state are not discontinuities. They are the phase state but wrapped within the interval $[-\pi, \pi]$. Figures 2.12 and 2.13 amplitudes are the normalized phase with respect to πh. Figure 2.14 shows the baseband CPFSK signal for the input used in Figures 2.12 and 2.13. No discontinuities are present due to the inherent memory characteristics of CPM signals. Figure 2.15 shows the passband CPFSK signal. It can be noticed how frequency changes based on the data input, increasing with a +1 input and decreasing with -1 input. Moreover, the frequency change is noticed to be instantaneous at the beginning of each interval and holds its value for the rest of the bit interval.

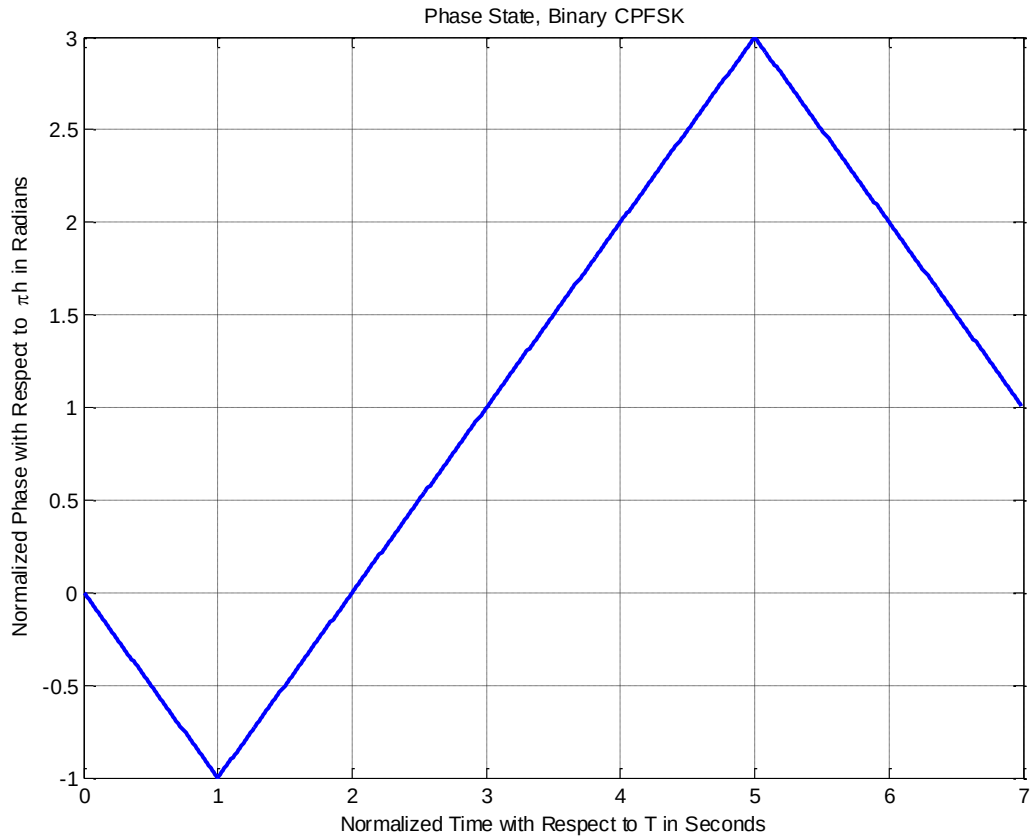

Figure 2.12: Phase State for CPFSK, $h = 1/2$

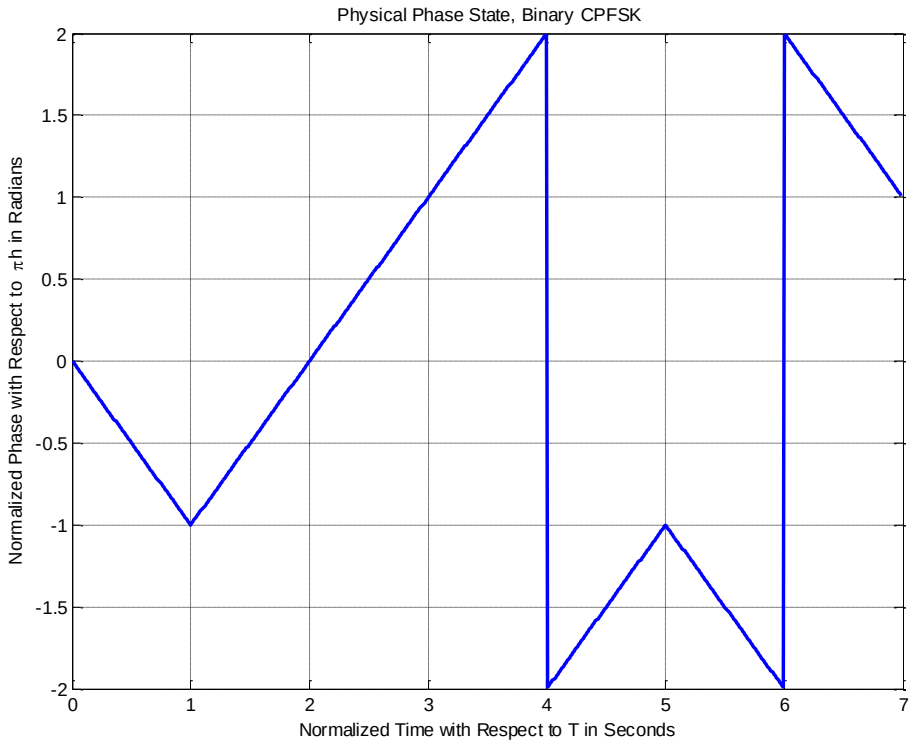

Figure 2.13: Physical Phase State for CPFSK, $h = 1/2$

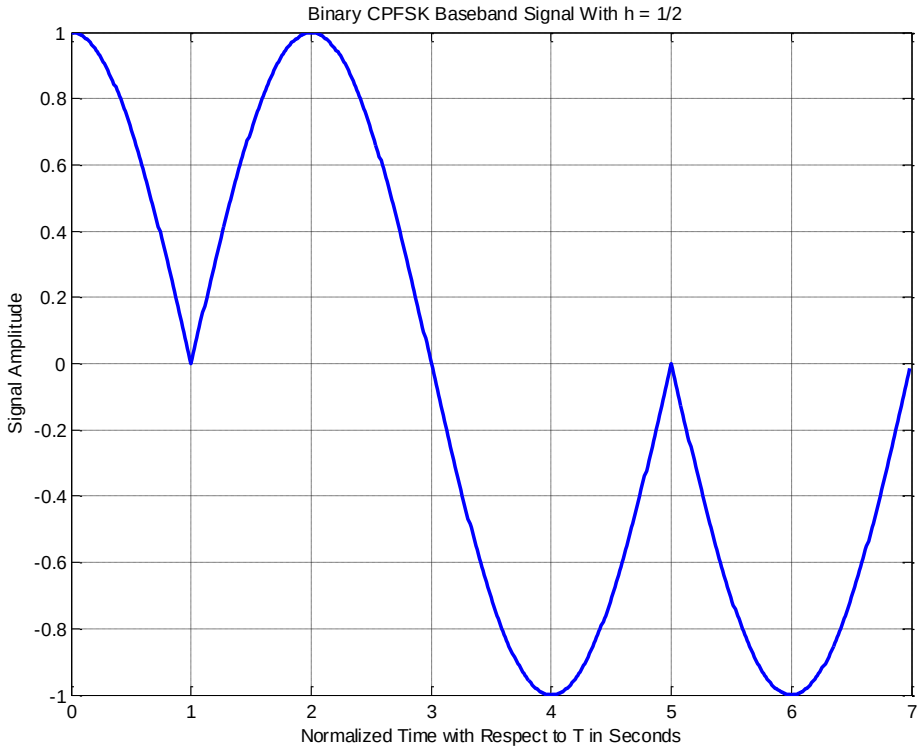

Figure 2.14: Binary CPFSK Baseband Signal with $h = 1/2$

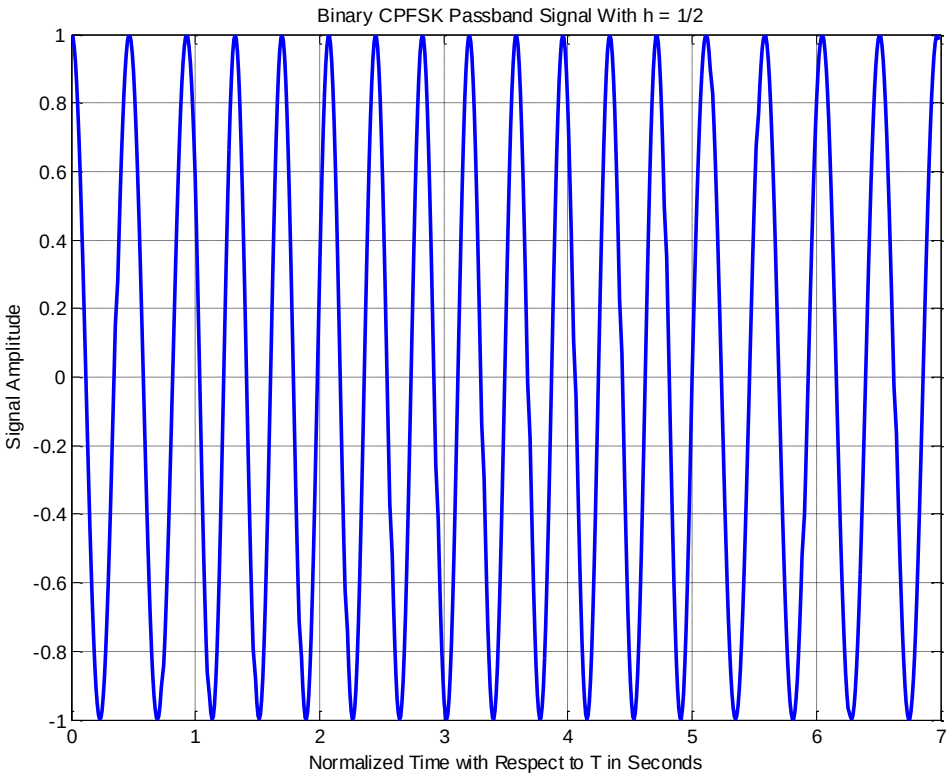

Figure 2.15: Binary CPFSK Passband Signal with $h = 1/2$

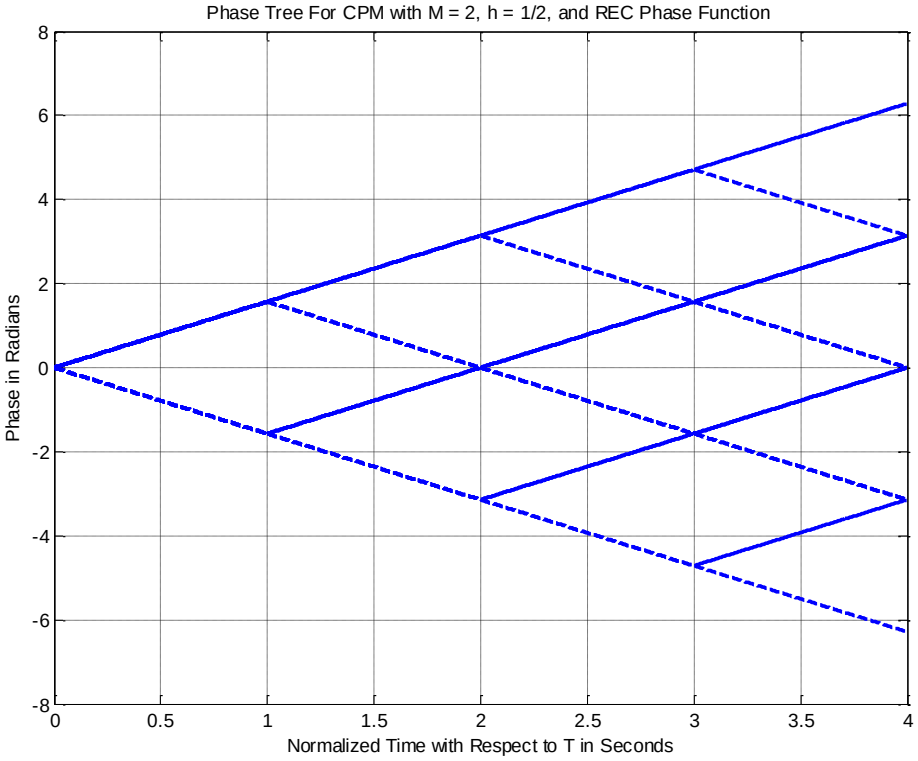

Figure 2.16: Phase Tree for CPFSK Normalized with Respect to $h = 1/2$

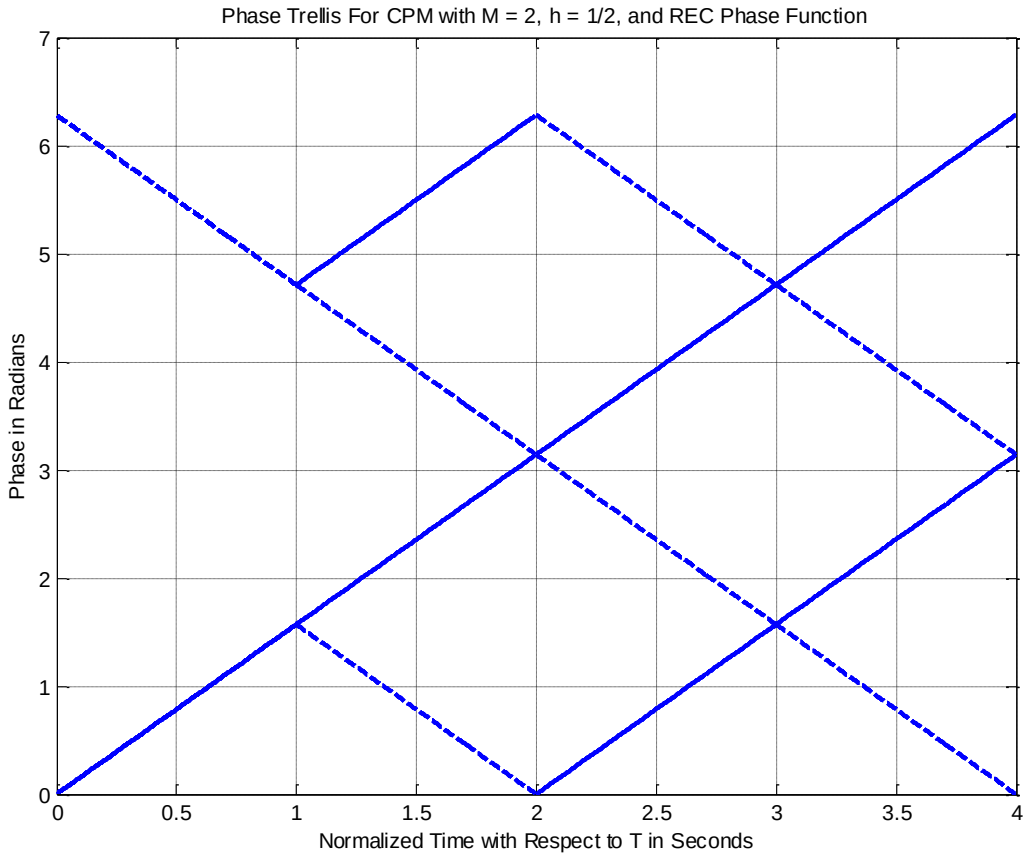

Figure 2.17: Phase Trellis for CPFSK Normalized with Respect to $h = 1/2$

Figures 2.16 and 2.17 show the phase tree and phase trellis for 2-CPFSK and $h = 1/2$, respectively. We emphasize that the phase transitions in the state trellis diagram in Figure 2.17 from one state to another are not true phase trajectories. They represent phase transitions for the terminal/observed states at the time instants $t = (i-1)T$, $1 \leq i \leq n$.

Figure 2.18 shows the phase cylinder for the phase states shown in Figure 2.12. The path wrapped around the phase cylinder of Figure 2.18 is only one of the possible paths that go all over the general cylinder shown in Figure 2.5. In other words, Figure 2.18 is one case of a more general case shown in Figure 2.5, and which case is shown depends on the randomly transmitted sequence. Since we are transmitting n-bits, then we will have M^n possible paths.

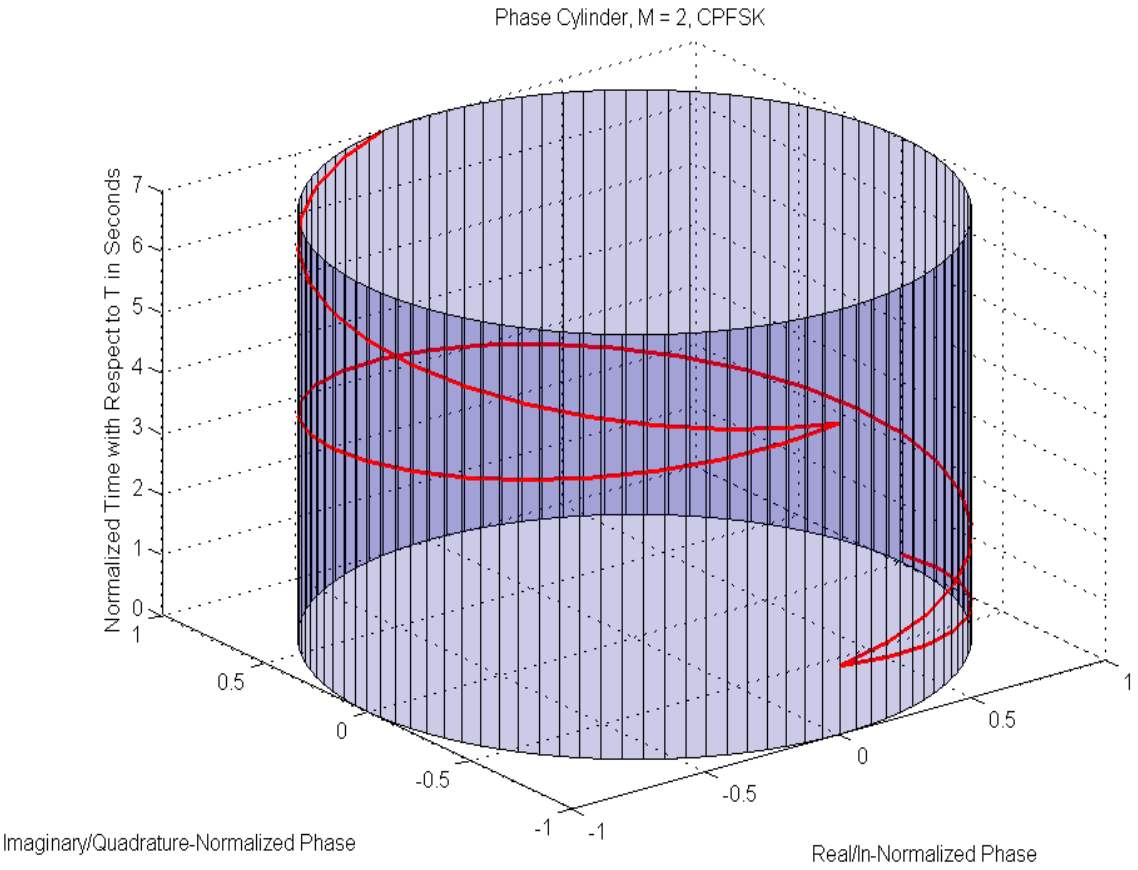

Figure 2.18: Phase Cylinder for 2-CPFSK, $h = 1/2$

2.6 Continuous Phase Chirp Keying (CPCK)

For the major part, CPCK has the same fundamentals as CPFSK, apart from the fact that each one of them uses a different phase function, which adds some new parameters in the case of CPCK. In CPCK, the phase function $g(t)$ is given by,

$$g(t) = \begin{cases} 0 & , \quad t \leq 0, t > T \\ 2\pi \int_0^t f(\tau) d\tau & , \quad 0 \leq t \leq T \\ \pi(h - w) = \pi q & , \quad t = T \end{cases} \tag{2.21}$$

and $f(t)$ is the instantaneous frequency deviation. For CPCK signaling

$$f(t) = \begin{cases} 0 & , \quad t < 0, t > T \\ \dfrac{h}{2T} - \dfrac{w}{T^2} t, & \quad 0 \leq t \leq T \end{cases} \tag{2.22}$$

And the CPCK phase function in Equation 2.21 becomes

$$g(t) = \begin{cases} 0 & , \quad t \le 0, t > T \\ \pi\left\{h\dfrac{t}{T} - w\left(\dfrac{t}{T}\right)^2\right\} & , \quad 0 \le t \le T \\ \pi(h-w) = \pi q & , \quad t = T \end{cases} \tag{2.23}$$

where h and w are dimensionless parameters, h represents the initial peak-to-peak frequency deviation divided by the bit rate $1/T$, and w stands for the frequency sweep width divided by $1/T$. We usually express h in terms of a third dimensionless parameter, q, where $h = q + w$. q and w are independent signal parameters. Note that $w = 0$ gives the continuous phase frequency shift keying (CPFSK) waveform where $h = q$ and $g(t) = t/2T$. Here, h is also called the modulation index. Following from Equation 2.21, 2.22 and 2.23, for full response CPCK, the function describing the phase is a little bit different than the one for CPFSK and is described as follows:

$$\phi(t, \boldsymbol{a}) = \sum_{k=1}^{i} a_k g(t-(k-1)T)$$

$$= a_i g(t-(i-1)T) + g(t=T)\sum_{k=1}^{i-1} a_k = \theta(t, a_i) + \theta_i$$

$$(i-1)T \le t \le iT, \tag{2.24}$$

where $\theta(t, a_i)$, the *instantaneous* phase is

$$\theta(t, a_i) = a_i g(t-(i-1)T) = a_i \pi\left\{h\frac{t-(i-1)T}{T} - w\left(\frac{t-(i-1)T}{T}\right)^2\right\}, \tag{2.25}$$

and θ_i, the *accumulated* phase or *phase state* is

$$\theta_i = g(t=T)\sum_{k=1}^{i-1} a_k = \pi q \sum_{k=1}^{i-1} a_k \tag{2.26}$$

For consistency, we show next the same type of plots for CPCK as that for CPFSK.

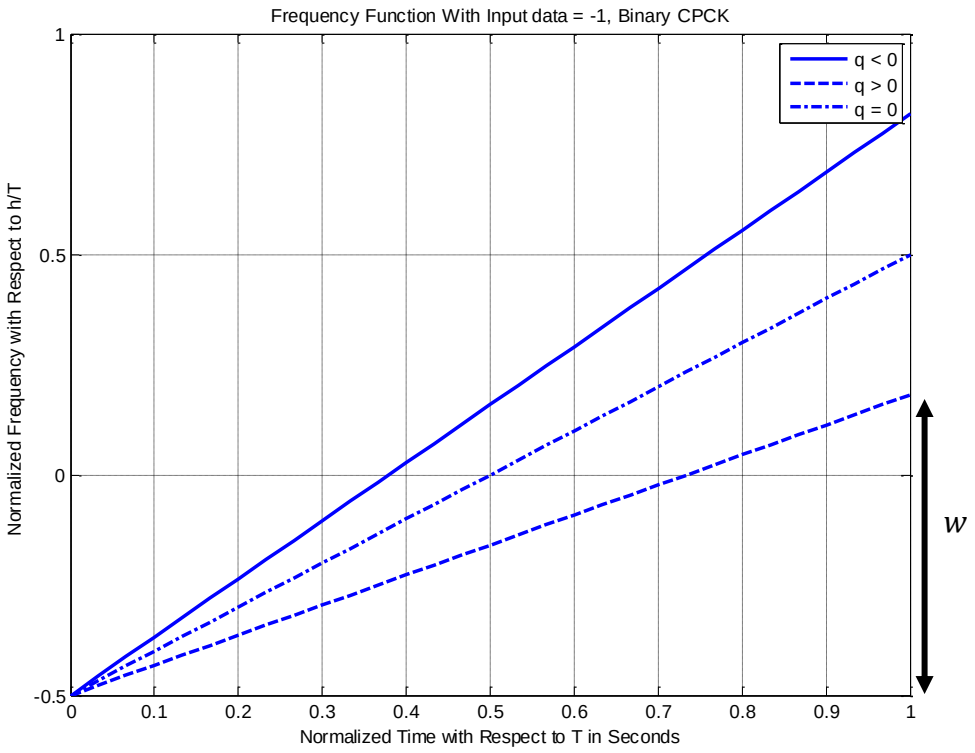

Figure 2.19: Instantaneous Frequency Deviation with Input Data −1

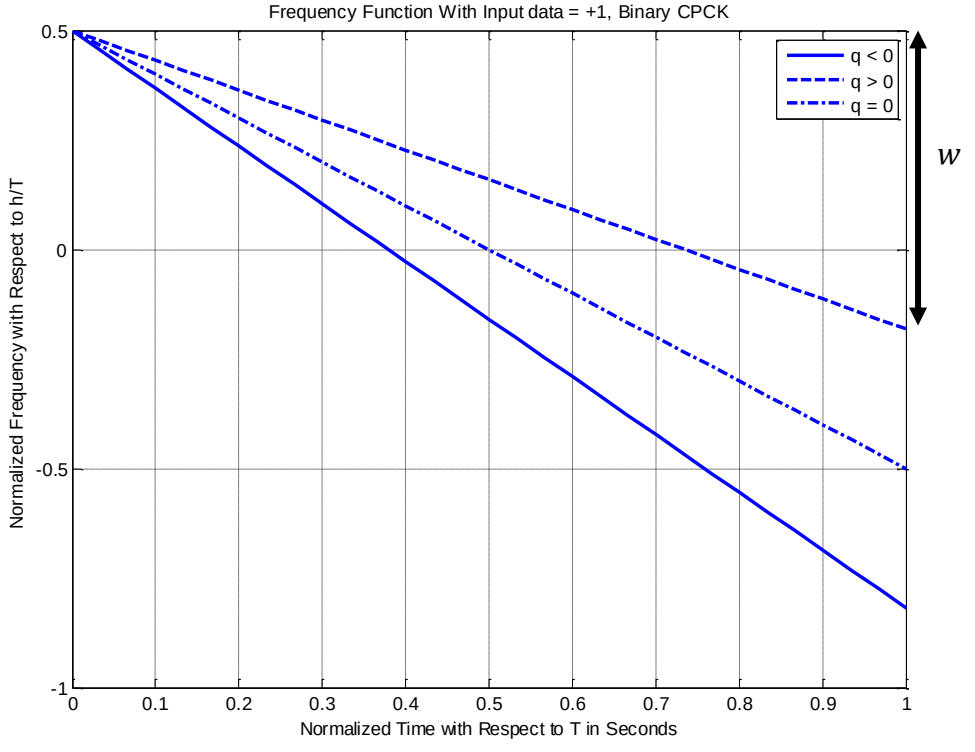

Figure 2.20: Instantaneous Frequency Deviation with Input Data +1

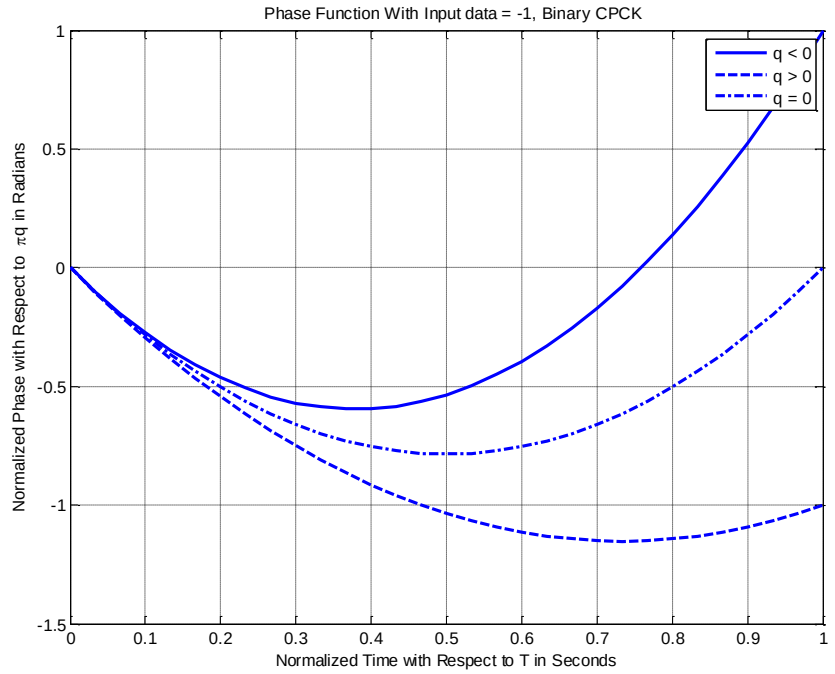

Figure 2.21: Phase Function with Input Data −1

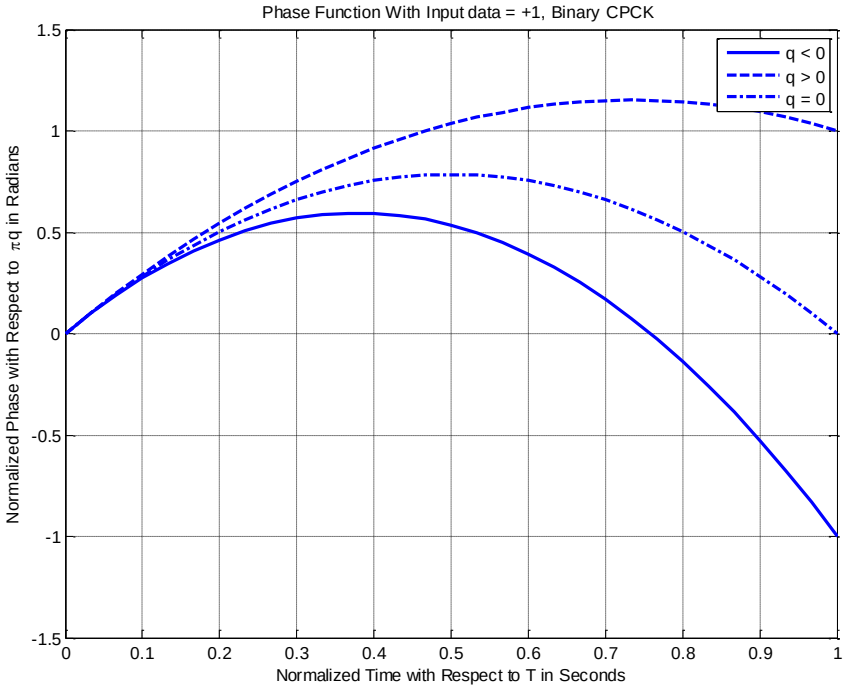

Figure 2.22: Phase Function with Input Data +1

Figures 2.19 and 2.20 show the frequency functions associated with data inputs −1 and +1, respectively. These graphs describe the behavior of the frequency during a bit

interval with a data input either -1 or $+1$. These Figures show that the frequency of the carrier signal varies linearly as a function of time, in response to the incoming data a_i, and hence, the corresponding phase of the signal varies in a nonlinear manner as shown in Figures 2.21 and 2.22.The Figures also show the effect of the parameter q, and it can be inferred from the graph that the value of q, which is in terms of the modulation index h and the frequency sweep width w, dictates the rate at which the frequency changes during a bit interval. Moreover, the different values of w associated with the different values of q can be found through

$$w = |f(t = 0) - f(t = T)|$$

Figures 2.19 and 2.20 indicate the way to find w graphically using the arrows on the side of the plots. Next, we plot the up-chirp, $a_i = -1$, and down-chip signals, $a_i = +1$, during one bit interval in Figures 2.23 and 2.24, respectively. It can be seen how the frequency changes during the i^{th} bit interval corresponding to the i^{th} data input.

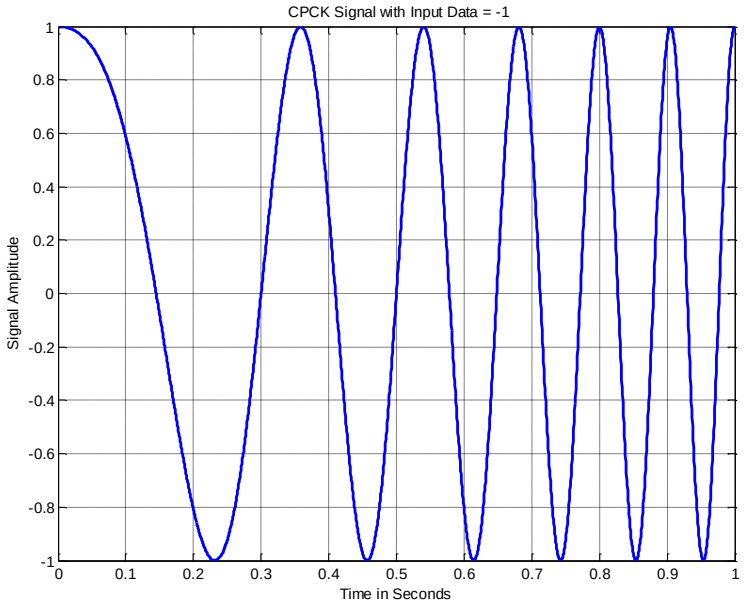

Figure 2.23: CPCK Signal with Input Data-1

In order to better understand CPCK signals, we provide the following plots. Figure 2.25 shows the phase state plot for 2-CPCK. Again, like in CPFSK, it can be inferred from the Figure that the transmitted sequence is [0 1 1 1 1 0 0], based on the curvature of phase

function within the bit interval. If it is concaved up, then the transmitted data bit is +1, otherwise it is a -1.

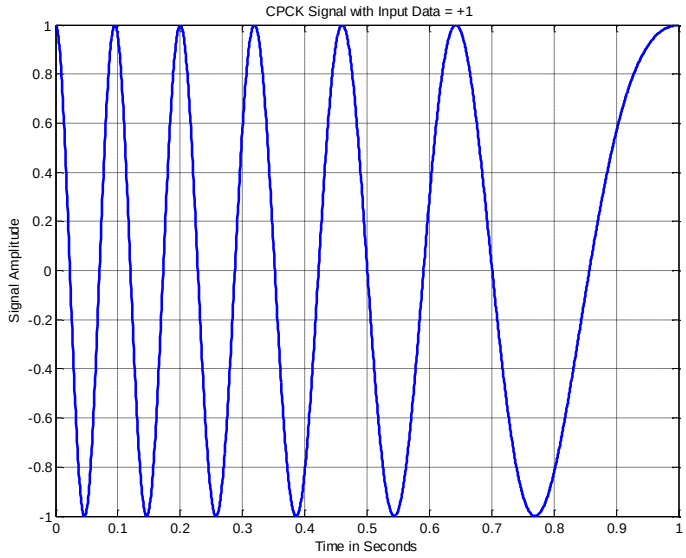

Figure 2.24: CPCK Signal with Input Data $+1$

Figure 2.26 shows the physical phase state, which is the observed phase. The jumps in the physical phase state are not discontinuities. They are the phase state but wrapped within the interval $[-\pi, \pi]$. Figures 2.25 and 2.26 amplitudes are the normalized phase with respect to πq.

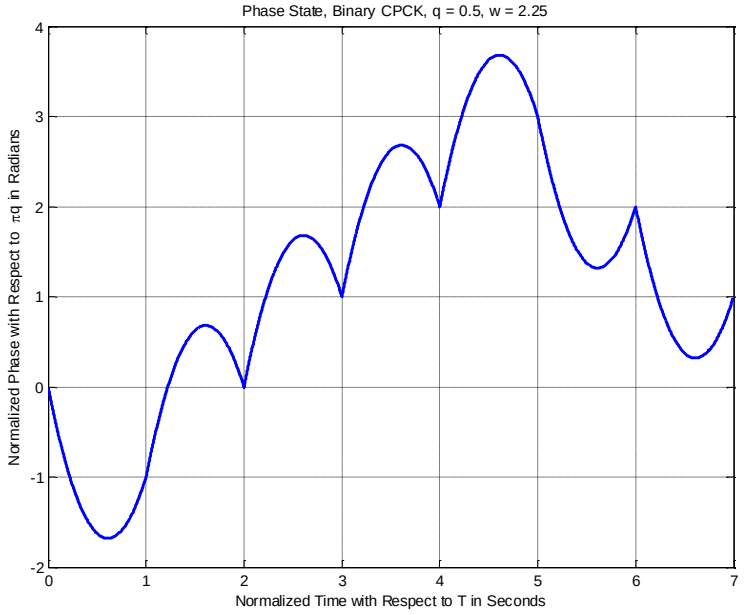

Figure 2.25: Phase State for CPCK

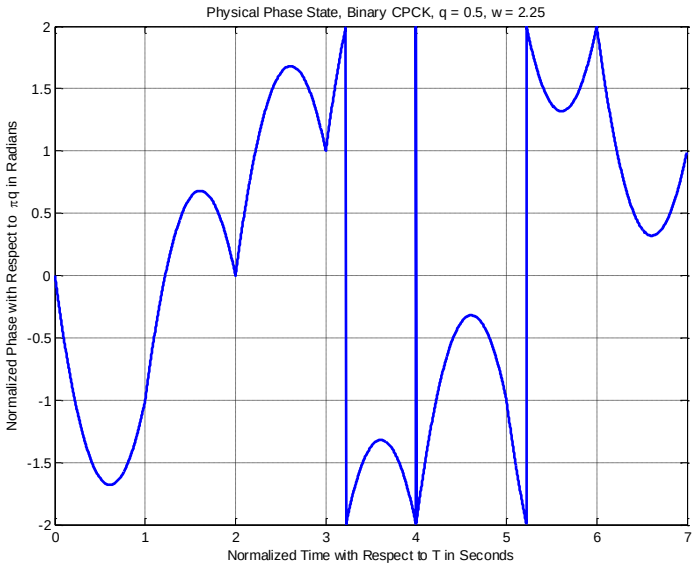

Figure 2.26: Physical Phase State for CPCK

Figure 2.27 shows the baseband CPCK signal for the input used in Figures 2.25 and 2.26. No discontinuities are present due to the inherent memory characteristics of CPM signals. Figure 2.28 shows the passband CPCK signal. It can be noticed how frequency changes based on the data input, decreasing with a +1 input and increasing with -1 input. Moreover, the frequency change is noticed to be linear starting at the beginning of each interval and keeps changing linearly till the end of the bit interval.

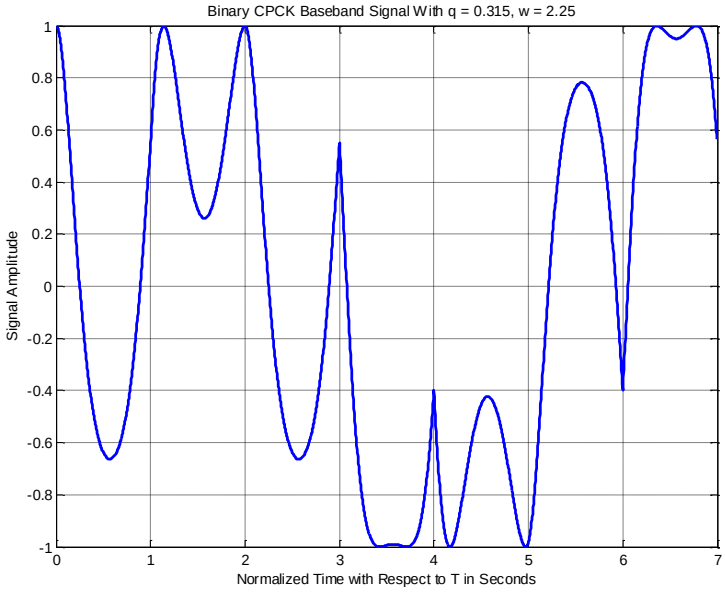

Figure 2.27: Binary CPCK Baseband Signal

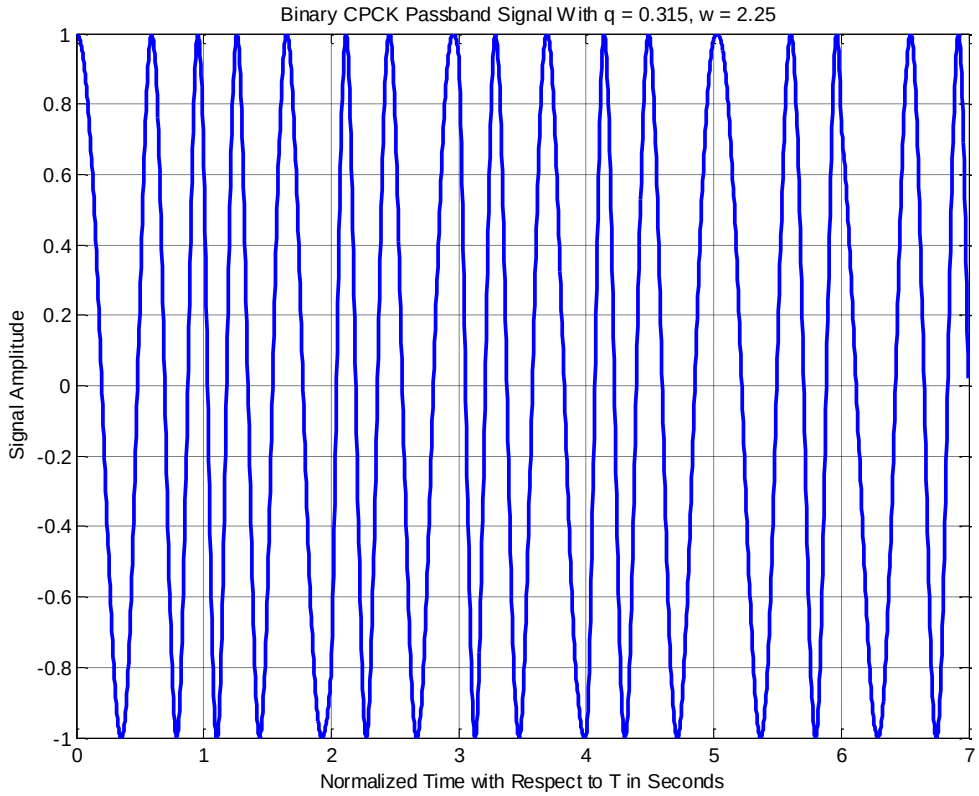

Figure 2.28: Binary CPCK Passband Signal

We demonstrate the difference between CPCK and CPFSK by comparing the passband signals for CPFSK and CPCK. During each time interval in CPFSK, the frequency changes to a different value based on the input data and is held constant. On the other hand, the frequency changes linearly in CPCK, either increasing or decreasing within one bit interval based on the input data. This indicates that the frequency changes in CPFSK are discontinuous, jumping from one level to the other, which can be inferred from Figures 2.8 and 2.9. On the other hand, in CPCK, the frequency is a linear continuous function, oscillating linearly between two frequency values.

Figures 2.29 shows the phase tree for 2-CPCK. The phase transitions shown in Figure 2.29 represent the true phase transitions at the time instants $t = iT$, $1 \leq i \leq n$.

Figure 2.30 shows the phase cylinder for the phase states shown in Figure 2.25. The path wrapped around the phase cylinder of Figure 2.30 is only one of the possible paths that go all over the general cylinder shown in Figure 2.5.

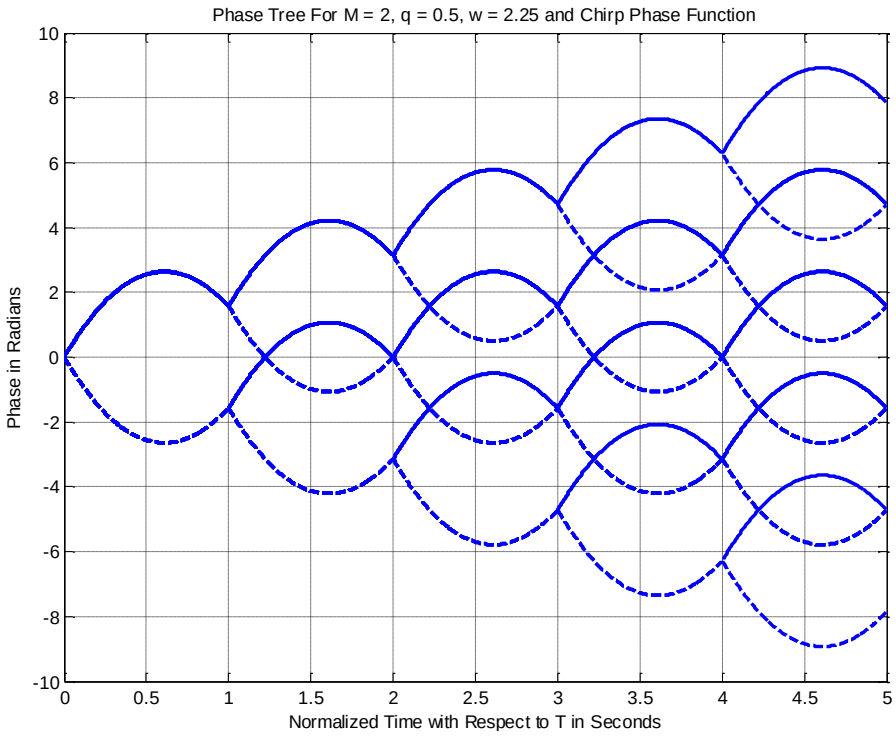

Figure 2.29: Phase Tree for CPCK

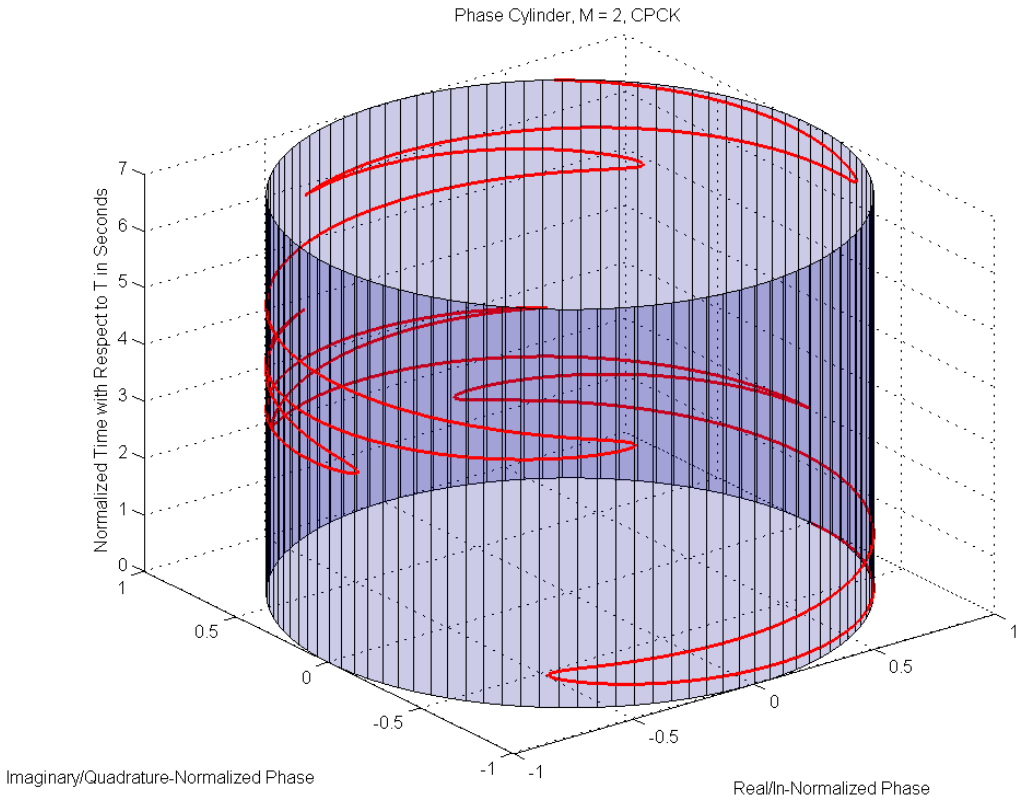

Figure 2.30: Phase Cylinder for CPCK

2.7 Summary

In this Chapter, we presented the concept, mathematical descriptions and properties of CPM signals. Moreover, we have laid the mathematical frame work required for the development of Continuous Phase Chirp Keying (CPCK) and Continuous Phase Frequency Shift Keying (CPFSK) signaling techniques, which will be used all through the thesis. It has been shown that the main difference between CPFSK and CPCK is in the way the frequency changes within the bit interval. This difference is attributed to properties associated with the different phase functions used. Figure 2.31 shows the combined phase tree for both CPFSK, in blue, and CPCK, in red. CPFSK can be considered as a special case of CPCK when the frequency sweep width, $w = 0$. MATLAB based graphs and Figures were provided for illustration purposes wherever possible.

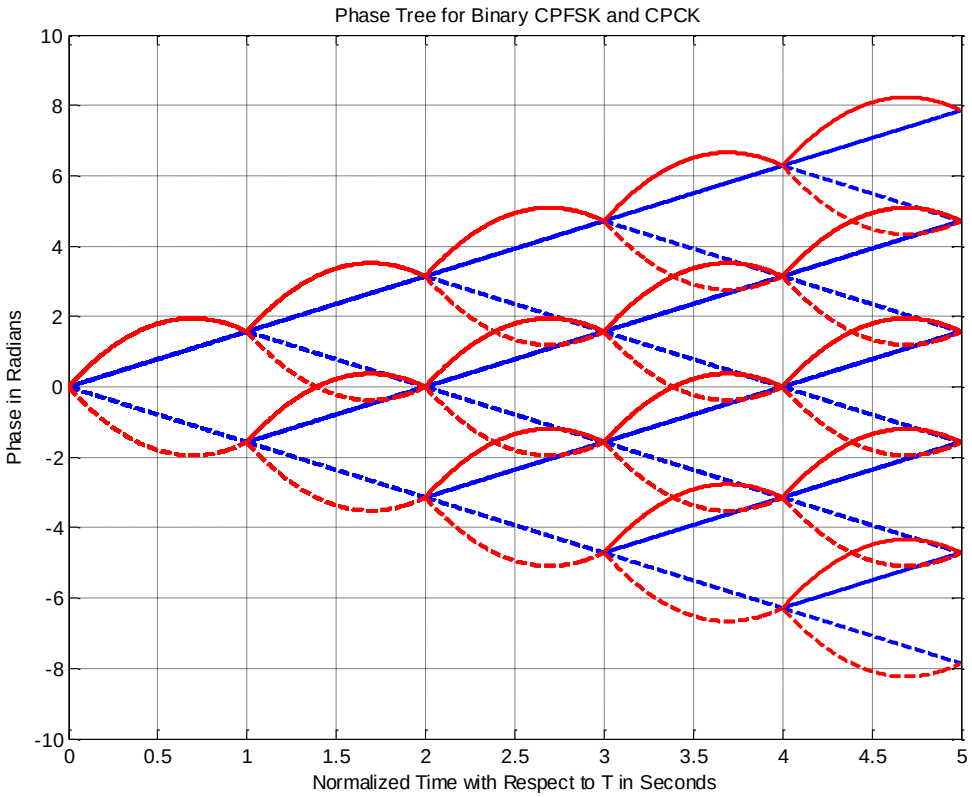

Figure 2.31: Phase Cylinder for CPCK

Chapter 3

Optimum and Sub-optimum Receivers for CPFSK and CPCK

When the signal has no memory, the general symbol-by-symbol detector, such as the ones employed for PSK, FSK, QPSK…etc., is optimum in the sense that it minimizes the probability of a symbol error. In contrast, for a transmitted signal that has memory, such as in CPM schemes, the optimum detector bases its decisions on observation of a *sequence* of received signals over successive signal intervals. There are mainly two types of receivers, based on the way the detection technique is applied, however; both of them are based on minimizing the probability of error using maximum-likelihood theory.

In this Chapter, we derive the structure of the optimum receiver for detection of CPM buried in AWGN.

The primary focus in this Chapter is to understand the relationship among modulation parameters, Signal-to-Noise Ratio (SNR) and number of observed symbols. The

relationship among those parameters are identified using extensive computer simulations. In the literature, receiver analyses are based on "high" and "low" SNR approximations, which gives rise to another major question, which is "What value of SNR that separates high-SNR from low-SNR when studying the effect of the different parameters on BER?" Moreover, we verify the results reported in the literature using simulation of the receivers. Also, we discuss the computational complexity involved in the analysis and simulation of the optimum receiver for CPFSK and CPCK.

First, we design a maximum a posteriori probability algorithm that makes decisions on the first symbol by observing the received waveform over n symbols. We then perform a detailed analysis to arrive at optimum and sub-optimum receivers for CPFSK and CPCK. Bounds on the performance of these receivers are then derived and illustrated for various CPFSK and CPCK signals.

We consider only the coherent case and it will be assumed that synchronization is established, i.e., that the carrier phase and the symbol timing are precisely known by the receiver. The channel is assumed to be an Additive White Gaussian Noise channel with one-sided power spectral density of N_0 $watts/Hz$.

3.1 Optimum Receiver using Bayesian MLRT

First, we start by developing the basic ideas of classical detection theory. The first step is a *Source* that generates an output. In the simplest case this output is one of two choices. We refer to them as hypotheses and label them H_1 and H_2 in the two-choice case referred to as binary decision-theory problem. More generally, the output might be one of M hypotheses, which we label H_1, H_2, . . . , H_M, and this type of problem is referred to as composite hypotheses problem. The basic components of a composite decision-theory problem are shown in Figure 3.1.

The second component of the problem is a *probabilistic transition mechanism*; the third is an observation space. The transition mechanism is considered as a device that knows which hypothesis is true. Based on this knowledge, it generates a point in the observation space according to some probability law.

In general, we confine our discussion to problems in which the observation space is finite-dimensional. In other words, the observations consist of a set of *N* numbers and can be represented as a point in an *N*-dimensional space. This class of problems is referred to as the *classical* decision problem.

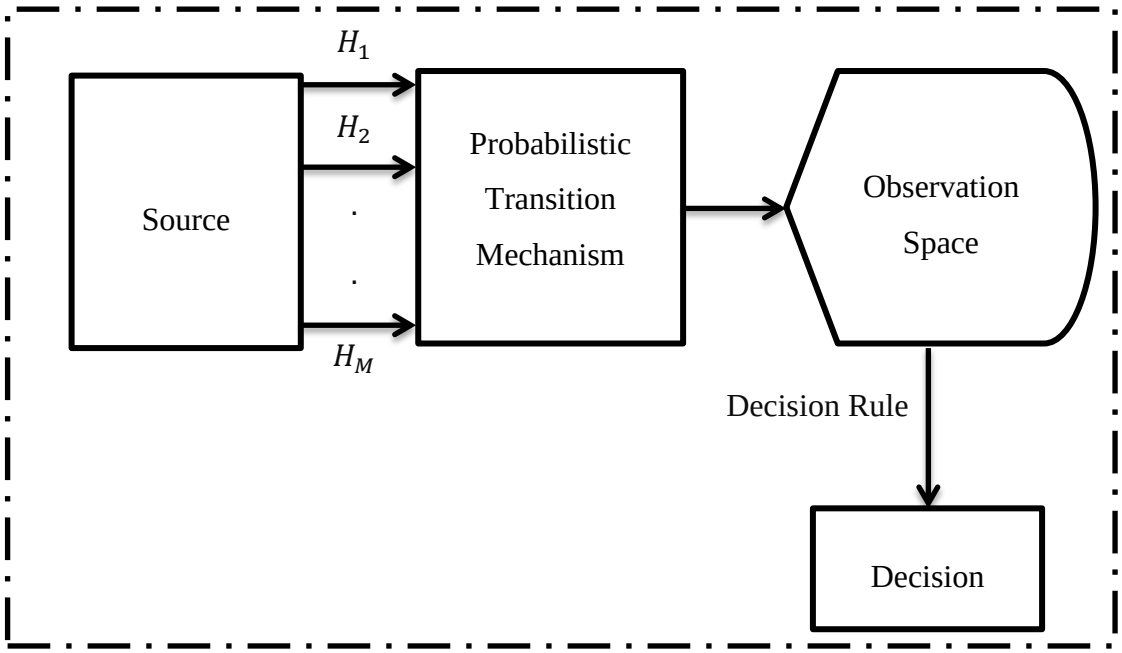

Figure 3.1 Components of a Decision Theory Problem

The fourth component of the detection problem is a *decision* rule. After observing the outcome in the observation space a guess is made on which hypothesis was true, and to accomplish this a decision rule that assigns each point to one of the hypotheses is developed.

As mentioned before, CPM signals have better bandwidth and energy performance due to the phase continuity constraint of CPM. Thus, obtaining this performance requires a multiple interval observation rather than the symbol-by-symbol decisions in memory-less modulation schemes.

The receivers in this section are quite general and apply to CPM schemes with any pulse shape and any modulation index, but we will specify them at the end of each section for CPFSK and CPCK schemes.

This receiver makes a decision about *one symbol only*, based on observation of a sequence of consecutive symbols. Once the decision is made, the receiver in principle starts from scratch again, processing the following symbol by sliding the observation interval. The received binary CPM signal during the i^{th} symbol is modeled as

$$r(t) = s(t, \boldsymbol{a}) + n(t) \tag{3.1}$$

where we use the notations from Chapter 2 for full response CPM

$$s(t, \boldsymbol{a}) = \sqrt{\frac{2E_b}{T}} \cos(2\pi f_c t + \phi(t, \boldsymbol{a}) + \phi_0), \quad t \geq 0, \tag{3.2}$$

where

$$\phi(t, \boldsymbol{a}) = \sum_{k=1}^{i} a_k g(t - kT), \qquad (i-1)T \leq t \leq iT, \tag{3.3}$$

ϕ_0 is the initial phase offset which is assumed to be zero for coherent detection without any loss of generality. In determining the optimum receiver structure for detecting symbol a_1, we shall use a shorthand notation developed in [10] for the received signal, so that Equation 3.1 becomes

$$r(t) = s(t, a_1, A_k) + n(t) \tag{3.4}$$

where a_1 is the first symbol, and A_k is the $(n-1)$-tuple $A_k = \{a_2, \dots, a_n\}$, where n is the observation interval. This is a classic composite-hypotheses probability theory problem in which the receiver chooses one hypothesis to be true. We have M^nhypotheses, where $M = 2$ for binary modulation case, under the source output of Figure 3.1, and they are all corrupted by noise.

The 2^n hypotheses are

$$H_{1,+1}: r(t) = s(t, a_1 = +1, A_1) + n(t)$$

$$H_{2,+1}: r(t) = s(t, a_1 = +1, A_2) + n(t)$$

.

.

$$H_{m,+1}: r(t) = s(t, a_1 = +1, A_m) + n(t)$$

$$H_{1,-1}: r(t) = s(t, a_1 = -1, A_1) + n(t)$$

$$H_{2,-1}: r(t) = s(t, a_1 = -1, A_2) + n(t)$$

.

.

$$H_{m,-1}: r(t) = s(t, a_1 = -1, A_m) + n(t) \quad (3.5)$$

where $m = 2^{n-1}$. Since we are only interested on making a decision on the first bit transmitted a_1, we assume full knowledge about which $A_j, j = 1,2, \dots, m$, has been transmitted. This reduces the previously stated composite hypotheses to a binary one of the following form

$$H_{+1}|A_j = H_1: r(t) = s(t, a_1 = +1, A_j) + n(t)$$

$$H_{-1}|A_j = H_2: r(t) = s(t, a_1 = -1, A_j) + n(t) \quad (3.6)$$

To establish the likelihood ratio test, we need the Probability Distribution Functions (PDF) for the previous hypotheses.

$$l = \frac{p(r(t)|H_1, A_j)}{p(r(t)|H_2, A_j)} \underset{-1}{\overset{+1}{\gtrless}} 1 \quad (3.7)$$

Usually, we decompose the signal in each hypothesis according to its basis functions set, however, we don't have a finite basis functions set that can perform such job. Therefore, we sample the output waveform each second and obtain N samples. Each noise sample is a zero-mean Gaussian random variable n with variance $\sigma^2 = N_o/2$. The noise samples at various instants are independent random variables and are independent of the source output. Thus, we have

$$H_1: r(zT_s) = s(zT_s, a_1 = +1, A_j) + n(zT_s)$$

$$H_2: r(zT_s) = s(zT_s, a_1 = -1, A_j) + n(zT_s) \quad (3.8)$$

where $1 \leq z \leq N$, and T_s is the sampling time. In order to simplify the notation, we drop the A_j, a_1 and T_s and the previous Equation becomes

$$H_1: r_z = s_{+1z} + n_z$$

$$H_2: r_z = s_{-1z} + n_z \quad (3.9)$$

In the case of AWGN, each sample point of r_i is a Gaussian random variable. Hence, each one of them will have a probability distribution function of the following form

$$p(r_z|H_1, A_j) = \frac{1}{\sqrt{2\pi\sigma^2}} \exp\left(\frac{-(r_z - E[r_z])^2}{2\sigma^2}\right)$$

$$p(r_z|H_2, A_j) = \frac{1}{\sqrt{2\pi\sigma^2}} \exp\left(\frac{-(r_z - E[r_z])^2}{2\sigma^2}\right) \quad (3.10)$$

where $E[r_z]$ is the expected value of the z^{th} Gaussian random sample, $\sigma^2 = N_o/2$.

$$p(r_z|H_1, A_j) = \frac{1}{\sqrt{2\pi\sigma^2}} \exp\left(\frac{-(r_z - s_{+1z})^2}{2\sigma^2}\right)$$

$$p(r_z|H_2, A_j) = \frac{1}{\sqrt{2\pi\sigma^2}} \exp\left(\frac{-(r_z - s_{-1z})^2}{2\sigma^2}\right) \quad (3.11)$$

Since we have N-such PDFs and they are all independent and uncorrelated, we can find the joint probability distribution function, which will approximate $p\big(r(t)\big|H_1, A_j\big)$ and $p\big(r(t)\big|H_2, A_j\big)$ as $N \to \infty$.

$$p\big(r(t)\big|H_1, A_j\big) = p\big(r_1\big|H_1, A_j\big) \times p\big(r_2\big|H_1, A_j\big) \times \ldots \times p\big(r_N\big|H_1, A_j\big)$$
$$= \prod_{z=1}^{N} p\big(r_z\big|H_1, A_j\big) = (2\pi\sigma^2)^{-N/2} \exp\left(\frac{-1}{2\sigma^2}\sum_{z=1}^{N}(r_z - s_{+1z})^2\right)$$

$$p\big(r(t)\big|H_2, A_j\big) = p\big(r_1\big|H_2, A_j\big) \times p\big(r_2\big|H_2, A_j\big) \times \ldots \times p\big(r_N\big|H_2, A_j\big)$$
$$= \prod_{z=1}^{N} p\big(r_z\big|H_2, A_j\big) = (2\pi\sigma^2)^{-\frac{N}{2}} \exp\left(\frac{-1}{2\sigma^2}\sum_{z=1}^{N}(r_z - s_{-1z})^2\right) \qquad (3.12)$$

After simplification, we get

$$l = \frac{\exp\left(\frac{-1}{N_o}\sum_{z=1}^{N}[r_z^2 - 2r_z s_{+1z} + s_{+1z}^2]\right) \overset{+1}{>} 1}{\exp\left(\frac{-1}{N_o}\sum_{z=1}^{N}[r_z^2 - 2r_z s_{-1z} + s_{-1z}^2]\right) \underset{-1}{<}} \qquad (3.13)$$

The true form of $r(t)$ is continuous, and we arrive at the original waveform as $N \to \infty$ in the time period of the observation which spans over n-bit time periods; $0 \to nT$.

$$\lim_{N\to\infty} l = \frac{\exp\left(\frac{-1}{N_o}\int_0^{nT}[r^2(t) - 2r(t)s_{+1}(t) + s_{+1}^2(t)]\,dt\right) \overset{+1}{>} 1}{\exp\left(\frac{-1}{N_o}\int_0^{nT}[r^2(t) - 2r(t)s_{-1}(t) + s_{-1}^2(t)]\,dt\right) \underset{-1}{<}} \qquad (3.14)$$

where

$$\int_0^{nT} s_{\pm 1}^2(t)dt = nE_b \qquad (3.15)$$

So finally, the Bayesian MLRT produces the following

$$\frac{\exp\left(\frac{2}{N_o}\int_0^{nT} r(t)s_{+1}(t)\,dt\right) \overset{+1}{>} 1}{\exp\left(\frac{2}{N_o}\int_0^{nT} r(t)s_{-1}(t)\,dt\right) \underset{-1}{<}} \qquad (3.16)$$

Additionally, we need to eliminate the factor of A_j, which is a random variable, by considering all possible sequences of A . This is performed mathematically by integrating over the PDF of A , $p(A)$. A is composed of $n-1$ binary random variables a_i such that

$$p(a_i) = \frac{1}{2}[\delta(a_i + 1) + \delta(a_i - 1)] \tag{3.17}$$

$p(a_i)$ is the density function of the i^{th} data bit, and the data are assumed to be independent. Hence, $p(A)$ is a joint probability of all $(n-1) - a_i s$, where $2 \le i \le n$

$$p(A) = p(a_2) \times p(a_3) \times \ldots \times p(a_n) = \prod_{i=2}^{n} p(a_i) \tag{3.18}$$

Thus,

$$\int_A p(A)dA = \int_{a_2} \int_{a_3} \ldots \int_{a_n} da_2 da_3 \ldots da_n \tag{3.19}$$

where the integral $\int_A dA$ is taken to mean the $n-1$ fold integral shown in the previous Equation. Going back to the MLRT Equation

$$l = \frac{\exp\left(\frac{2}{N_o}\int_0^{nT} r(t)s_{+1}(t)\,dt\right)}{\exp\left(\frac{2}{N_o}\int_0^{nT} r(t)s_{-1}(t)\,dt\right)} = \frac{\int_A \exp\left(\frac{2}{N_o}\int_0^{nT} r(t)s\,(t, a_1 = +1, A)\,dt\right)p(A)dA}{\int_A \exp\left(\frac{2}{N_o}\int_0^{nT} r(t)s\,(t, a_1 = -1, A)\,dt\right)p(A)dA} \tag{3.20}$$

Carrying out the integration, the MLRT becomes,

$$\frac{\exp\left(\frac{2}{N_o}\int_0^{nT} r(t)s\,(t, a_1 = +1, A_1)\,dt\right) + \cdots + \exp\left(\frac{2}{N_o}\int_0^{nT} r(t)s\,(t, a_1 = +1, A_m)\,dt\right)}{\exp\left(\frac{2}{N_o}\int_0^{nT} r(t)s\,(t, a_1 = -1, A_1)\,dt\right) + \cdots + \exp\left(\frac{2}{N_o}\int_0^{nT} r(t)s\,(t, a_1 = -1, A_m)\,dt\right)} \tag{3.21}$$

Using the MLRT, the receiver structure is defined in Figure 3.2, where

$$x_{\pm 1j} = \exp\left(\frac{2}{N_o}\int_0^{nT} r(t)s\left(t, a_1 = \pm 1, A_j\right)dt\right), \quad 1 \le j \le m \tag{3.22}$$

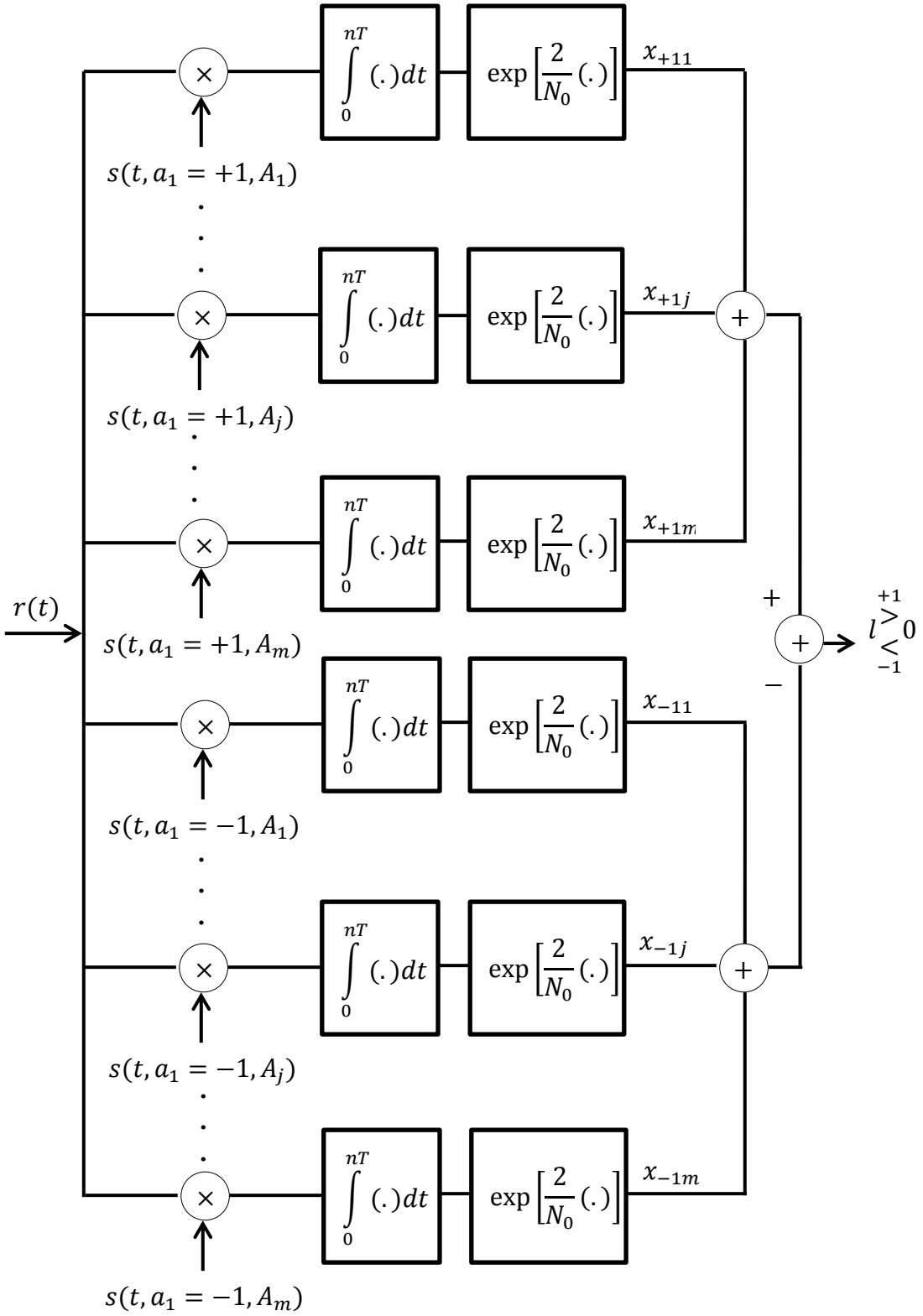

Figure 3.2: Block Diagram of Optimum Coherent Receiver

The receiver correlates the received waveform with each of the m possible transmitted signals beginning with data $+1$, then forms the sum of the $\exp(\frac{2}{N_o}c_j)$ where c_j is the correlation of the received waveform of the j^{th}. A similar operation of correlating and summing for the m possible signals with a data -1 is performed and the decision is based on the polarity of the difference of the two sums.

$x_{\pm 1j}$ is a log-normal random variable. When taking $[\ln(x_{\pm 1j})]$, we get the Gaussian random variable back. The performance of the optimum coherent receiver shown in Figure 3.2 with the log-normal variable is very complex to be mathematically analyzed. For Gaussian random variables, finding the joint probability distribution in order to determine the BER can be mathematically computed. However, in the CPM optimum receiver case, that joint probability distribution function passes through the exponential factor, which is considered as a transformation function, transforming the random variable and rendering it very complex to be analyzed and computationally exhaustive to find the joint probability distribution. Even simulating the optimum performance in MATLAB using the receiver structure in Figure 3.2 is not applicable. This is due to the problem that the generated Gaussian random variable never have the *exact* theoretical values of the mean and variance desired, and can have a difference from the theoretical value of up to the 10^{-2}. That is fine if the decision was to be based before the exponential stage. However, once it passes through the exponential block and transforms into a log-normal variable, a small difference of 10^{-2} grows exponentially to diverge the mean of the random variable from the desired theoretical value by a big margin, and it gets even worse for the variance.

Since the performance of the CPM optimum coherent receiver is very complex to be computed analytically, we resort to bounding the optimum performance by the performance of two sub-optimum receivers. One receiver performance is tight at high-SNR and the other is tight at low-SNR. Both receivers are used together to give a very reasonable and tight *bound* at all SNR values.

3.2 Average Matched Filter (AMF) Receiver

This receiver is based on approximating $x_{\pm 1j}$ at low values of E_b/N_0 as follows

$$x_{\pm 1j} \approx 1 + \frac{2}{N_0}\int_0^{nT} r(t)s\left(t, a_1 = \pm 1, A_j\right) dt \tag{3.23}$$

Using this Equation in the MLRT Equation,

$$l = \frac{\sum_{j=1}^{m} \exp\left(\frac{2}{N_o}\int_0^{nT} r(t)s\left(t, a_1 = +1, A_j\right) dt\right)}{\sum_{j=1}^{m} \exp\left(\frac{2}{N_o}\int_0^{nT} r(t)s\left(t, a_1 = -1, A_j\right) dt\right)} = \frac{\sum_{j=1}^{m} x_{+1j}}{\sum_{j=1}^{m} x_{-1j}} \underset{-1}{\overset{+1}{\gtrless}} 1 \tag{3.24}$$

the receiver becomes,

$$\int_0^{nT} r(t)\sum_{j=1}^{m} s\left(t, a_1 = +1, A_j\right) dt \underset{-1}{\overset{+1}{\gtrless}} \int_0^{nT} r(t)\sum_{j=1}^{m} s\left(t, a_1 = -1, A_j\right) dt$$

$$\int_0^{nT} r(t)\overline{s}(t, a_1 = +1)dt \underset{-1}{\overset{+1}{\gtrless}} \int_0^{nT} r(t)\overline{s}(t, a_1 = -1)dt$$

$$\int_0^{nT} r(t)[\overline{s}(t, a_1 = +1) - \overline{s}(t, a_1 = -1)]dt \underset{-1}{\overset{+1}{\gtrless}} 0$$

$$\Lambda \underset{-1}{\overset{+1}{\gtrless}} 0 \tag{3.25}$$

where

$$\overline{s}(t, a_1 = \pm 1) = \sum_{j=1}^{m} s\left(t, a_1 = \pm 1, A_j\right) \tag{3.26}$$

$$\Lambda = \int_0^{nT} r(t)[\overline{s}(t, a_1 = +1) - \overline{s}(t, a_1 = -1)]dt \tag{3.27}$$

It can be inferred from the previous Equation that this sub-optimum receiver, which gives the upper bound on BER at low-SNR, correlates the received waveform with the average waveform given data $+1$ and the average waveform given a data -1, and makes a

decision based on the largest of those correlations. Figure 3.3 shows the low-SNR receiver structure. Such a receiver is also referred to as the Average Matched Filter (AMF) Receiver.

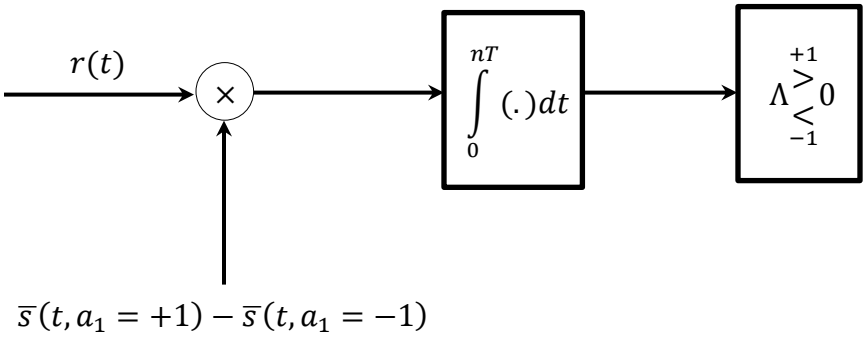

Figure 3.3: Block Diagram of Sub-Optimum Low-SNR Coherent Receiver

Λ is the decision variable for the low-SNR coherent receiver shown in Figure 3.3. Λ is a Gaussian random variable, and hence we only need the mean and variance to compute the probability of error. The mean of Λ will depend on the transmitted signal and therefore the probability of error depends on the transmitted sequence. We assume the sequence $s(t, a_1 = +1, A_j)$ has been transmitted. Λ can then be interpreted as follows:

$$\Lambda = E\left[\Lambda \middle| s(t, a_1 = +1, A_j)\right] + \sqrt{Var(\Lambda)}.N(0,1) \tag{3.28}$$

where $N(0,1)$ is a standard normally distributed random variable with zero-mean and unity-variance, and $E[.]$ denotes the expected value of the argument. The mean of Λ is given by

$$E\left[\Lambda \middle| s(t, a_1 = +1, A_j)\right] = \int_0^{nT} s(t, a_1 = +1, A_j).[\bar{s}(t, a_1 = +1) - \bar{s}(t, a_1 = -1)]dt \tag{3.29}$$

The variance of Λ is independent of a particular transmitted sequence and is given by,

$$Var(\Lambda) = E\left[\left(\Lambda - E\left[\Lambda | s(t, a_1 = +1, A_j)\right]\right)^2\right] \tag{3.30}$$

Equation 3.30 reduces to

$$Var(\Lambda) = \int_0^{nT} \int_0^{nT} n(t_1)n(t_2)[\overline{s}(t_1,+1) - \overline{s}(t_1,-1)][\overline{s}(t_2,+1) - \overline{s}(t_2,-1)]\, dt_1 dt_2 \tag{3.31}$$

We know that

$$\int_0^{nT} \int_0^{nT} n(t_1)n(t_2)\, dt_1 dt_2 = R(t_1 - t_2) = \frac{N_0}{2}\delta(t_1 - t_2) \tag{3.32}$$

is the auto correlation function for an Gaussian random variable with $N_0/2$ variance. And hence the integration will only exist if $t_1 - t_2 = 0$. Thus

$$Var(\Lambda) = \frac{N_0}{2} \int_0^{nT} [\overline{s}(t, a_1 = +1) - \overline{s}(t, a_1 = -1)]^2 dt \tag{3.33}$$

Therefore, the probability of error, given $s(t, a_1 = +1, A_j)$ has been transmitted, is

$$\Pr\left(\varepsilon \middle| s(t, a_1 = +1, A_j)\right) = Q\left[\frac{E\left[\Lambda \middle| s(t, a_1 = +1, A_j)\right]}{\sqrt{Var(\Lambda)}}\right] \tag{3.34}$$

where

$$Q(x) = \int_x^{\infty} \frac{1}{\sqrt{2\pi}} \exp\left(-\frac{\tau^2}{2}\right) d\tau \tag{3.35}$$

The probability of error is given by averaging over all the possible transmitted sequences,

$$P(\varepsilon) = \sum_{j=1}^{m} P\left(\varepsilon \middle| s(t, a_1 = +1, A_j)\right) P(A_j) = \frac{1}{m} \sum_{j=1}^{m} P\left(\varepsilon \middle| s(t, a_1 = +1, A_j)\right) \tag{3.36}$$

The mean and variance can be found based on the CPM scheme being used, and the probability of error is affected by the specific modulation parameters for each scheme and the number of bit-observations n. Eventually, after a certain n, the BER does not show any further improvements and that is set as the optimal observation interval. This is proved through computer simulations and studying the minimum distance criteria in

Chapter 4. Next we derive the BER associated with this sub-optimum receiver for both CPFSK and CPCK. It is important to note here that the CPM signal changes every i^{th} bit. Therefore, the mean and variance will be changing at each bit interval. The procedure for the following calculations is to compute the contribution to the mean and the variance of the i^{th} bit, one bit at a time, and sum over the n bits.

3.2.1 CPFSK Performance

In CPFSK signaling format, the mean and the variance for the AMF receiver can be shown to be

$$E\left[\Lambda\middle|s\left(t,a_1=+1,A_j\right)\right]=E_1+\sum_{i=2}^{n}E_i \tag{3.37}$$

where

$$E_1=E_b(1-\operatorname{sinc}(2h)) \tag{3.38}$$

$$E_i=E_b\sin(\pi h)\cos^{i-2}(\pi h)\left[\sin(\theta_i)+\frac{a_i}{2\pi h}.[\cos(\theta_i)-\cos(2\pi h a_i+\theta_i)]\right], \tag{3.39}$$

$$\theta_i=\pi h\sum_{k=1}^{i-1}a_k \tag{3.40}$$

$$Var(\Lambda)=E_bN_o\left[1-\operatorname{sinc}(2h)+\frac{(1-\cos(2\pi h))(1+\operatorname{sinc}(2h))(\cos^{2n-2}(\pi h)-1)}{2(\cos^2(\pi h)-1)}\right] \tag{3.41}$$

Next, we examine the effect of one variable on the BER while holding the other variables constant. Since Binary Phase Shift Keying (BPSK) is regarded to be the best binary modulation scheme, it is used as a benchmark for comparing BER performances in all the following studies. First, we investigate the effect of observation interval, n, on the BER.

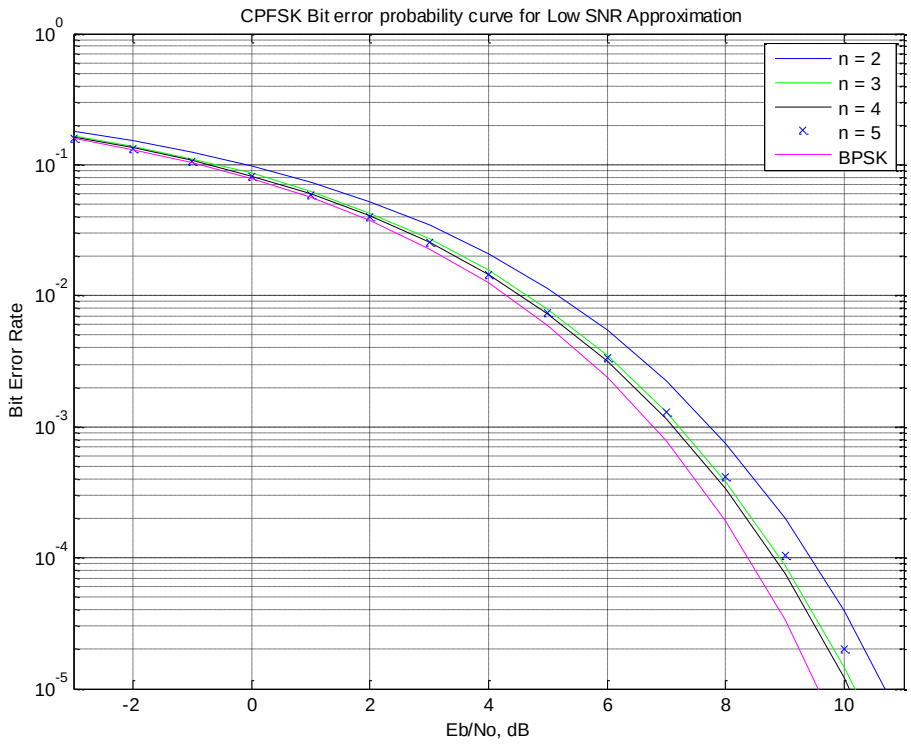

Figure 3.4: CPFSK AMF BER vs. SNR at Different n

Figure 3.4 shows how the AMF BER performance varies as n increases. We noticed that after n exceeds a certain value, different for different SNR values, the performance starts to slightly degrade before saturating at a certain level. Table 3.1 shows BER observations for $SNR = 0$ dB and $SNR = 6$ dB. This is elaborated in Figure 3.5. For low values of SNR, improvements in BER can be witnessed beyond $n = 3$; however, that is true up till a certain value of SNR, at which no matter what the SNR value is, the BER reaches its minimum value at $n = 3$, for that value of SNR.

Table 3.1: CPFSK BER Observations for $SNR = 0$ & 6 dB

n	$BER/SNR = 0$ dB	$BER/SNR = 6$ dB
2	9.769×10^{-2}	5.444×10^{-3}
3	8.584×10^{-2}	3.490×10^{-3}
4	8.225×10^{-2}	3.158×10^{-3}
5	8.145×10^{-2}	3.372×10^{-3}
6	8.137×10^{-2}	3.578×10^{-3}
7	8.143×10^{-2}	3.710×10^{-3}
8	8.150×10^{-2}	3.782×10^{-3}

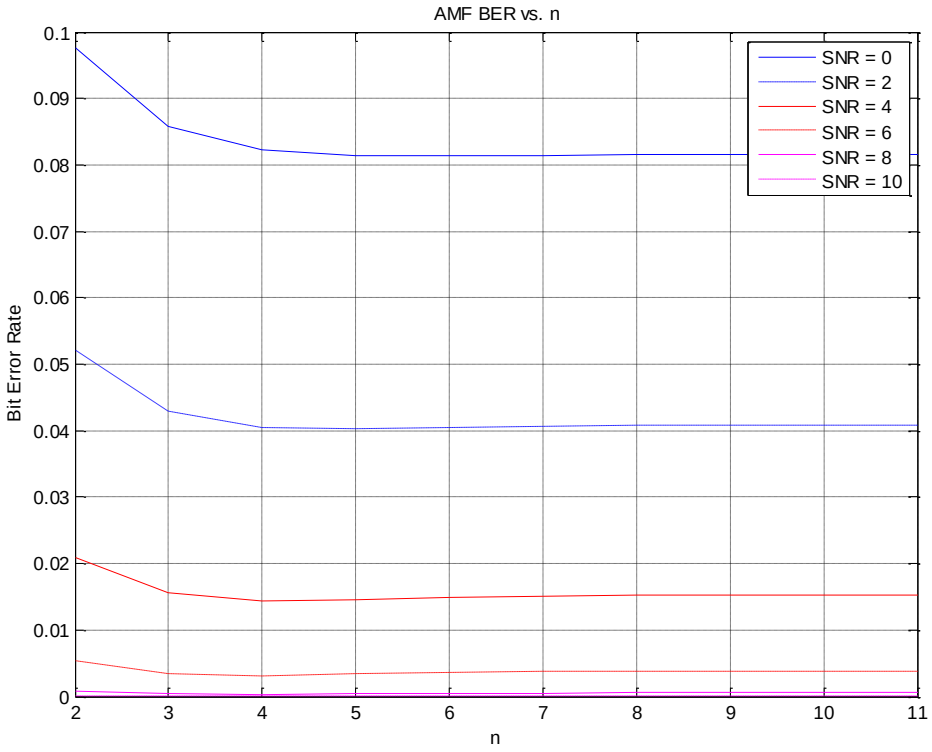

Figure 3.5: CPFSK AMF *BER* vs. *n*

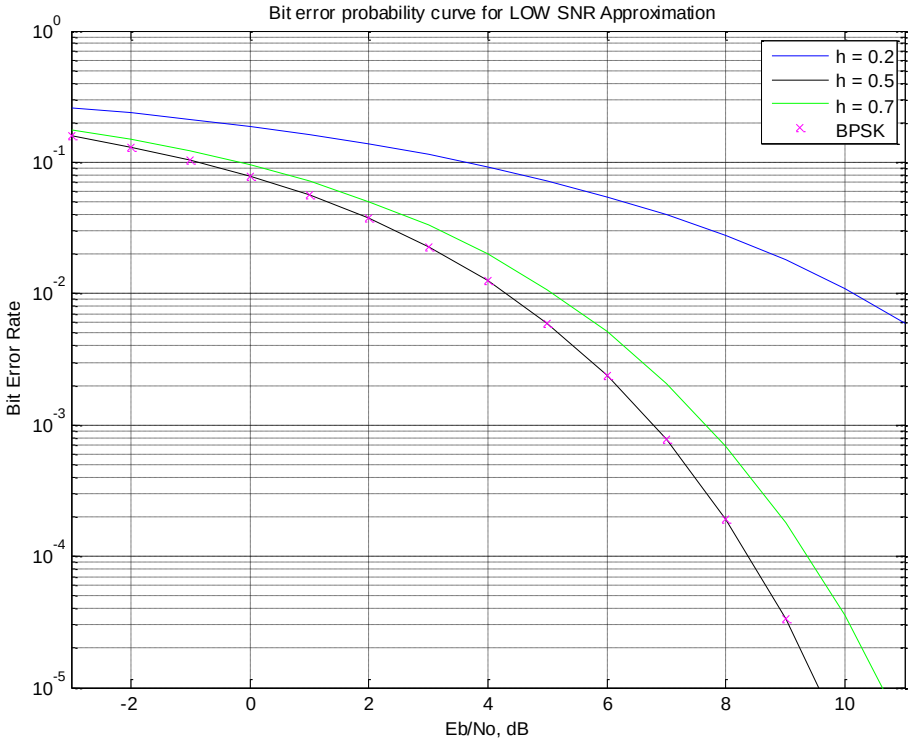

Figure 3.6: CPFSK AMF *BER* vs *SNR* for Different *h*

Figure 3.6 shows the effect of h, the modulation index, when set to different values. It shows that as h increases, CPFSK AMF receiver performance keeps on improving till it reaches the performance of BPSK (CPFSK; $h = 0.5$). Afterwards, the performance starts degrading again, which is shown in Figure 3.7 for different SNR. Moreover, to witness the effect of n on BER for different values of h, we plotted Figure 3.8. In Figures 3.7, 3.8 and 3.10, the BER is normalized by the minimum value of BER at all h.

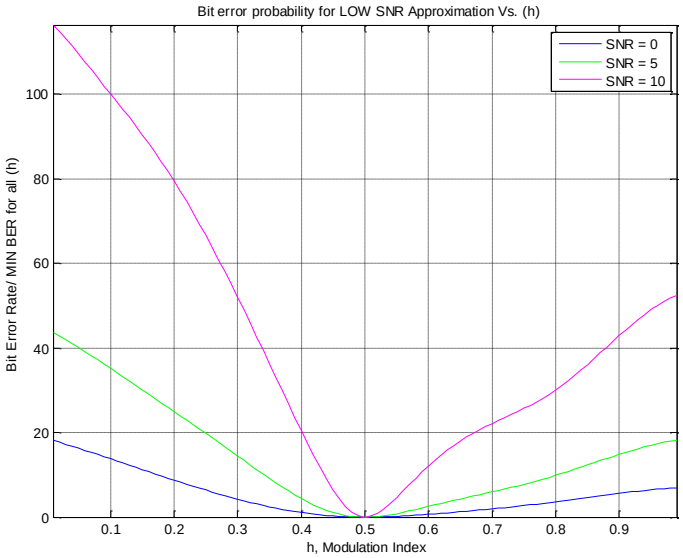

Figure 3.7: CPFSK AMF BER vs. h for Different SNR

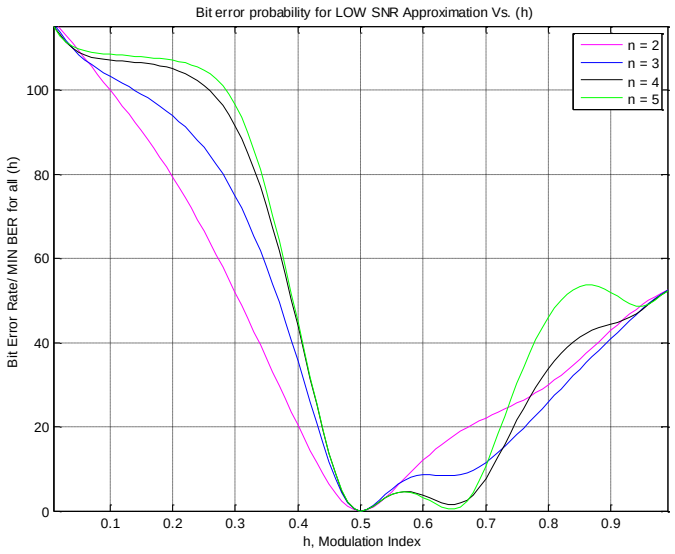

Figure 3.8: CPFSK AMF BER vs. h for Different n at $SNR = 6$ dB

Two main observations are concluded from Figure 3.8. The first is that for all n, the AMF BER for $h = 0.5$ is the same, which is equal to the BER performance of BPSK. In order to confirm this conclusion, we plot Figure 3.9, which shows the performance for CPFSK $h = 0.5$ for different n. Moreover, Figure 3.8 shows that as n increases, the next nearest BER performance to that of BPSK occurs at $h = 0.646$, and this is apparent at high-SNR values. The conclusion is backed with the plot in Figure 3.10.

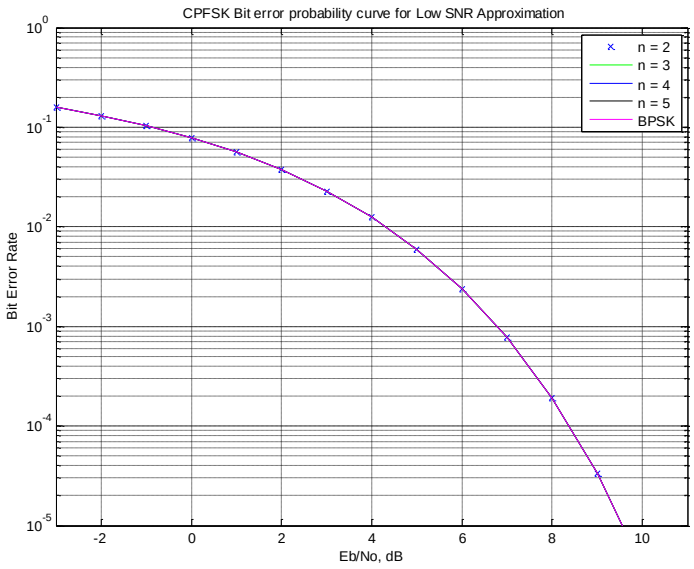

Figure 3.9: CPFSK AMF BER vs. SNR for Different n at $h = 0.5$

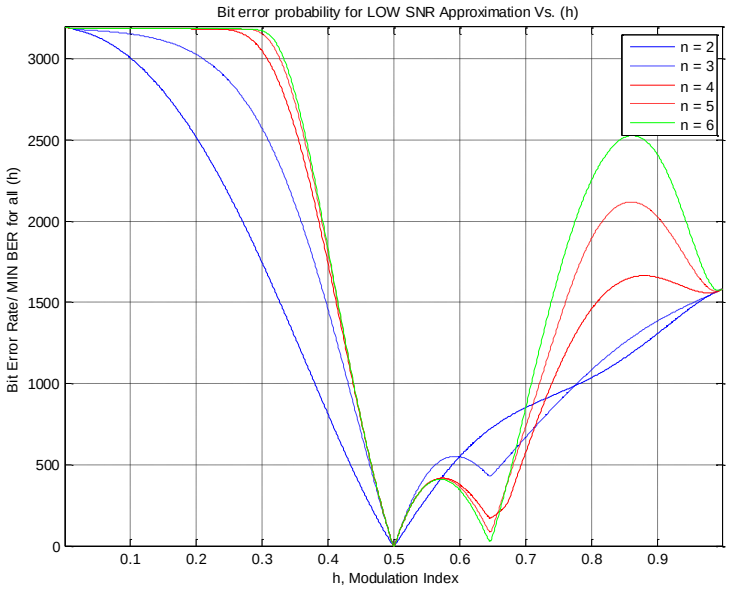

Figure 3.10: CPFSK AMF BER vs. h for Different n at $SNR = 12$ dB

Figure 3.10 serves as a guide when designing a system with bandwidth constraints, where for a certain n; receiver complexity, one can decide from Figure 3.10 the best value of h that accommodates the bandwidth in use and minimizes the BER. Next, we try to capture the combined effect of n and h on BER performance at certain values of SNR in 3D plots and contours graphs.

3D plots and contours will be further used in the thesis, so we will be providing a general description for how these graphs were plotted and how to interpret them. All these graphs are showing the BER performance vs. Different modulation parameters; n, h, q and w. Each graph is normalized by the $\min\{BER\}$ corresponding to that graph. The plotted BER is described by the following Equation

$$10\log_{10}\frac{BER}{\min\{BER\}}$$

Thus, wherever $\min\{BER\}$ exists in each of these graphs, it will be shown as a zero point on the vertical z-axis. The color-bar used in these 3D plots and contours is the following

The far left, dark blue, indicates 0, where the far right, dark red, indicated the highest value corresponding to that graph. The vertical axis in the 3D plots describes how much the BER at the corresponding coordinates is worse or greater than the $\min\{BER\}$. For example, if $10\log_{10}\frac{BER}{\min\{BER\}} = 5$, it means that all locations resulting in that BER value offers a loss of performance 5 times more relative to the $\min\{BER\}$, or the actual value at that location is 5 times the $\min\{BER\}$. Moreover, all points within a 3D or a contour plot that have the same color means that they all have the same value of BER.

Contours plots are actually a different way of viewing 3D plots, in which a 3D plot is viewed from its top. Each line with a different color within a contour plot describes *one* BER value and the axes show all the coordinates, or the different sets of modulation parameters, that result in that BER value. Any empty region in a contour plot that is surrounded by dark blue lines indicates the location of $\min\{BER\}$ corresponding to that contour and its 3D plot, where empty regions surrounded by dark red lines indicates the location of $\max\{BER\}$.The same plotting method is used throughout the thesis.

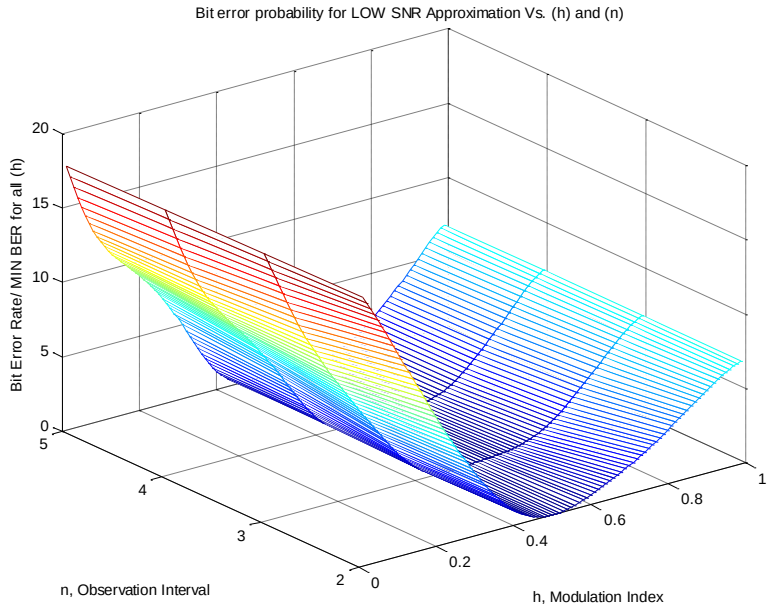

Figure 3.11: 3D Graph for CPFSK AMF BER vs. h and n, $SNR = 0$ dB

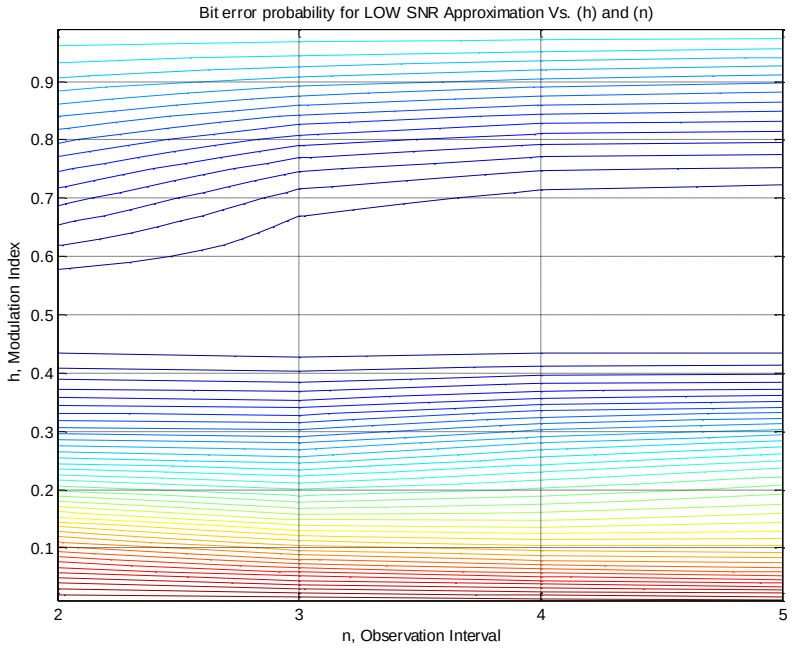

Figure 3.12: Contours of CPFSK AMF BER vs. h and n, $SNR = 0$ dB

The BER in Figures 3.11 and 3.12 are log-normalized with respect to the $min\{BER\}$, for all h, which occurs at $h = 0.5$, as concluded previously. The contours of Figure 3.12 are a cross-section in Figure 3.11 3D plot. All the lines with the same color represent one BER value. So the contours indicate that given a certain BER threshold at a certain SNR value, there are many combinations of h and n that give the same BER performance. The

empty space in the middle of Figure 3.12 complies with the results from Figure 3.8, regarding the$min\{BER\}$ occurrence at $h = 0.5$. The blue lines around $h = 0.5$, has the next $min\{BER\}$ value to that provided by $h = 0.5$. We have produced similar Figures for higher values of SNR in Figures 3.13 and 3.14.

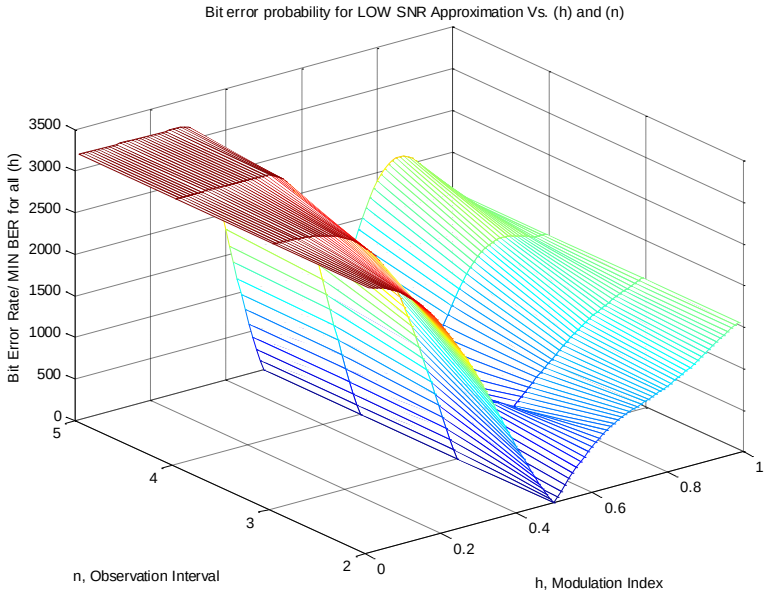

Figure 3.13: 3D Graph for CPFSK AMF BER vs. h and n, $SNR = 12$ dB

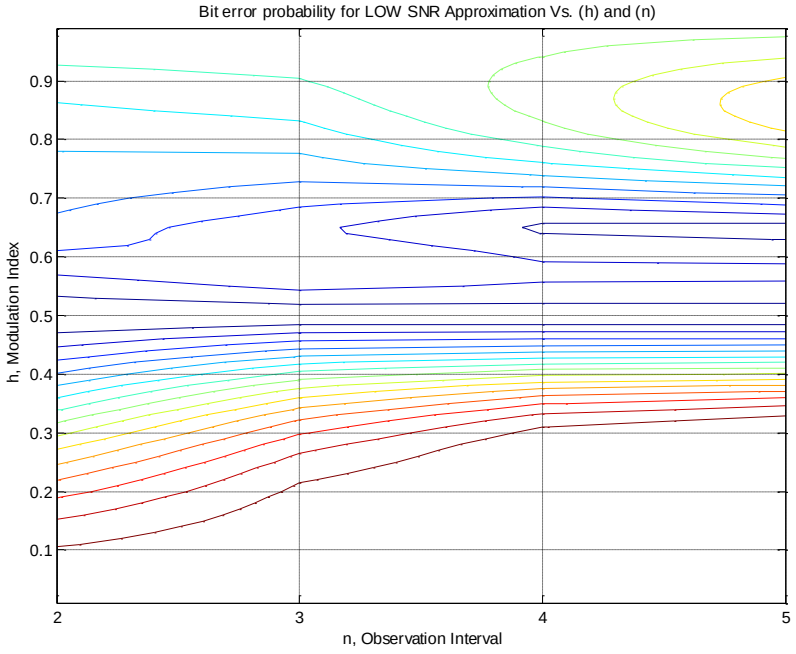

Figure 3.14: Contours of CPFSK AMF BER vs. h and n, $SNR = 12$ dB

3.2.2 CPCK Performance

In CPCK signaling format, the mean and the variance for the AMF receiver can be shown to be

$$E\left[\Lambda\middle|s\left(t,a_1=+1,A_j\right)\right]=\int_0^{nT} s\left(t,a_1=+1,A_j\right)[\bar{s}(t,a_1=+1)-\bar{s}(t,a_1=-1)]dt$$

$$=\sum_{u=1}^{m}\sum_{i=1}^{n}\int_{(i-1)T}^{iT} s_i\left(t,+1,A_j\right)[s_i(t,+1,A_u)-s_i(t,-1,A_u)]dt \qquad (3.42)$$

where

$$s_k(t,\pm1,A_z)=\begin{cases} s\,(t,\pm1,A_z), & (i-1)T\le t\le iT \\ 0\quad\ , & Otherwise \end{cases} \qquad (3.43)$$

Using the following complex envelope notation,

$$\int s_1(t)s_2(t)dt=\frac{1}{2}Re\int u_1(t)u_2^*(t)dt \qquad (3.44)$$

$E\left[\Lambda\middle|s\left(t,a_1=+1,A_j\right)\right]$ can be expressed as

$$\sum_{u=1}^{m}\sum_{i=1}^{n}\left[\frac{E_b}{T}\int_0^T\cos\left(\Delta\beta_i(t,j,u)\right)dt-\frac{E_b}{T}\int_0^T\cos\left(\Delta\phi_i(t,j,u)\right)dt\right] \qquad (3.45)$$

where

$$\Delta\phi_i(t,j,u)=\left(a_{ji}-a_{ui}\right)g(t)+\pi q\sum_{k=1}^{i-1}\left(a_{jk}-a_{uk}\right) \qquad (3.46)$$

$$\Delta\beta_i(t,j,u)=\begin{cases} 0\quad\ , & i=1 \\ \Delta\phi_i(t,j,u)-2\pi q, & i=2,\dots,n \end{cases} \qquad (3.47)$$

$\Delta\phi_i(t,j,u)$ and $\Delta\beta_i(t,j,u)$ describe the phase difference between the signals $s\left(t,+1,A_j\right)$ and $s(t,-1,A_u)$ during the i^{th} bit interval with the data difference term (i.e., difference

between sequences $\{a_1 = +1, A_j\}$ and $\{a_1 = -1, A_u\}$ during the i^{th}bit interval) is given by

$$a_{ji} - a_{ui} = \begin{cases} 0, & a_{ji} = a_{ui} \\ \pm 2, & a_{ji} = -a_{ui} = \pm 1 \end{cases} \tag{3.48}$$

Similarly, assuming that $s(t, -1, A_z)$ was sent, it can be shown that

$$E[\Lambda | s(t, a_1 = -1, A_z)] = -E\big[\Lambda \big| s\big(t, a_1 = +1, A_j\big)\big], \qquad z = m - 1 - j \tag{3.49}$$

The variance is given by

$$Var(\Lambda) = \frac{N_o}{2} \int_0^{nT} [\bar{s}(t, +1) - \bar{s}(t, -1)]^2 dt$$

$$= \frac{N_o}{2} [\sum_{j=1}^{m} \int_0^{nT} s\big(t, +1, A_j\big). [\bar{s}(t, +1) - \bar{s}(t, -1)]\, dt]$$

$$- \sum_{r=1}^{m} \int_0^{nT} s(t, -1, A_r). [\bar{s}(t, +1) - \bar{s}(t, -1)]\, dt$$

$$= \frac{N_o}{2} \left[\sum_{j=1}^{m} E\big[\Lambda \big| s\big(t, a_1 = +1, A_j\big)\big] - \sum_{z=1}^{m} E[\Lambda | s(t, a_1 = -1, A_z)] \right]$$

$$= N_o \left[\sum_{j=1}^{m} E\big[\Lambda \big| s\big(t, a_1 = +1, A_j\big)\big] \right] \tag{3.50}$$

Since there are more modulation parameters in CPCK than that of CPFSK, it is better to analyze the system directly in 3D. Figures 3.15, 3.17 and 3.19 show the log 3D plots for CPCK AMF receiver performance vs. q and w at $SNR = 6$ dB for different values of n. The performance reported by these Figures is normalized by the min$\{BER\}$ for all q and w. Using computer search, it was found that $min\{BER\}$ occurs at $q = 0.5$ and $q = 1.5$ independent of both parameters, w and n, and the minimum value is equal to that of BPSK at $SNR = 6$ dB. After trying for several SNR values, it was concluded that BPSK performance can be achieved using CPCK AMF receiver with only setting $q = 0.5$ or

$q = 1.5$. Figures 3.16, 3.18 and 3.20 show the contours corresponding to the 3D plots reported in Figures 3.15, 3.17 and 3.19. Supporting the previous conclusion, empty regions can be seen around $q = 0.5$ and $q = 1.5$ irrespective of n, w and SNR value.

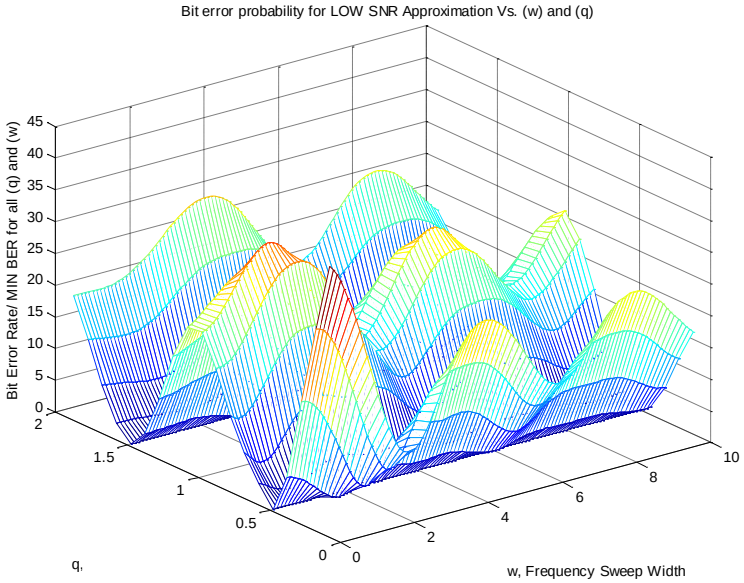

$min\{BER\} = 2.388 \times 10^{-3}$ at $q = 0.5$ and $q = 1.5$

Figure 3.15: 3D Graph for CPCK AMF BER vs. q and w, $SNR = 6$ dB, $n = 2$

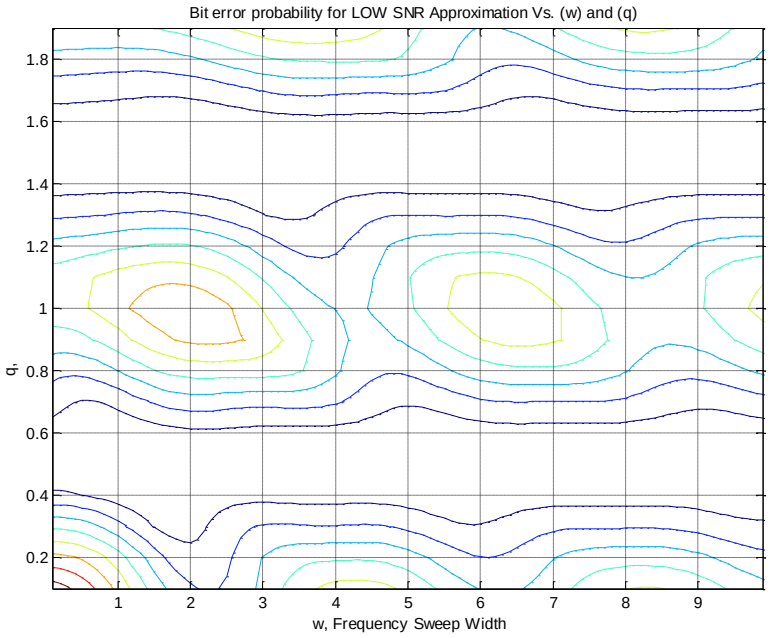

$min\{BER\} = 2.388 \times 10^{-3}$ at $q = 0.5$ and $q = 1.5$

Figure 3.16: Contours of CPCK AMF BER vs. q and w, $SNR = 6$ dB, $n = 2$

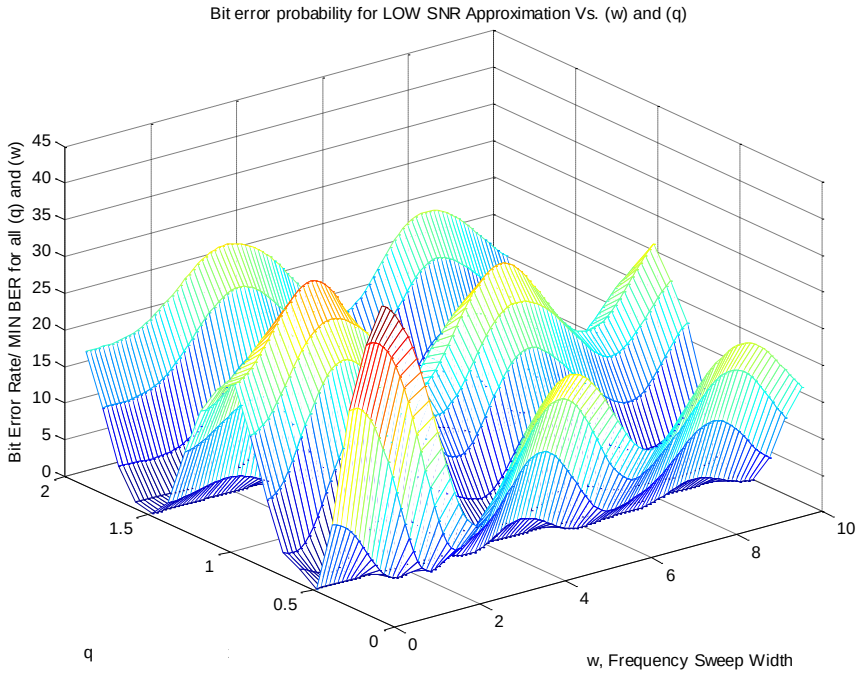

$min\{BER\} = 2.388 \times 10^{-3}$ at $q = 0.5$ and $q = 1.5$

Figure 3.17: 3D Graph for CPCK AMF BER vs. q and w, $SNR = 6$ dB, $n = 3$

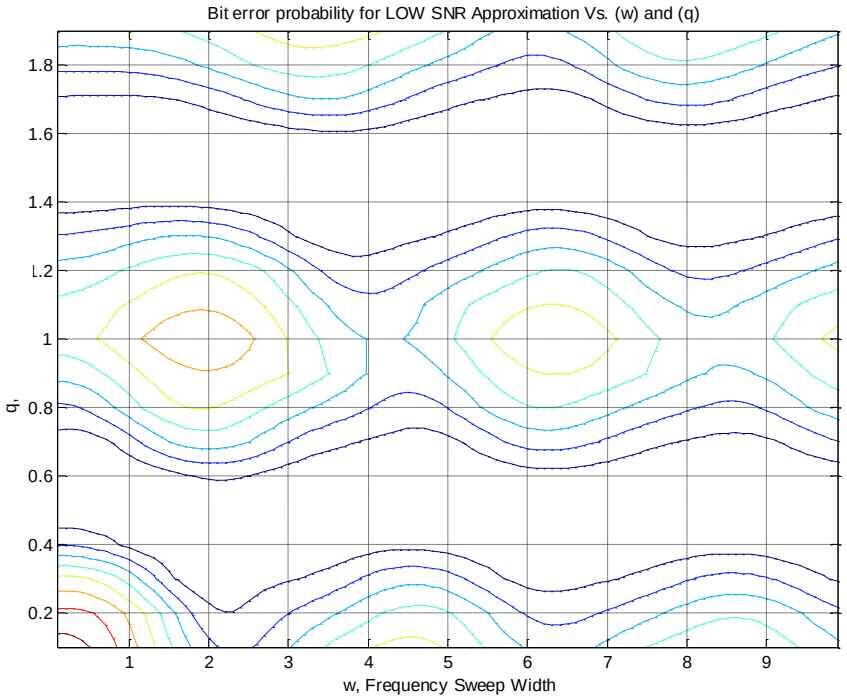

$min\{BER\} = 2.388 \times 10^{-3}$ at $q = 0.5$ and $q = 1.5$

Figure 3.18: Contours of CPCK AMF BER vs. q and w, $SNR = 6$ dB, $n = 3$

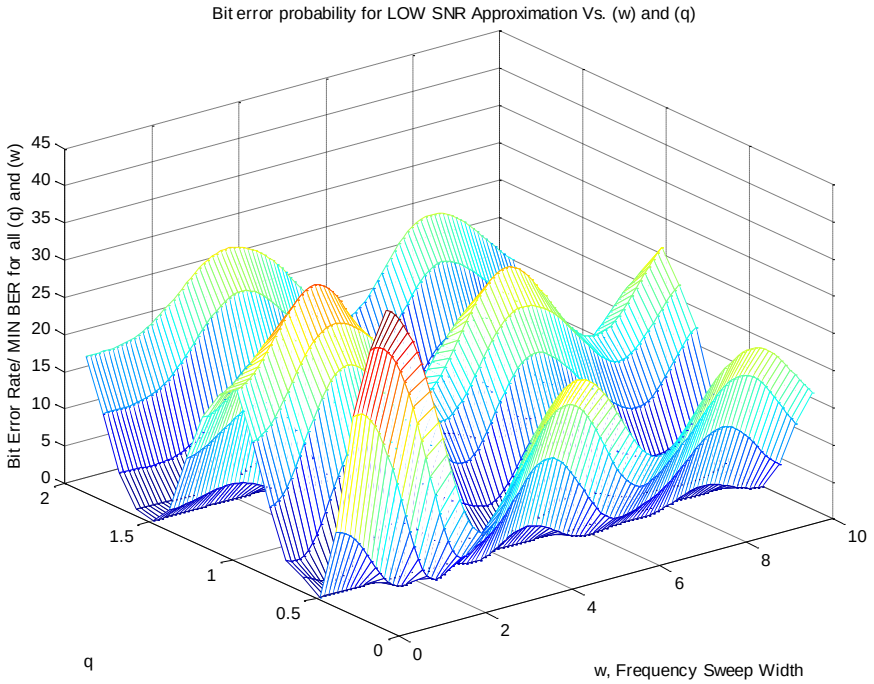

$min\{BER\} = 2.388 \times 10^{-3}$ at $q = 0.5$ and $q = 1.5$

Figure 3.19: 3D Graph for CPCK AMF BER vs. q and w, $SNR = 6$ dB, $n = 4$

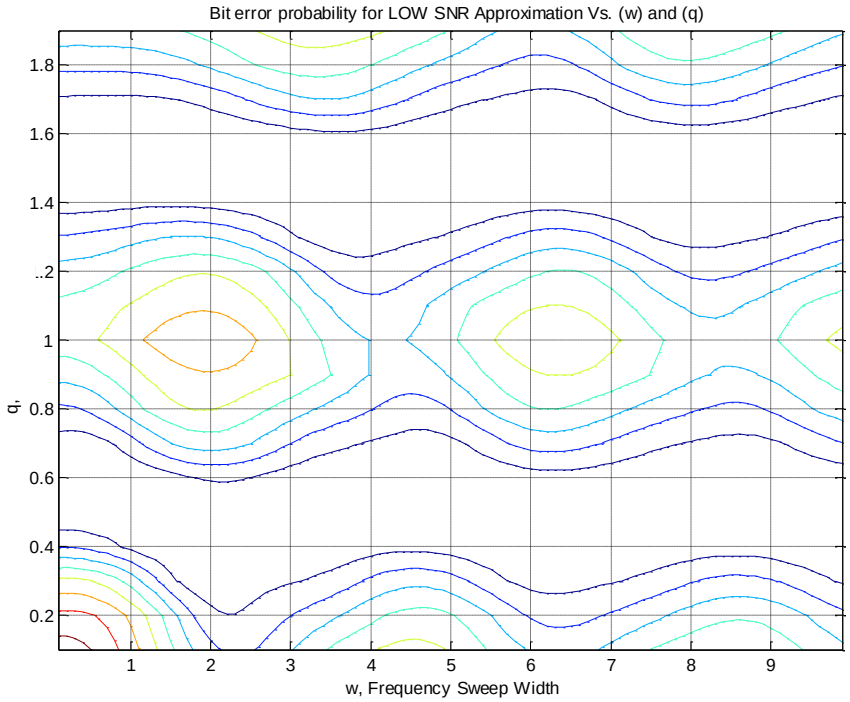

$min\{BER\} = 2.388 \times 10^{-3}$ at $q = 0.5$ and $q = 1.5$

Figure 3.20: Contours of CPCK AMF BER vs. q and w, $SNR = 6$ dB, $n = 3$

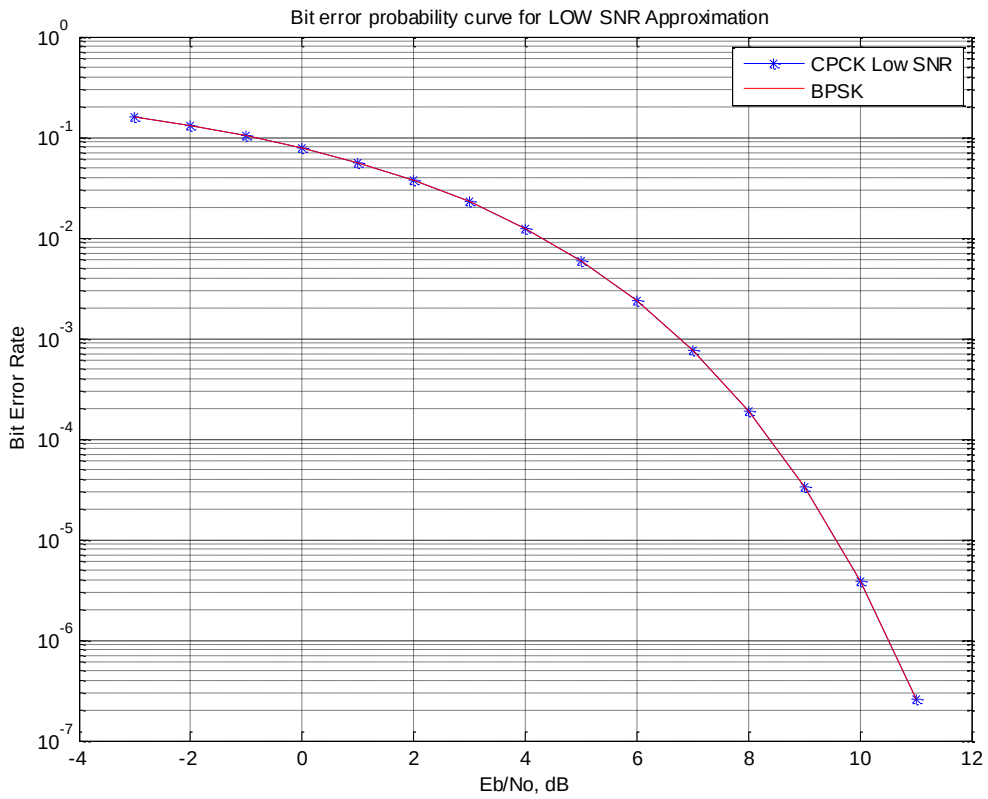

Figure 3.21: CPCK AMF BER vs. SNR, for $q = 0.5$ or 1.5. Any Value for n and w

Figure 3.21 shows the BER performance for $q = 0.5$ or $q = 1.5$, which matches BPSK performance for all n and w. The q values yielding BPSK performance were found by searching the region $0 \leq q \leq 2$. Other values for q can exist outside these boundaries.

3.3 High-SNR Receivers

Two sub-optimum receivers are produced using high-SNR approximation, and both will be used in conjunction with the AMF receiver from the previous section in producing a tight bound on the BER performance of the optimal receiver. This receiver is based on approximating $x_{\pm 1j}$ at high values of E_b/N_0 as follows

$$\sum_{j=1}^{m} x_{\pm 1j} \cong \tilde{x}_{\pm 1} \tag{3.51}$$

where

$$\tilde{x}_{\pm 1} = \max\{x_{\pm 1j}; j = 1, \dots, m\} \tag{3.52}$$

will yield a sub-optimum decision rule which closely approximates the optimum decision rule of the optimum receiver of Figure 3.2. Since the function $\exp(.)$ is monotonic, $\tilde{x}_{\pm 1}$ is an equivalent test parameter suggesting that the corresponding sub-optimum receiver should compute all $x_{\pm 1j}$ and produce a decision depending on the largest of these. This will be used in conjunction with the other The sub-optimum receiver's decision rule is therefore given by

$$l = \frac{\max\{x_{+1j}; j = 1, \dots, m\}}{\max\{x_{-1j}; j = 1, \dots, m\}} \underset{-1}{\overset{+1}{\gtrless}} 1 \tag{3.53}$$

Assuming that $s(t, a_1 = +1, A_j)$ has been transmitted, then the conditional probability of error is given by

$$P\left(\varepsilon \middle| s(t, a_1 = +1, A_j)\right)$$
$$= \Pr\left[\left(x_{+1j} \le x_{-11}\right) \cup \left(x_{+1j} \le x_{-12}\right) \cup \dots \cup \left(x_{+1j} \le x_{-1m}\right) \middle| s(t, a_1 = +1, A_j)\right] \tag{3.54}$$

Using the union bound, the conditional probability of bit error can be written as,

$$P\left(\varepsilon \middle| s(t, a_1 = +1, A_j)\right) \le \sum_{u=1}^{m} \Pr\left[\left(x_{+1j} \le x_{-1u}\right) \middle| s(t, a_1 = +1, A_j)\right] \tag{3.55}$$

where we have used the inequality

$$P(A + B + C) \le P(A) + P(B) + P(C) \tag{3.56}$$

The *upper* bound $\tilde{P}(\varepsilon)$ on the error rate of the optimum coherent receiver $P(\varepsilon)$ is then given by

$$P(\varepsilon) \le \tilde{P}(\varepsilon) = \frac{1}{m} \sum_{j=1}^{m} \sum_{u=1}^{m} Q\left[\sqrt{\frac{E_b}{N_o} D_n^2(j, u)}\right] \tag{3.57}$$

where $D_n^2(j, u)$ is the normalized distance squared between the signals $s(t, a_1 = +1, A_j)$ and $s(t, a_1 = -1, A_u)$, given by,

$$D_n^2(j,u) = \frac{1}{2E_b}\int_0^{nT} \left|s\left(t, a_1 = +1, A_j\right) - s(t, a_1 = -1, A_u)\right|^2 dt = n - n\rho(j,u) \quad (3.58)$$

where

$$\rho(j,u) = \frac{1}{nE_b}\int_0^{nT} s\left(t, a_1 = +1, A_j\right) s(t, a_1 = -1, A_u) dt \quad (3.59)$$

For large SNR, the error rate is mainly determined by the minimum of all distance-squared values,

$$D_n^2 = \min\{ D_n^2(j,u); j,u = 1, \dots, m\} \quad (3.60)$$

It is possible, therefore, to compare different coherent systems (at high-SNR) by simply comparing their respective minimum distances. Using PSK (${D_1}^2 = 2$) as a benchmark, an estimate of the SNR gain (in decibels) relative to PSK is then obtained from

$$G_n = 10 \log_{10}\left(\frac{{D_n}^2}{2}\right) \quad (3.61)$$

We will carry out a study of the minimum distance properties of CPM signals in Chapter 4. It is useful to construct a lower bound on the performance of the coherent CPM receiver in order to test the tightness of the upper bound introduced above. The lower bound is obtained by supposing that for each transmitted sequence, the receiver needs only to decide between that sequence and its nearest neighbor. This receiver will perform *at least* as well as the receiver which does not know which of two sequences. The performance of this receiver is a lower bound to the performance of the optimum CPM receiver presented in section 3.1. This lower bound on the probability of error can be written as

$$P(\varepsilon) \geq \tilde{P}_l(\varepsilon) = \frac{1}{m}\sum_{j=1}^{m} Q\left[\sqrt{\frac{E_b}{N_o} D_n^2}\right] \quad (3.62)$$

$$D_n^2 = \min\{ D_n^2(j,u); u = 1, \dots, m\} \quad (3.63)$$

Figure 3.23 shows the high-SNR approximation receiver.

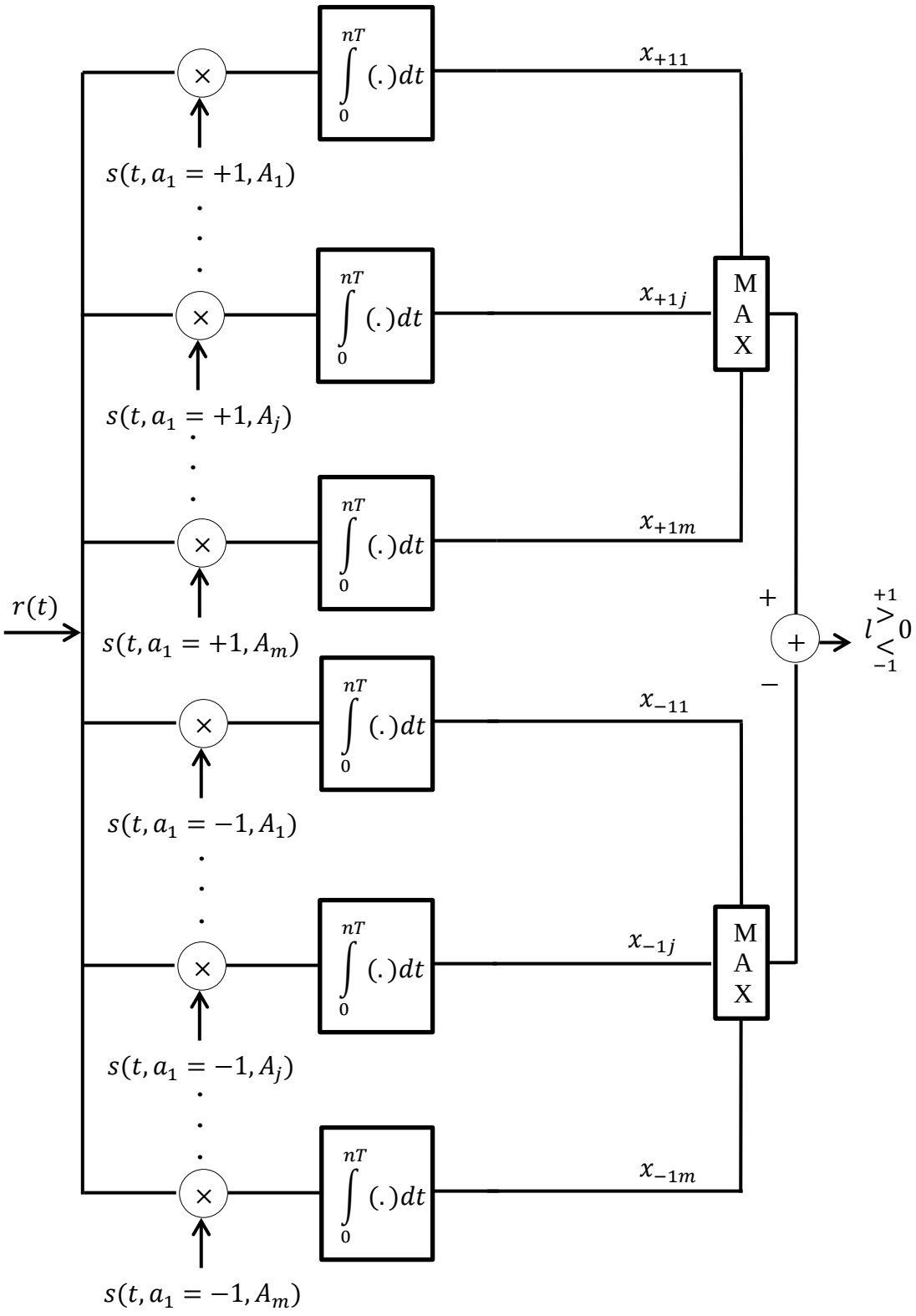

Figure 3.22: Block Diagram of Sub-Optimum High-SNR Receiver

3.3.1 CPFSK Performance

We need to evaluate the correlation function $\rho(j,u)$ in order to find the high-SNR upper and lower bounds for CPFSK performances. It can be shown that,

$$\rho(j,u) = \frac{1}{n}\sum_{i=1}^{n} \operatorname{sinc}\left(\frac{h}{2}\left(a_{ji} - a_{ui}\right)\right).\cos\left[\frac{\pi h}{2}\left(a_{ji} - a_{ui}\right) + \pi h \sum_{k=1}^{i-1}\left(a_{jk} - a_{uk}\right)\right] \quad (3.64)$$

First, we start by plotting the upper bound and lower bound for CPFSK BER performance for $n = 2,3$ and 4, $h = 0.715$ in Figure 3.22. It can be seen that at higher values of SNR the lower bound meets with the upper bound to form an even tighter bound. It can also be seen that as n increases, there is a noticeable improvement in the BER performance, which suggests carrying more comparisons in order to have an idea of how the different parameters affect the BER. Figure 3.24 shows the BER performance for high-SNR approximation for CPFSK.

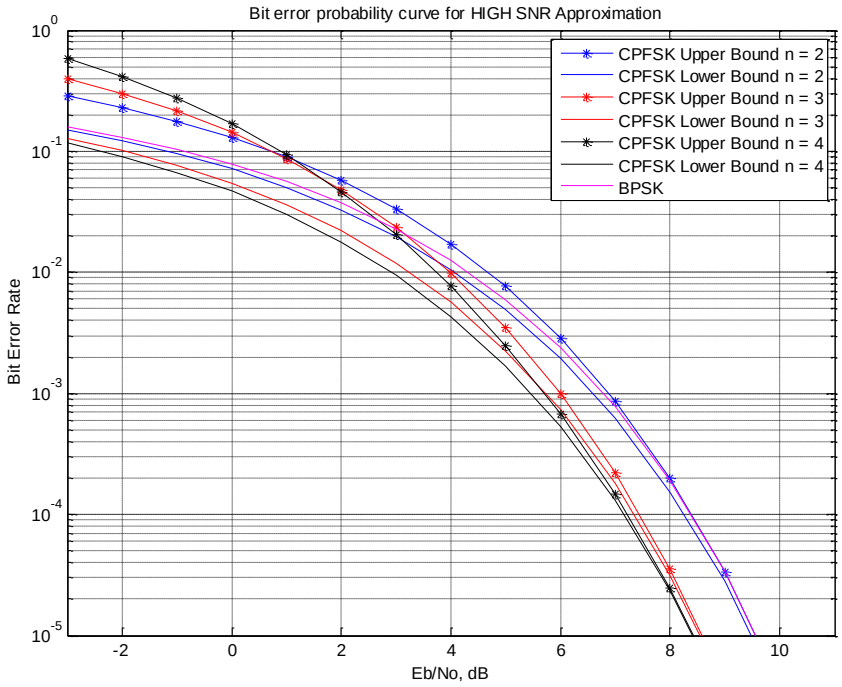

Figure 3.23: BER for High-SNR CPFSK for $h = 0.715, n = 2,3,4$

Next, we investigate the effect of h and n together on the BER performance for different values of SNR. It is observed from Figure 3.24 that there is a gap between the upper

bound and the lower bound at low-SNR, $SNR = 0$, which means that these bounds are not tight at low-SNR. On the other hand, in Figure 3.25, it can be seen that these two bounds have merged together for $SNR = 12$ dB. These graphs provide multiple options, in terms of values of n and h, when it comes to designing a system to meet a certain BER, subject to bandwidth and receiver complexity constraints. It is noted that the choice of h decides the bandwidth and n decides the complexity of the receiver.

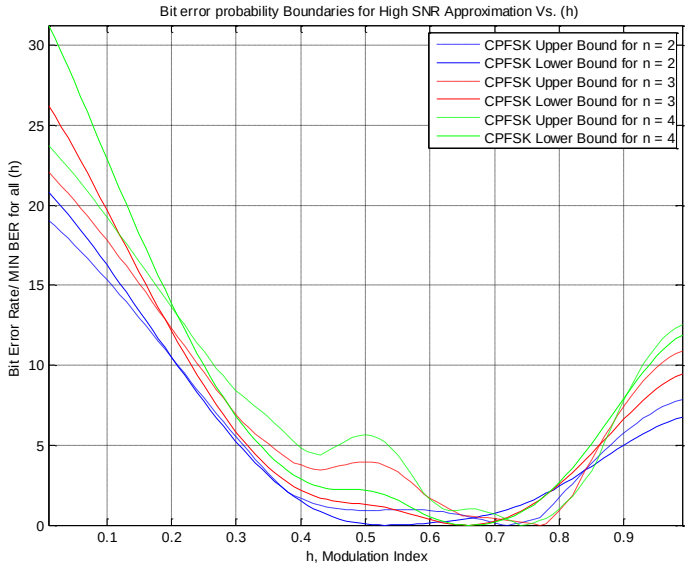

Figure 3.24: High-SNR CPFSK BER vs. h and n for $SNR = 0$ dB

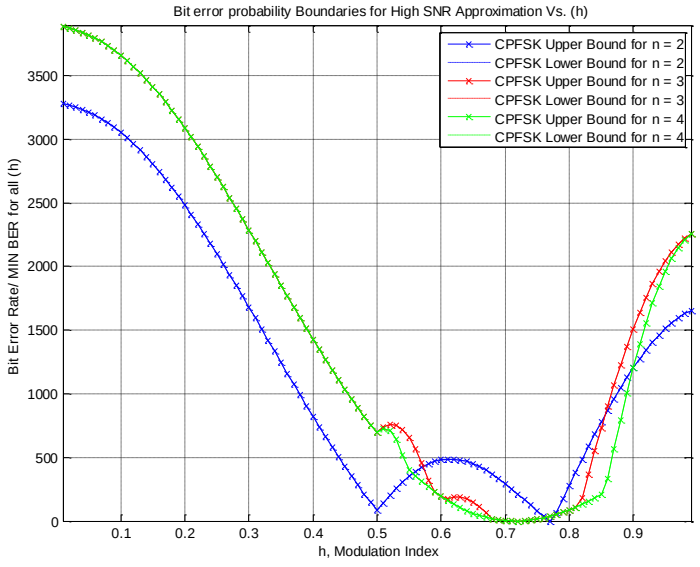

Figure 3.25: High-SNR CPFSK BER vs. h and n for $SNR = 12$ dB

The graphs in these Figures reveal that $min\{BER\}$ is somewhat in the region between $h = 0.5$ and $h = 0.8$. As n increases, the min$\{BER\}$ occurs at $h = 0.715$. This is related to the minimum distance of CPM signals, which will be explained in more detail in Chapter 4. We usually take the upper bound performance as a measure for the optimum receiver, since the lower bound assumes perfect conditions. It can also be seen from Figures 3.24 and 3.25 that the next nearest $min\{BER\}$ occurs at $h = 0.5$. Next; we plot the contours for the upper bound BER vs. h and n in Figures 3.26 and 3.27. Comparing these results to that of the AMF receivers, it can be inferred that the region [0.5, 0.75] has the two $min\{BER\}$ points for both receivers, which is shown in Table 3.2.

Table 3.2: min{BERs} for AMF and High-SNR Receivers

$min\{BER\}$	AMF (low-SNR)	Union Bound (high-SNR)
First Minimum	$h = 0.500$	$h = 0.715$
Second Minimum	$h = 0.646$	$h = 0.500$

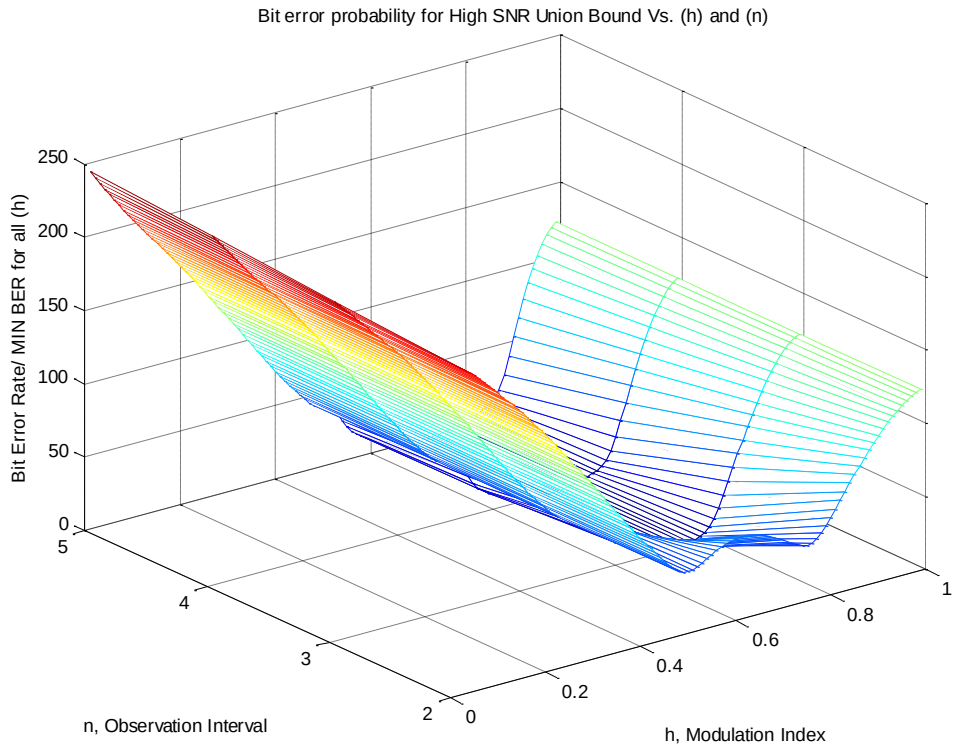

Figure 3.26: 3D Graph for CPFSK Union Bound BER vs. h and n, $SNR = 12$ dB

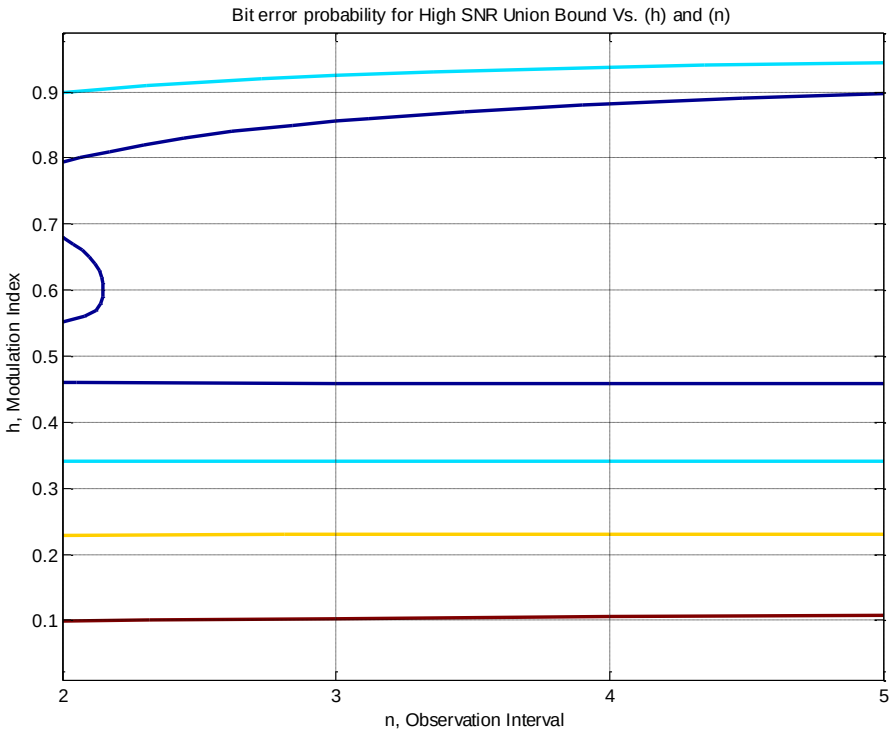

Figure 3.27: Contours of CPFSK Union Bound BER vs. h and n, $SNR = 12$ dB

3.3.2 CPCK Performance

We just need to evaluate the correlation function $\rho(j,u)$ in order to find the high-SNR upper and lower bounds for CPCK performances. It can be shown that

$$\rho(j,u) = \frac{1}{T}\sum_{i=1}^{n}\int_{(i-1)T}^{iT}\cos\left(\left(a_{ji}-a_{ui}\right)\pi\left[h\frac{t-(i-1)T}{T}-w\left(\frac{t-(i-1)T}{T}\right)^2\right]+\theta_i\right)dt \tag{3.65}$$

where

$$\theta_i = \pi q\sum_{k=1}^{i-1}a_{jk}-a_{uk} \tag{3.66}$$

For $i \geq 1$,

$$\rho(j,u)|_{i\geq 1} = \frac{\cos(\psi)}{2\sqrt{w}}\left[C[u_h]-C[u_l]\right]+\frac{\sin(\psi)}{2\sqrt{w}}\left[S[u_h]-S[u_l]\right] \tag{3.67}$$

For $i = 1$, $a_{ji} = -a_{ui} = +1$, the parameters of Equation 3.67 are

$$\psi = \frac{\pi(q+w)^2}{2w}, \qquad u_h = -\frac{h}{\sqrt{w}}, \qquad u_l = \frac{2w-h}{\sqrt{w}} \tag{3.68}$$

For $i \geq 2$, $a_{ji} > a_{ui}$, the parameters of Equation 3.67 are

$$\psi = \frac{\pi(q+w)^2}{2w} + \theta_i, \qquad u_h = -\frac{h}{\sqrt{w}}, \qquad u_l = \frac{2w-h}{\sqrt{w}} \tag{3.69}$$

For $i \geq 2$, $a_{ji} < a_{ui}$, the parameters of Equation 3.67 are

$$\psi = \frac{\pi(q+w)^2}{2w} - \theta_i, \qquad u_h = -\frac{h}{\sqrt{w}}, \qquad u_l = \frac{2w-h}{\sqrt{w}} \tag{3.70}$$

For $i \geq 2$, $a_{ji} = a_{ui} = \pm 1$,

$$\rho(j,u)|_{i\geq 2} = \cos\theta_i \tag{3.71}$$

In all cases, $C(x)$ and $S(x)$ are the Fresnel integrals, which require numerical evaluation, and are given by:

$$C(x) = \int_0^x \cos\left(\frac{\pi u^2}{2}\right) du\,, \qquad S(x) = \int_0^x \sin\left(\frac{\pi u^2}{2}\right) du \tag{3.72}$$

Again, since CPCK involves two modulation parameters, we use 3D plots in order to study the relation between the BER and the combinations of modulation parameters. Figures 3.28, 3.30 and 3.32 shows the 3D plots for CPCK; Union Upper Bound vs. q and w for $SNR = 6$ dB, $n = 2$,3 and 4, respectively. The parameters that minimizes BER at a certain SNR value can also be found by studying the minimum distance properties of CPCK. Again, all the graphs are normalized by their respective $min\{BER\}$. Figures 3.29, 3.31 and 3.33 show the contours of their corresponding 3D plots. For CPFSK high-SNR receiver, the minimum BER occurred at $h = 0.715$ for all n and SNR values. On the other hand, for CPCK high-SNR receiver, the minimum BER occurs at different points for different n for all SNR values. Using the 3D plots and their corresponding contours, the min$\{BER\}$ was found at the set of points (q, w) reported in Table 3.3.

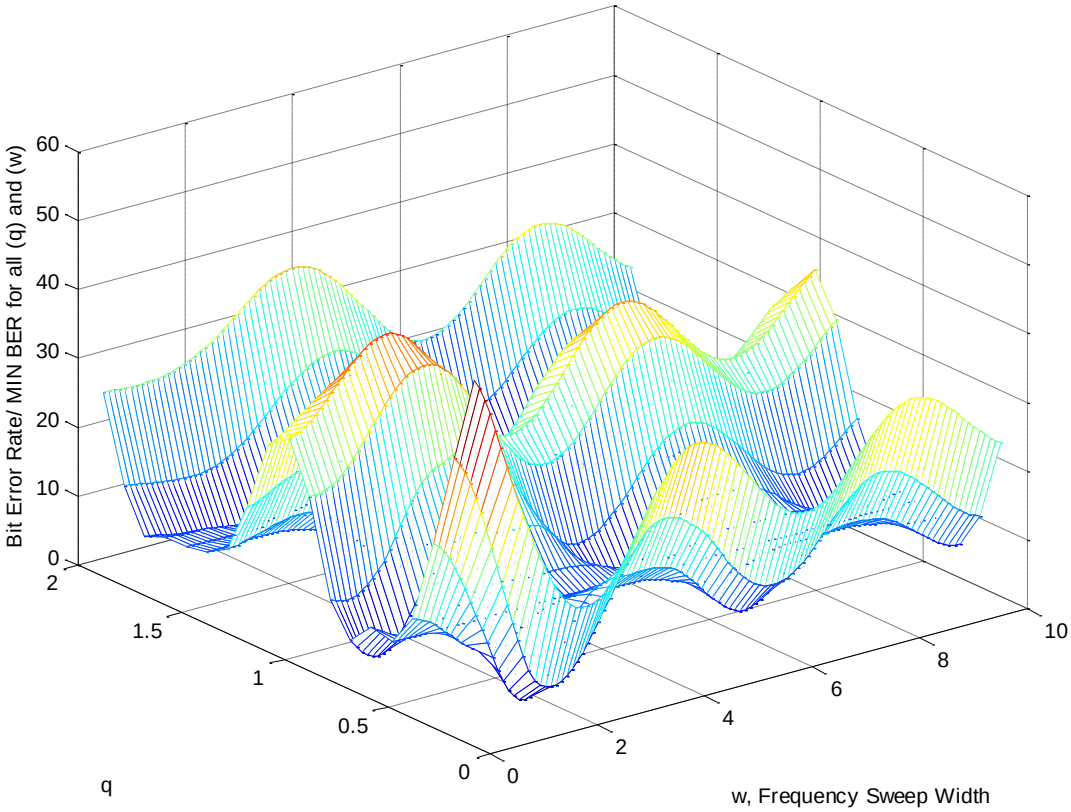

$$min\{BER\} = 1.232 \times 10^{-3}$$

Figure 3.28: 3D plot for CPCK Union Bound BER vs. q and w, $n = 2$, $SNR = 6$ dB

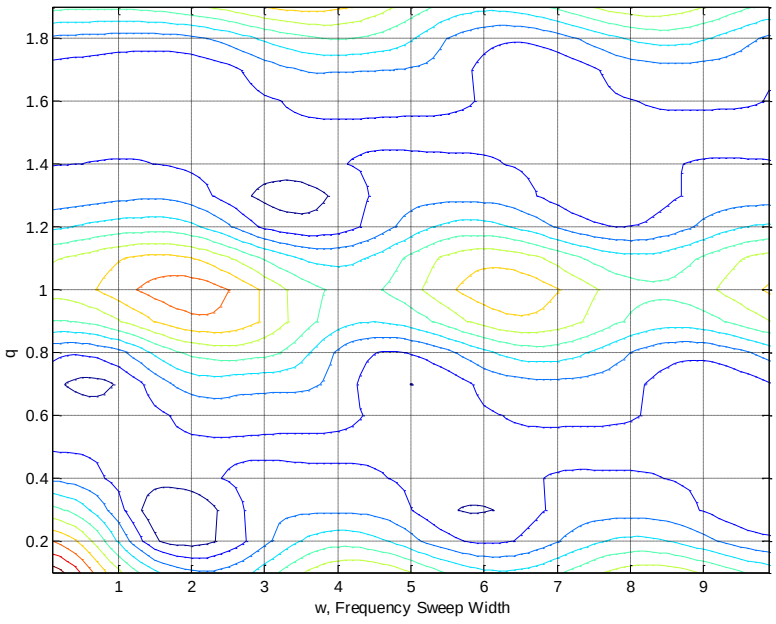

Figure 3.29: Contours of CPCK Union Bound BER vs. q and w, $n = 2, SNR = 6$ dB

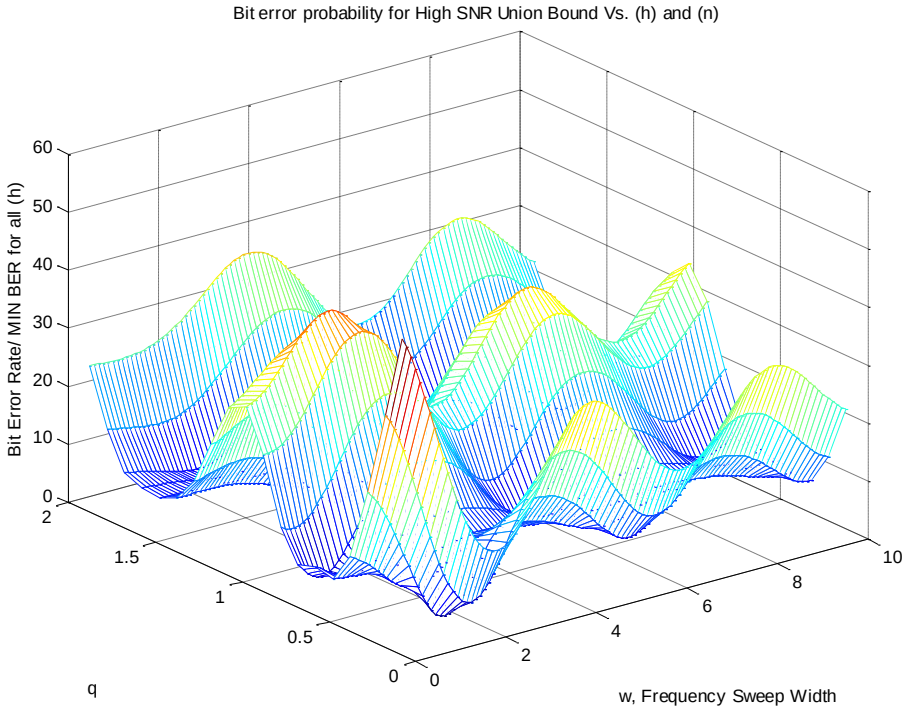

$$min\{BER\} = 6.459\ x\ 10^{-4}$$

Figure 3.30: 3D plot for CPCK Union Bound BER vs. q and w, $n = 3$, $SNR = 6$ dB

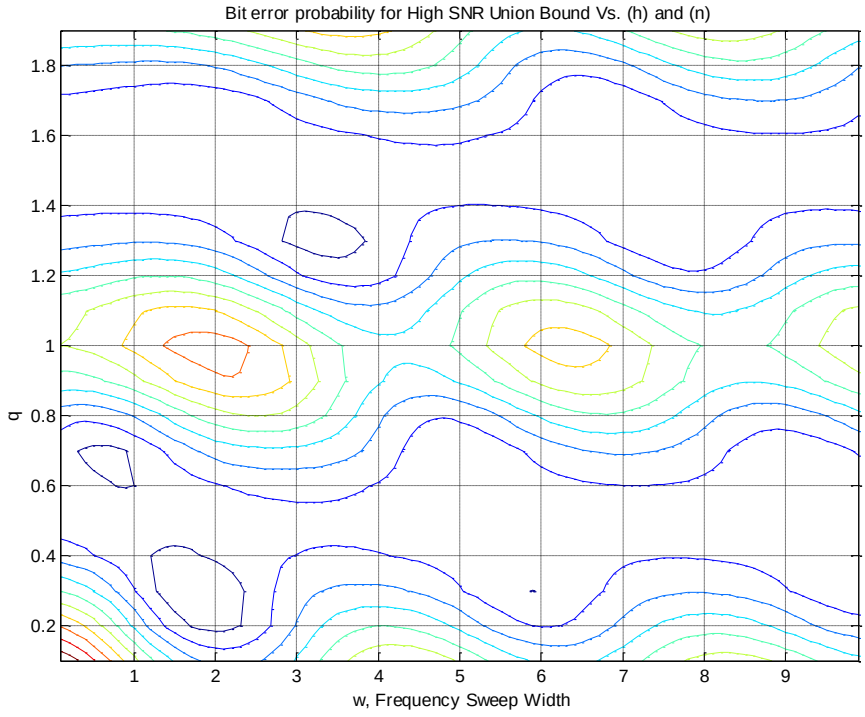

Figure 3.31: Contours of CPCK Union Bound BER vs. q and w, $n = 3, SNR = 6$ dB

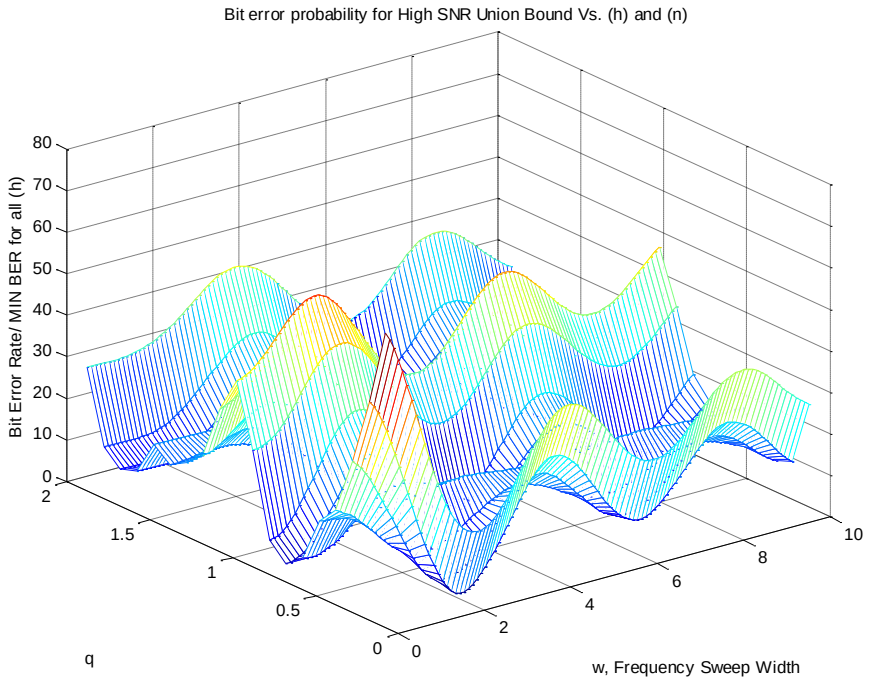

$$min\{BER\} = 4.242\ x\ 10^{-4}$$

Figure 3.32: 3D plot for CPCK Union Bound BER vs. q and w, $n = 4$, $SNR = 6$ dB

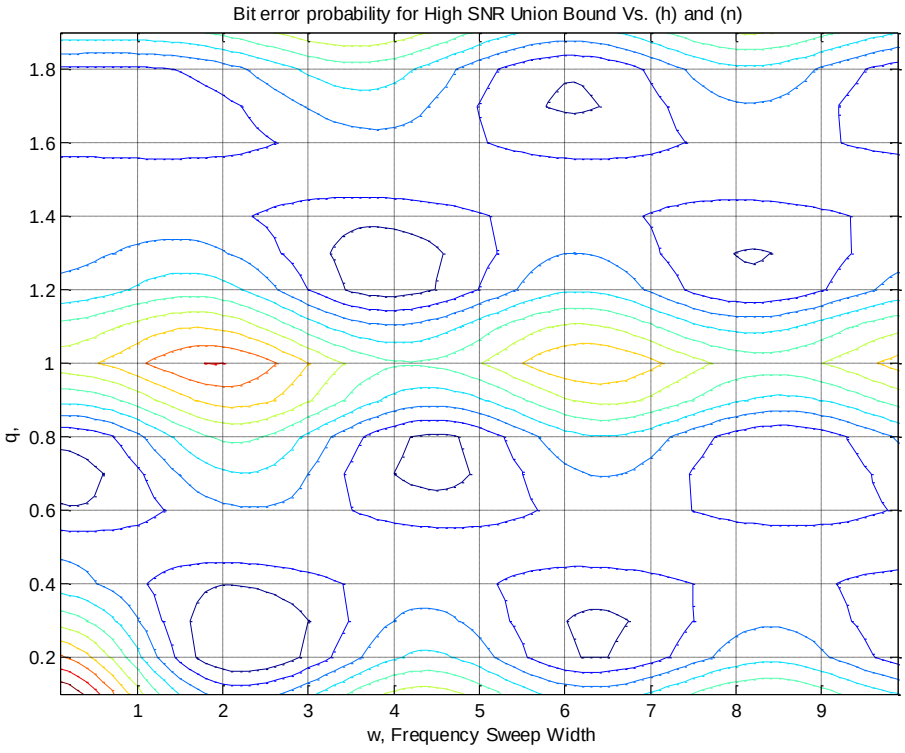

Figure 3.33: Contours of CPCK Union Bound BER vs. q and w, $n = 4, SNR = 6$ dB

In Table 3.3, the best values of q and w that minimizes union upper bound for $n = 2,3$ and 4 are shown. These values were found using the 3D plots shown in the previous Figures. It is observed that there exist several sets of parameters (q, w) that give the same BER threshold, which gives communication systems designers more flexibility when trying to meet the design criteria and constraints.

Table 3.3: q, w and n Values for Union Bound Receiver shown in Figure 3.34

n	(q, w)	$\min\{BER\}$ at $SNR = 6$ dB
2	$(0.28, 1.85)$	1.232×10^{-3}
3	$(0.24, 2.06)$	$6.459\ x\ 10^{-4}$
4	$(0.23, 2.22)$	$4.242\ x\ 10^{-4}$

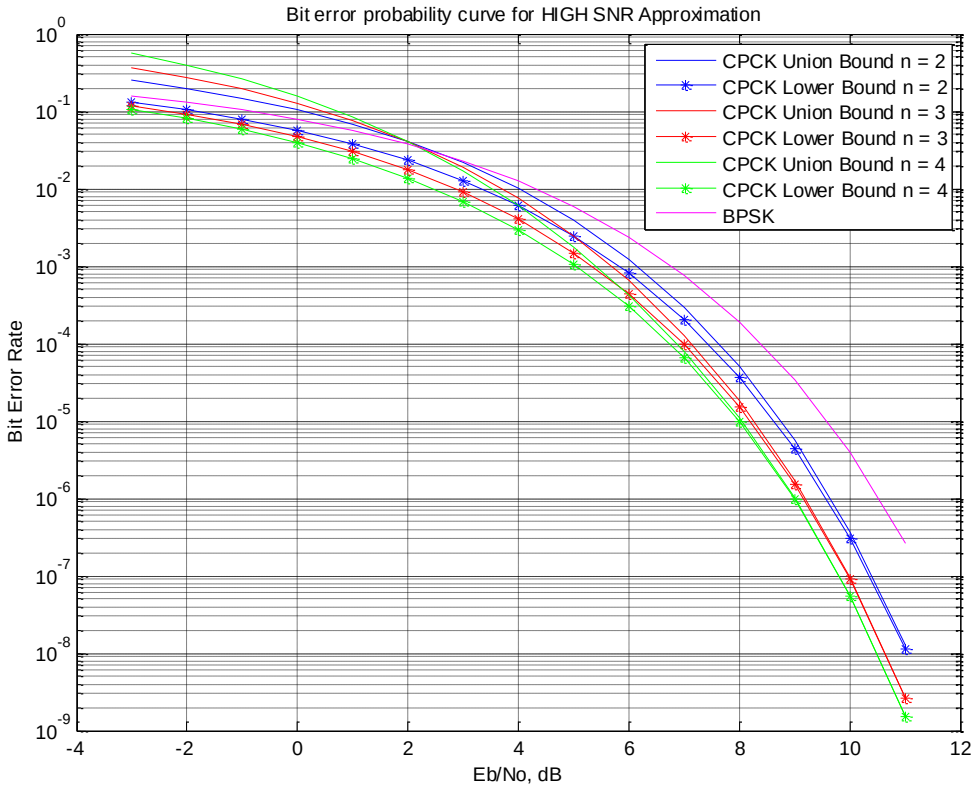

Figure 3.34: CPCK Union Bound Receiver BER

3.4 Composite Performance Bounds

Again, there is still the question of "What threshold that separates high-SNR from low-SNR when studying the effect of the different parameters on BER?" In this section, we plot the composite bound, derived from the performance of the AMF and high-SNR

receivers for both CPFSK and CPCK. The optimum performance for CPFSK and CPCK will be bounded by these composite bound. Figures 3.35 and 3.36 show the performance of CPFSK and CPCK with respect to BPSK, respectively. From these composite bounds plots, it is noticed that at a certain SNR value, the upper bound is decided using the high-SNR upper bound instead of the AMF receiver bound. Thus, the point at which the optimum receiver performance gets upper bounded by the upper bound of the high-SNR receiver instead of the AMF, can be considered as the SNR value that separates high- and low-SNR for any set of modulation parameters and n. Figure 3.37 combines the results of Figures 3.35 and 3.36 into a single Figure to compare the performances of CPFSK with CPCK. Parameters used for composite bound are: for CPFSK, $n = 4$ and $h = 0.715$, and for CPCK, $n = 4, w = 2.2$ and $q = 0.23$. From Figure 3.37, using high-SNR upper bound, it is noted that CPCK has SNR advantage of 0.65 dB and 1.50 dB relative to CPFSK and BPSK, respectively. We carried out simulations to verify the mathematical analysis provided in the thesis, and Figure 3.38 shows that the simulation results comply with the results due to the theoretical derivations.

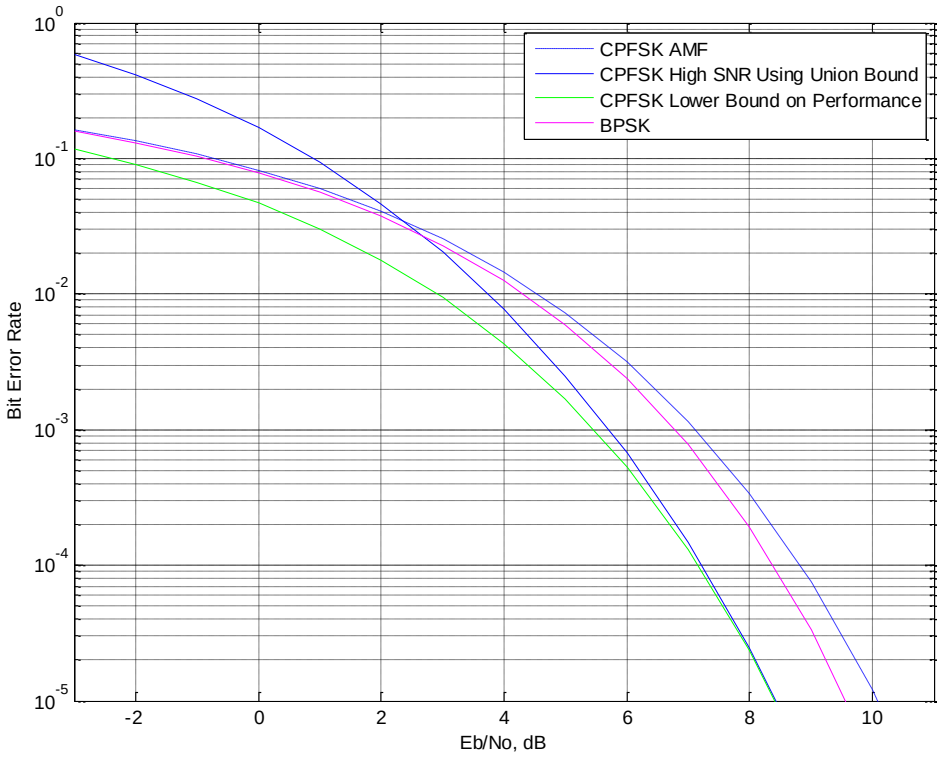

Figure 3.35: Composite Bound on CPFSK

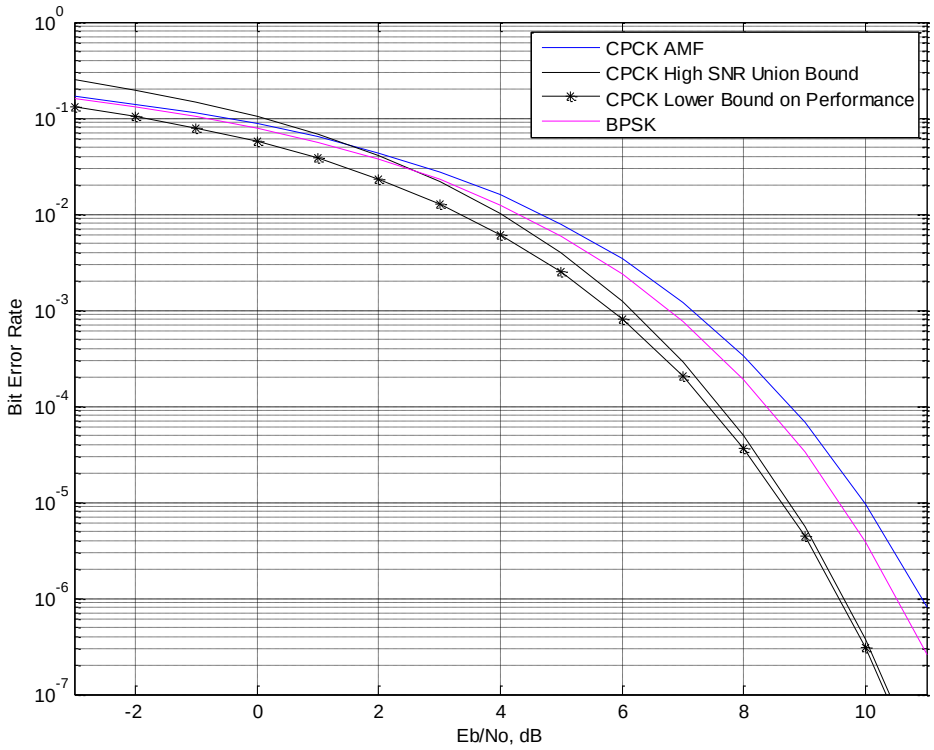

Figure 3.36: Composite Bound on CPCK

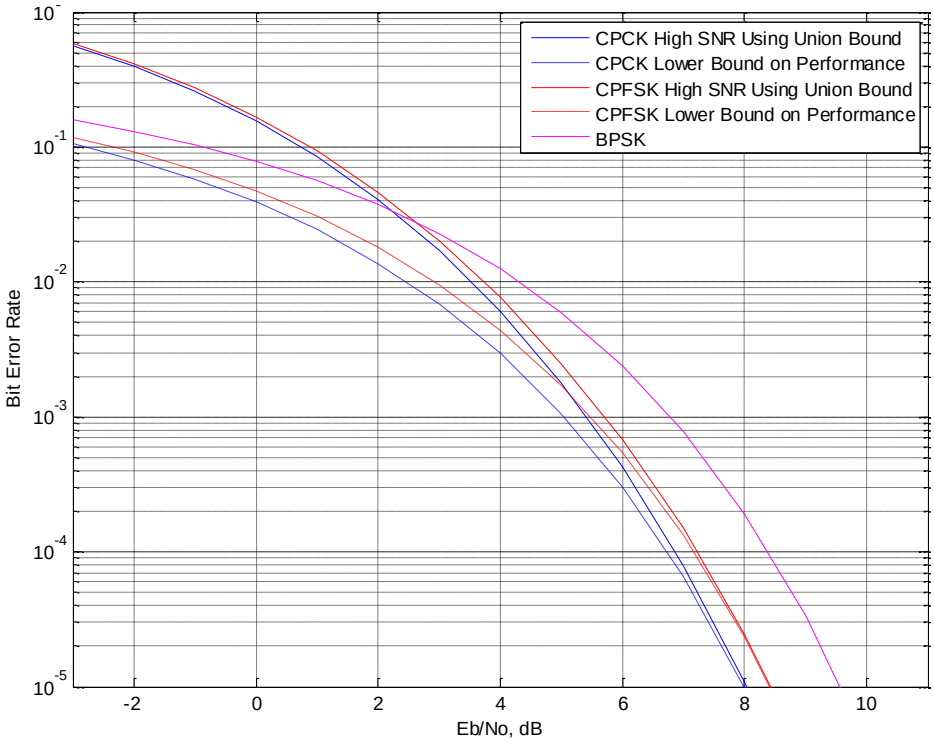

Figure 3.37: CPFSK and CPCK Union Bounds, $n = 4$

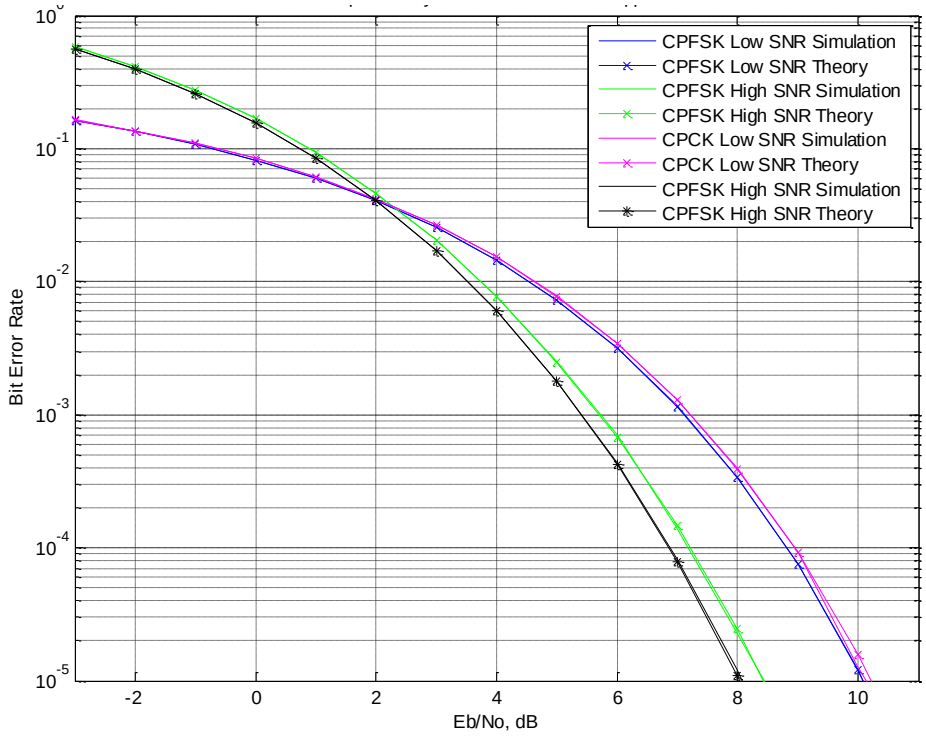

Figure 3.38: CPFSK and CPCK AMF and Union Bound Receivers Simulation

3.5 Summary and Results

In this Chapter, we have examined one of the two main Maximum Likelihood Detectors for CPM. Optimum CPM MLRT-based receiver was derived, and block diagram for receiver implementation has been provided. Also, we have discussed the computational complexity involved in analyzing and simulating the optimum receiver for CPFSK and CPCK. Since the optimum receiver is very complex to be mathematically analyzed, two approximations have been used to arrive at sub-optimum receivers for low- and high-SNR values. At low-SNR, sub-optimum AMF receiver is thoroughly examined for CPFSK and CPCK. It was shown that the AMF performance of CPFSK with $h = 0.5$ matches that of BPSK for all n. Moreover, it was shown that as n increases, the next nearest BER performance to that of BPSK occurs at $h = 0.646$. For CPCK, it was found that $min\{BER\}$ occurs at $q = 0.5$ and $q = 1.5$ independent of SNR value w and n, yielding BPSK performance. The q values yielding BPSK performance for CPCK were found by searching the region $0 \leq q \leq 2$. Other values for q can exist outside these boundaries.

Using high-SNR approximation, sub-optimum high-SNR receiver has been provided for CPFSK and CPCK. This receiver has provided two bounds for CPFSK and CPCK optimum receiver, an upper bound and a lower bound. Different plots and graphs have been provided in both cases in order to study the relationships between BER and the different modulation parameters for both CPFSK and CPCK, such as: E_b/N_0 vs. h, E_b/N_0 vs. h & n, E_b/N_0 vs. q & n, E_b/N_0 vs. w & n…etc. In general, for CPFSK and CPCK, the BER performance improved as the length of the observation interval n increased. However, that amount of improvement decreased with each increment of the observation interval length. This indicated that increasing the length of the observation interval beyond a certain limit provided only marginal BER improvement and higher receiver complexity. Moreover, for CPFSK, it has been noted that optimum performance is achieved at $h = 0.715$ for all n, and near optimum performance is achieved at $h = 0.5$ for all n. In addition, the difference in performance between the upper bound and the lower bound at low-SNR was relatively big, which means that these bounds are not tight at low-SNR; however, the performance corresponding to both bounds would meet at high-SNR values. For CPCK, 3D plots were used in order to study the relation between BER and the combinations of modulation parameters. Wherein CPFSK high-SNR receiver the minimum BER occurred at $h = 0.715$ for all n and SNR values, for CPCK high-SNR receiver, the minimum BER occurs at different points for different n for all SNR values. Using the 3D plots and their corresponding contours, the set of points (q, w) where min$\{BER\}$ occurs were found. The high-SNR numerical results are best summarized in Table 3.4.

Table 3.4: Optimum CPFSK and CPCK high-SNR Systems Parameters

CPFSK		
n	h	min$\{BER\}$ at $SNR = 6$ dB
2	0.715	2.858×10^{-3}
3	0.715	$9.938\,x\,10^{-4}$
4	0.715	$6.758\,x\,10^{-4}$
CPCK		
n	(q, w)	min$\{BER\}$ at $SNR = 6$ dB
2	$(0.28, 1.85)$	1.232×10^{-3}
3	$(0.24, 2.06)$	$6.459\,x\,10^{-4}$
4	$(0.23, 2.22)$	$4.242\,x\,10^{-4}$

In order to better understand the performance of high-SNR approximation, one needs to understand the distance properties associated with each signaling scheme. Therefore, we have proposed studying the distance criteria for CPFSK and CPCK in Chapter 4. The different graphs for AMF receiver and high-SNR receiver provided in this Chapter helps system designers by giving multiple options, in terms of values of n and h, in order to meet a certain BER, subject to different bandwidth and receiver complexity constraints. It is noted that the choice of h, q and w decides the bandwidth and n decides the complexity of the receiver.

Moreover, in order to answer the question of "What threshold that separates high-SNR from low-SNR when studying the effect of the different parameters on BER?", plots of the composite bounds, derived from the performance of the AMF and high-SNR receivers for both CPFSK and CPCK were provided. The optimum performance for CPFSK and CPCK will be bounded by these composite bound. It was noticed that if a threshold is assumed for a set of modulation parameters, it is not necessarily the same for another set of modulation parameters. Even for CPFSK and CPCK with relatively similar modulation parameters, $q_{CPCK} = h_{CPFSK}$ and n, the same threshold does not comply. However, after plotting the composite bound for CPFSK and CPCK, it was noticed that at a certain SNR value, the upper bound is decided using the high-SNR upper bound instead of the AMF. Thus, the point at which the optimum receiver performance gets upper bounded by the upper bound of the high-SNR receiver instead of the AMF, can be considered as the SNR value that separates high- and low-SNR for any set of modulation parameters and n. A comparison between optimum CPFSK; $n = 4$ and $h = 0.715$, and optimum CPCK; $n = 4, w = 2.2$ and $q = 0.23$ performance showed that CPCK has SNR advantage of 0.65 dB and 1.50 dB relative to CPFSK and BPSK, respectively. Computer Simulations were carried out to verify the mathematical analysis provided in the thesis, and simulation results complied with the results of the theoretical derivations.

In general, a BER expression for CPFSK and CPCK can be given in the following format,

$$P(e)|_{CPFSK} = f(SNR, n, h) \tag{3.73}$$

$$P(e)|_{CPCK} = f(SNR, n, q, w) \tag{3.74}$$

In addition, CPCK has been found more flexible than CPFSK, from a design point of view, in the sense that CPCK allowed for the manipulation of more parameters, which gave better control on the modulation scheme, and this can be inferred from Equations 3.73 and 3.74. In general, CPCK can achieve superior BER performances to that of CPFSK.

Chapter 4

Viterbi Receiver for CPFSK and CPCK

The immense capabilities of CPM signaling techniques encouraged designers to use CPM in many real-life communication applications; however, when it comes to demodulation of CPM, the receiver complexity is always a huge drawback. The complexity associated with the MLRT-based optimum receiver was examined in Chapter 3. In such a receiver, frame-by-frame detection strategy is employed. Maximum Likelihood Detection (MLD) Theory offers another solution for detection of CPM signals by taking advantage of the inherent memory/sequence characteristics of CPM. Essentially, it operates using a sequence detection strategy, which is Maximum Likelihood Sequence Estimation (MLSE). Receivers employing MLSE are referred to as Viterbi receivers. This detection approach is based on searching for the minimum Euclidean distance path through the trellis that characterizes the memory in the transmitted signal. Viterbi detector is the practical implementation of Maximum Likelihood Detection for CPFSK and CPCK signals.

Since Viterbi receiver utilizes the concept of minimum distance, we first start the Chapter by studying the minimum distance properties for both signaling schemes.

4.1 Minimum Distance Properties for CPFSK and CPCK

First, we start by setting the Equations for the case of general CPM, and then we specify them for CPFSK and CPCK. This will help us in estimating a limiting value on the SNR gain $G_n$for CPFSK and CPCK. Assuming narrow-band signals, i.e., $w_c T \gg 2\pi w$, passband signals may be represented by their complex envelopes and it can be shown that distance Equation from Chapter 3 can be written as,

$$D_n{}^2(j,u) = n - \sum_{i=1}^{n} \frac{1}{T} \int_0^T \cos\big(\Delta\phi_i(t,j,u)\big)dt \qquad (4.1)$$

$\Delta\phi_i(t,j,u)$ describes the phase difference between the signals $s\big(t,+1,A_j\big)$ and $s(t,-1,A_u)$ during the i^{th} bit interval with the data difference term (i.e., difference between sequences $\{a_\delta = +1, A_j\}$ and $a_\delta = -1, A_u\}$ during the i^{th}bit interval) is given by

$$a_{jk} - a_{uk} = \begin{cases} 0, & a_{jk} = a_{uk} \\ \pm 2, & a_{jk} = -a_{uk} = \pm 1 \end{cases} \qquad (4.2)$$

The optimum coherent receiver produces a decision on the first bit a_1 among the n observed bits, and an upper bound on the minimum distance squared $D_B{}^2$ is always determined by the two data sequences $(+1,-1,x,x,\dots)$ and $(-1,+1,x,x,\dots)$ where the $x's$ indicate that the sequences are identical after the second bit. This will upper bound the optimal coherent receiver: that is,

$$D_n{}^2 \leq D_B{}^2 \qquad (4.3)$$

$D_B{}^2$ can be interpreted as the maximum minimum (free) distance for a system with a specific set of modulation parameters. This will be used later in finding the Viterbi Receiver's upper bound on BER.

4.1.1 Minimum Distance Properties of CPFSK

$$\Delta\phi_i(t,j,u) = \frac{(a_{ji} - a_{ui})t}{T} + \pi h \sum_{k=1}^{i-1} (a_{jk} - a_{uk}) \tag{4.4}$$

$$D_n{}^2 \leq D_B{}^2(h) = 2 - 2\,\mathrm{sinc}(h)\cos(\pi h) \tag{4.5}$$

The previous Equation suggests that $D_B{}^2(h) \leq 4$ indicating that the SNR gain G_n has an upper limit of 3 dB. But, in order to find a tighter upper bound, $D_B{}^2(h)$ was computed for all possible values of h. Regions where $D_B{}^2(h) < 2$ are of no interest to us since there is no SNR gain corresponding to those values of h. Since we constrain h to take values in the range [0,1], $D_B{}^2(h)$ has one global maxima at $h = 0.715$, $\max\{D_B{}^2(h)\} = 2.434$. This actually supports the observations in Chapter 3 for CPFSK, that is the CPFSK's union bound for CPFSK, would reach its optimum value when $h = 0.715$.

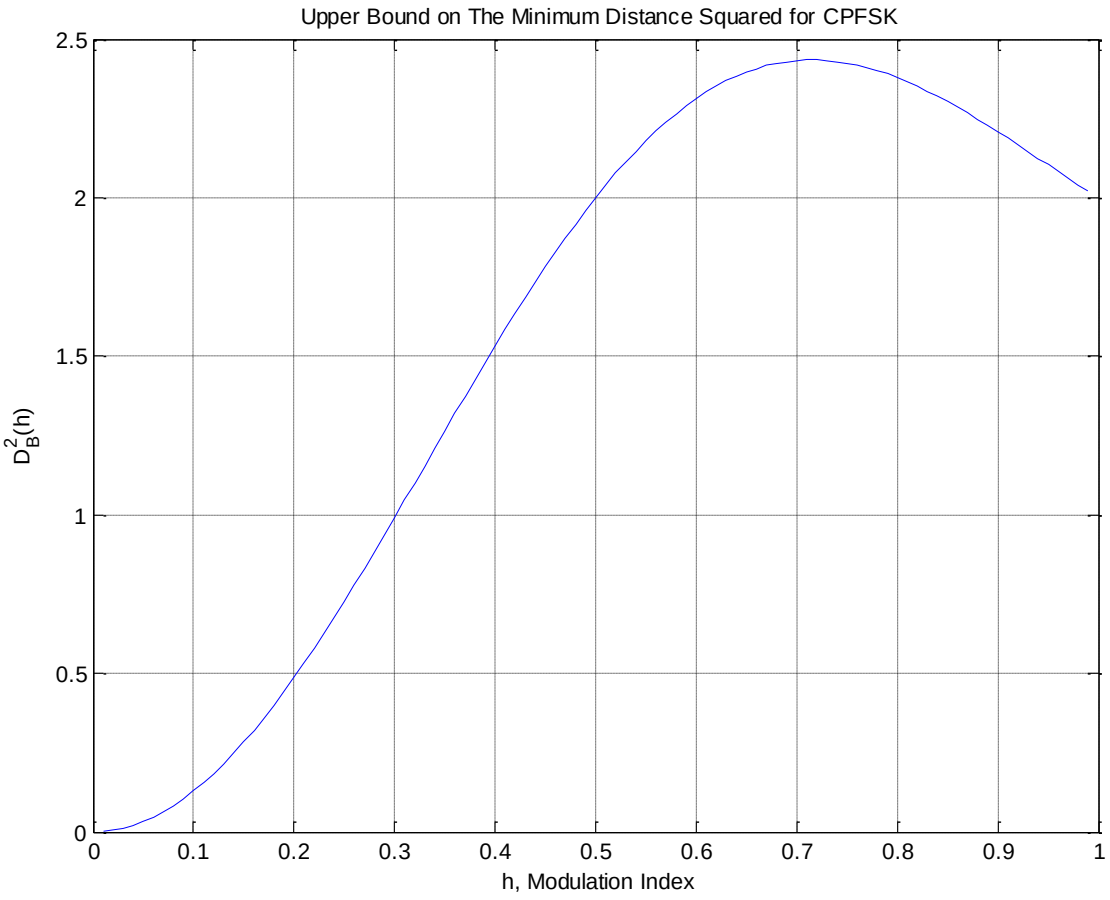

Figure 4.1: Upper Bound on the Minimum Distance Squared for CPFSK at all h

Also, It can be seen that ${D_n}^2(j,u)$ is minimized for data sequences that differ only in the decision bit position ($a_{j1} = -a_{u1}$ and $a_{jk} = a_{uk}, k = 2, \dots n$) independent of the n value; for all n. ${D_n}^2$ for such sequence is

$$ {D_n}^2(n,h) = n(1 - \cos(2\pi h)) + \cos(2\pi h) - \operatorname{sinc}(h)\cos(\pi h) \qquad (4.6) $$

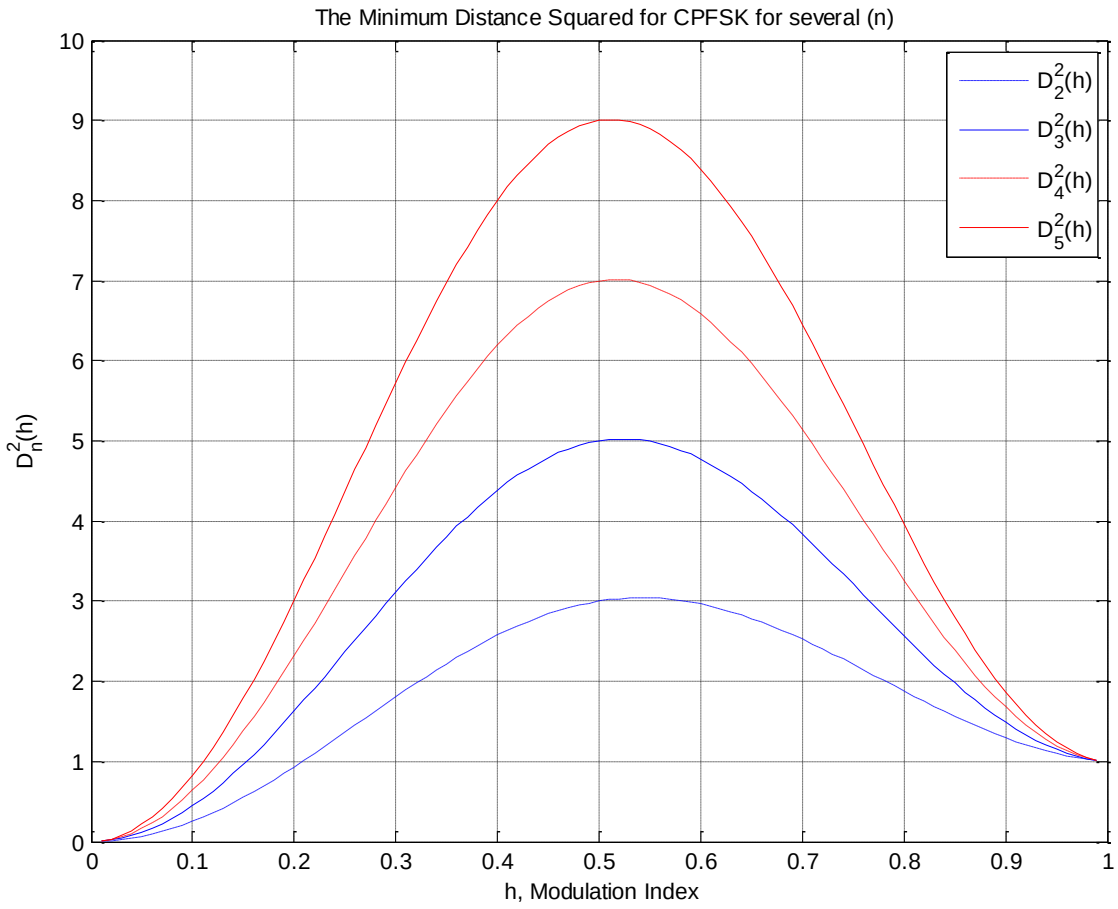

Figure 4.2: CPFSK Minimum Distance Squared with First Bit Difference Only

This implies that as we increase the observation interval when comparing such sequences ($a_{j1} = -a_{u1}$ and $a_{jk} = a_{uk}, k = 2, \dots n$), we have SNR gain according to the following Equation

$$ G_n = 10\log_{10}({D_n}^2/2) = 10\log_{10}\left({D_n}^2(n,h)/2\right) \qquad (4.7) $$

It is important to understand that the actual ${D_n}^2$ will always be smaller than the global maxima of its bound. For some $h \neq 0.715$, however, a ${D_n}^2$ close to this maxima may be obtained. With this assumption, the maximum value of ${D_B}^2(h) = 2.434$ indicates that the SNR gain G_n will be limited to about 0.85 dB.

In order to verify this, using Equations 4.1 and 4.4, we run an exhaustive computer search to find the parameters maximizing ${D_n}^2$ and G_n for different n and h, and we report the results in Table 4.1. The results shows that the closest we can get to the upper bound is at $h-\text{value} = 0.71$. Moreover, it is showing that the maximum SNR gain attainable for CPFSK is achieved at $n = 3$, so it can be called the optimum observation interval, where further observations don't add benefits to the system.

Table 4.1: CPFSK Signal Parameters Maximizing ${D_n}^2$ and G_n

n	h	${D_n}^2$	G_n
2	0.765	2.051	0.11
3	0.710	2.434	0.85
4	0.710	2.434	0.85
5	0.710	2.434	0.85

4.1.2 CPCK Minimum Distance Properties

$$\Delta\phi_i(t,j,u) = (a_{ji} - a_{ui})g(t) + \pi q \sum_{k=1}^{i-1}(a_{jk} - a_{uk}) \tag{4.8}$$

$${D_n}^2 \leq {D_B}^2(q,w) = 2 - \frac{2\cos(\pi q)}{T}\int_0^T \cos\left\{2\pi w\left(\frac{t}{T}\right)^2 - \frac{2\pi(q+w)t}{T} + \pi q\right\}dt \tag{4.9}$$

$${D_B}^2(q,w) = 2 - \frac{\cos(\pi q)}{\sqrt{w}}.[\cos\left(\frac{\pi(q^2+w^2)}{2w}\right)\left[C\left(\frac{w-q}{\sqrt{w}}\right) + C\left(\frac{w+q}{\sqrt{w}}\right)\right]$$

$$+ \sin\left(\frac{\pi(q^2+w^2)}{2w}\right)\left[S\left(\frac{w-q}{\sqrt{w}}\right) + S\left(\frac{w+q}{\sqrt{w}}\right)\right]] \tag{4.10}$$

Equation 4.10 suggests that ${D_B}^2(q,w) \leq 4$ indicating that the SNR gain G_n has an upper limit of 3 dB. But, in order to find a tighter upper bound, ${D_B}^2(q,w)$ was computed for all

possible values of q, w. From Equation 4.11, it can be inferred that ${D_B}^2(q,w) = {D_B}^2(-q,w) = {D_B}^2(|q|,w)$. Since more parameters control the CPCK performance than that of CPFSK, we provide Figures 4.3 and 4.4. These graphs are 3D plots for ${D_B}^2$ vs. q and w. Regions where ${D_B}^2(q,w) < 2$ are of no interest to us since there is no SNR gain corresponding to those values of q, w. ${D_B}^2(q,w)$ has many local maxima for integer values of q and the global maxima at $(q,w) = (0.2.4)$, $\max\{{D_B}^2(q,w)\} = 2.93$. For $q = 0$ or $w = 0$, one needs to work out the problem starting from Equation 4.10, and take out the intended parameter. That was done for plotting ${D_B}^2(q,0)$ and ${D_B}^2(0,w)$. Of course, ${D_B}^2(q,0)$ is the CPFSK case that was plotted in the previous section as ${D_B}^2(h)$. By manipulating q and restricting the values assigned to it, one can arrive at simpler expressions for the ${D_n}^2(q,w)$. For example, limiting q to only take integer values would cancel some terms in the ${D_n}^2(q,w)$ as will be seen next.

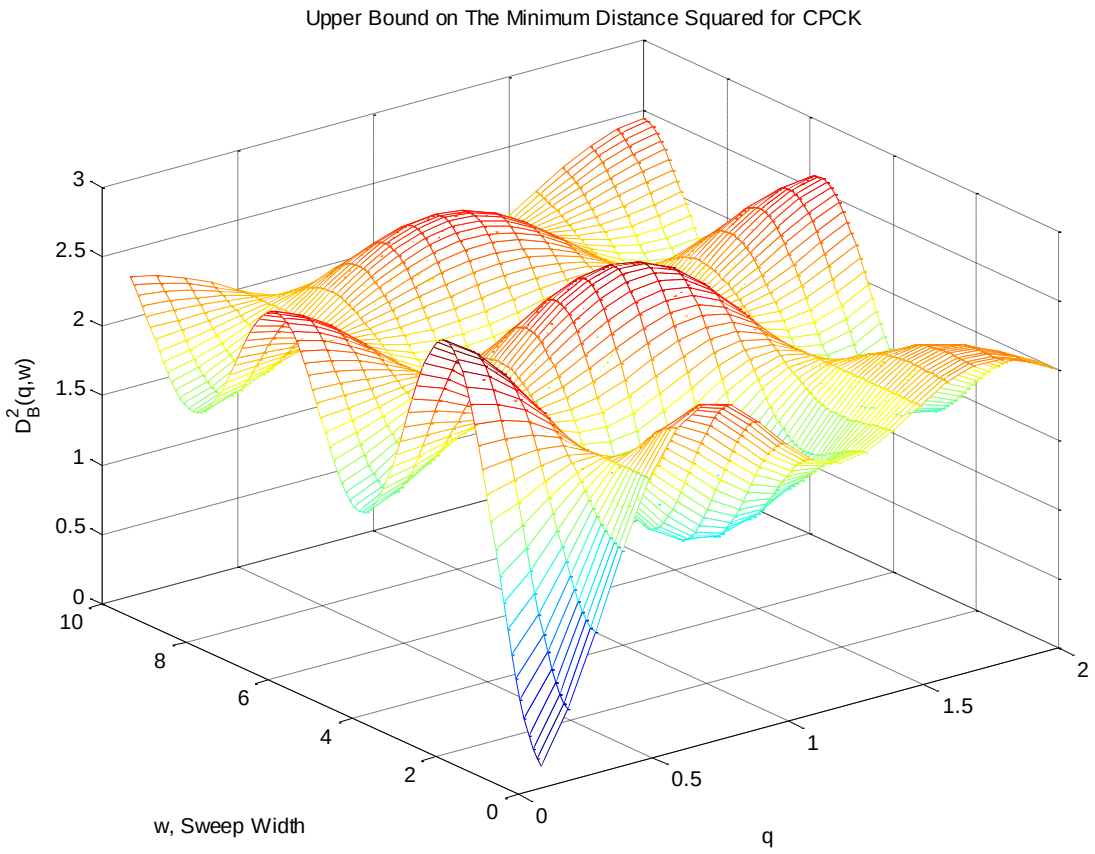

Figure 4.3: Upper Bound on the Minimum Distance Squared for CPCK for all q&w

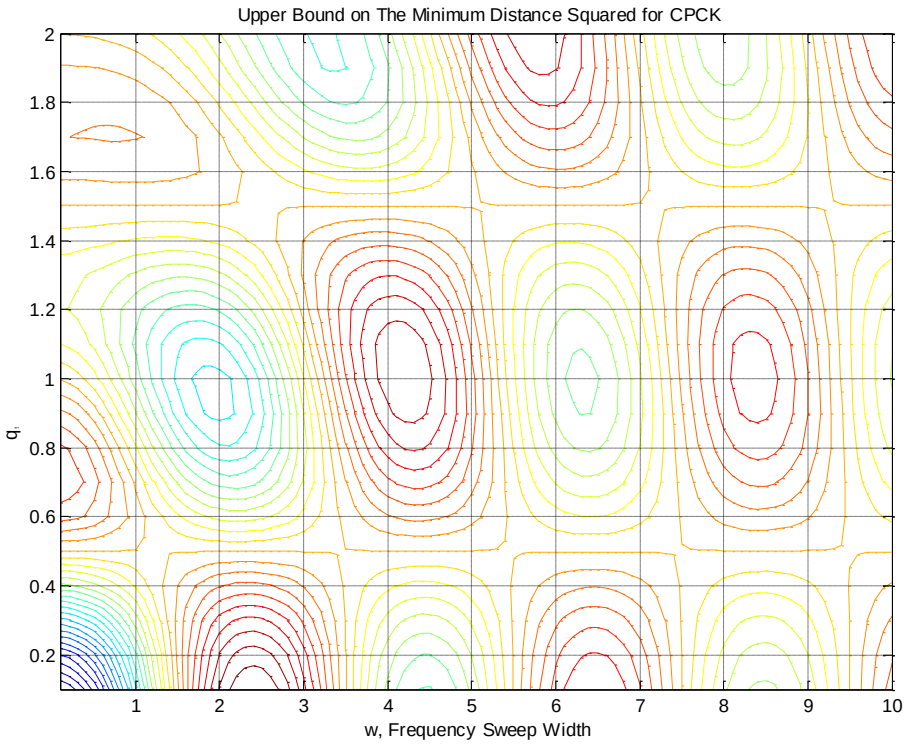

Figure 4.4: Contours for Upper Bound on Minimum Distance Squared for CPCK

For $q = 0, \pm 1, \pm 2, \ldots$, it is found that ${D_n}^2$ reduces to

$$ {D_n}^2(j,u) = n - \sum_{i=1}^{n} \frac{1}{T} \int_0^T \cos\Big(\big(a_{ji} - a_{ui}\big) g(t) \Big)\, dt\,, \quad q = 0, \pm 1, \pm 2, \ldots \qquad (4.11) $$

And it can be shown that ${D_n}^2(j,u)$ is minimized, independent of n, for data sequences that differ only in the decision bit position ($a_{j1} = -a_{u1}$ and $a_{jk} = a_{uk}, k = 2, \ldots n$), then it follows,

$$ {D_n}^2 = 1 - \frac{1}{T} \int_0^T \cos\big(2g(t)\big)\, dt\,, \quad q = 0, \pm 1, \pm 2, \ldots \qquad (4.12) $$

for all n, implying that one bit observation is optimum, i.e, no SNR gain results from observing the received signal beyond the one bit. Hence, the actual ${D_n}^2$ will always be smaller than the global maxima of its bound. For some $q \neq 0, \pm 1, \pm 2, \ldots$, however, a ${D_n}^2$

close to this maxima may be obtained. With this assumption, the maximum value of ${D_B}^2(q,w) = 2.93$ indicates that the SNR gain G_n will be limited to about 1.66 dB.

In order to verify this, using Equations 4.1 and 4.12, we run exhaustive computer search to find the parameters maximizing ${D_n}^2$ and G_n for different n and q and w, and we report the results in Table 4.2. We only carried the simulations up till $n = 4$, because it is noticed that SNR gain increase is not as major from $n = 3$ to $n = 4$ and we are approaching the upper bound value for SNR gain of 1.66 dB. So, $n = 4$ can be called the optimum observation interval, where further observations don't add major benefits to the system.

Table 4.2: CPCK Signal Parameters Maximizing ${D_n}^2$ and G_n

n	q	w	${D_n}^2$	G_n
2	0.250	1.55	2.571	1.09
3	0.192	2.05	2.774	1.42
4	0.156	2.36	2.827	1.50

4.2 Optimum Viterbi Receiver

The Viterbi algorithm (VA) is an optimal solution to the problem of estimating the state sequence of a discrete time finite state Markov process observed in memory-less noise The VA is optimum in the sense that the maximum likelihood estimate of the sequence of states is obtained. The Viterbi algorithm performs recursively to choose those sequences that maximize the log likelihood function up to the i^{th} symbol interval. Since a specific sequence of state transitions gives a unique sequence of data symbols, a maximum likelihood estimate of the data sequence is also obtained. This is referred to as maximum likelihood sequence estimation (MLSE).

In this section, we describe a class of optimum receivers based on the maximum likelihood sequence estimation, which is optimal in the sense that it minimizes the BER, when decoding an *infinitely* long sequence, meaning that the optimal performance of the Viterbi decoder is achieved as $n \to \infty$. We start by a quick recap from Chapter 2, redefining the terms according to the Viterbi's optimal requirement. We know the that the information carrying phase can be expressed as follows,

$$\phi(t,\boldsymbol{a}) = \sum_{k=-\infty}^{i} a_k g(t-(k-1)T) = \theta(t,a_i) + \theta_i, \qquad (i-1)T \le t \le iT, (4.13)$$

For h and $g(t)$ and for any symbol interval i, the phase $\phi(t,\boldsymbol{a})$ is defined by a_i, the correlative state vector $(a_{i-1}, a_{i-2}, \dots, a_{i-L+1})$ and the phase state θ_i, where

$$\theta_i = \left[g(t=T) \sum_{k=-\infty}^{i-1} a_k \right] \bmod 2\pi \qquad (4.14)$$

The number of correlative states is finite and equal to $M^{(L-1)}$. Since we are working with full response CPM, $L = 1$, we don't have a correlative state vector. For rational modulation indices the phase tree is reduced to a phase trellis. In this Chapter, we define the modulation index as follows

$$h = 2v/p \ (v, p \text{ integers}) \qquad (4.15)$$

There are p different phase states with values $\left[0, \frac{2\pi}{p}, 2\frac{2\pi}{p}, \dots, (p-1)\frac{2\pi}{p}\right]$. The total state vector is defined by the 1-tuple $S_i = (\theta_i)$, and the number of such states is p. All of these properties are critical to the receiver structures in this section.

Usually, phase states and correlative states are assigned to the nodes in the phase tree. The root node is arbitrarily given phase state 0. Each node in the tree is labeled with the state S_i. The state trellis diagram can be derived from the phase tree by viewing the phases modulo 2π. By folding the phase tree into a cylinder, the so-called phase cylinder is obtained, which was illustrated in Chapter 2. The receiver observes the signal $r(t) = s(t,\boldsymbol{a}) + n(t)$, where the noise $n(t)$ is AWGN. The maximum likelihood sequence estimating (MLSE) receiver maximizes the following log likelihood function,

$$\log_e[p_{r(t)|\tilde{\boldsymbol{a}}}(r(t)|\tilde{\boldsymbol{a}}) \approx \int_{-\infty}^{\infty} [r(t) - s(t,\tilde{\boldsymbol{a}})]^2 dt \qquad (4.16)$$

with respect to the *infinitely* long estimated sequence $\tilde{\boldsymbol{a}}$. The maximizing sequence $\tilde{\boldsymbol{a}}$ is the maximum likelihood sequence estimate and $p_{r(t)|\tilde{\boldsymbol{a}}}$ is the probability density function for the observed signal $r(t)$ conditioned on the infinitely long sequence $\boldsymbol{a}$. It is equivalent to maximize the correlation

$$J(\tilde{\boldsymbol{a}}) = \int_{-\infty}^{\infty} r(t)s(t,\tilde{\boldsymbol{a}})dt \tag{4.17}$$

In principle, Equation 4.18 states the basic principle for a correlation receiver, in which all possible transmitted signals $s(t,\tilde{\boldsymbol{a}})$ are correlated with the received signal and the data sequence $\tilde{\boldsymbol{a}}$ maximizing the correlation is chosen as the received data. This is not a feasible structure in practice, not even with reasonably short data bursts. That is due to the sheer number of correlations associated with an n-bit long sequence, which is 2^n correlations. Now define

$$J_i(\tilde{\boldsymbol{a}}) = \int_{-\infty}^{iT} r(t)s(t,\tilde{\boldsymbol{a}})dt \tag{4.18}$$

Thus, we can write

$$J_i(\tilde{\boldsymbol{a}}) = J_{i-1}(\tilde{\boldsymbol{a}}) + Z_i(\tilde{\boldsymbol{a}}) \tag{4.19}$$

where

$$Z_i(\tilde{\boldsymbol{a}}) = \int_{(i-1)T}^{iT} r(t)\cos[2\pi f_c t + \phi(t,\tilde{\boldsymbol{a}})]\,dt \tag{4.20}$$

By using the above formulas it is possible to calculate the function $J_i(\tilde{\boldsymbol{a}})$ recursively through Equation 4.20 and the metric $Z_i(\tilde{\boldsymbol{a}})$. This metric can be recognized as a correlation between the received signal and an estimated signal over the i^{th} symbol interval. The possible extensions of those sequences are portrayed in the state trellis shown in Chapter 2. The receiver computes $Z_i(\tilde{\boldsymbol{a}}_i, \tilde{\theta}_i)$ for all M possible sequences $\tilde{\boldsymbol{a}}_i$ and all p possible $\tilde{\theta}_i$. This makes pM different values of Z_i. Rewriting Equation 4.20 using Equation 4.14 yields

$$Z_i(\tilde{\boldsymbol{\alpha}}_i, \tilde{\theta}_i) = \int_{(i-1)T}^{iT} r(t) \cos\left[2\pi f_c t + \theta(t, \tilde{\boldsymbol{\alpha}}_i) + \tilde{\theta}_i\right] dt \qquad (4.21)$$

Now, it can be seen that $Z_i(\tilde{\boldsymbol{\alpha}}_i, \tilde{\theta}_i)$ is obtained by feeding the signal $r(t)$ into a filter and sampling the output of the filter at $t = iT$; and that a bank of such filters must be used. The receiver correlates the received signal over *one symbol interval* with all possible transmitted alternatives over that symbol interval. By using the finite state description of the signals, the correlation receiver can now be implemented without *exponential growth* of the number of receiver signal alternatives. The noise $n(t)$ can be expressed in the band-pass form

$$n(t) = x(t) \cos 2\pi f_c t - y(t) \sin 2\pi f_c t \qquad (4.22)$$

Using the basic quadrature receiver of Figure 4.5, the received quadrature components are

$$\hat{I}(t) = \left[\sqrt{\frac{2E_b}{T}}\, I(t) + x(t)\right] \qquad (4.23)$$

$$\hat{Q}(t) = \left[\sqrt{\frac{2E_b}{T}}\, Q(t) + y(t)\right] \qquad (4.24)$$

The LP-filters only remove double carrier frequency terms. Thus,

$$r(t) = I(t) \cos(2\pi f_c t) - Q(t) \sin(2\pi f_c t) + n(t) \qquad (4.25)$$

By inserting these components in $Z_i(\tilde{\boldsymbol{\alpha}}_i, \tilde{\theta}_i)$ and omitting double frequency terms, we have

$$Z_i(\tilde{\boldsymbol{\alpha}}_i, \tilde{\theta}_i) = \cos\tilde{\theta}_i \int_{(i-1)T}^{iT} \hat{I}(t) \cos[\theta(t, \tilde{\boldsymbol{\alpha}}_i)]\, dt + \cos\tilde{\theta}_i \int_{(i-1)T}^{iT} \hat{Q}(t) \sin[\theta(t, \tilde{\boldsymbol{\alpha}}_i)]\, dt$$
$$+ \sin\tilde{\theta}_i \int_{(i-1)T}^{iT} \hat{Q}(t) \cos[\theta(t, \tilde{\boldsymbol{\alpha}}_i)]\, dt - \sin\tilde{\theta}_i \int_{(i-1)T}^{iT} \hat{I}(t) \sin[\theta(t, \tilde{\boldsymbol{\alpha}}_i)]\, dt \qquad (4.26)$$

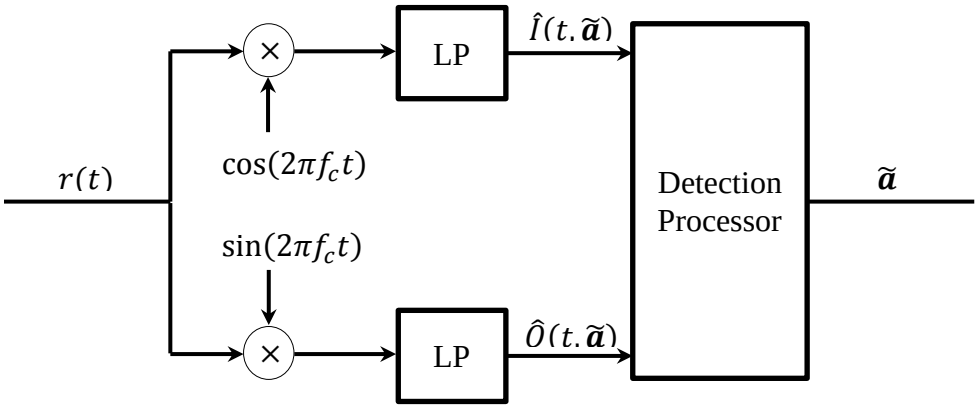

Figure 4.5 Basic Quadrature Receiver

Note that the receiver of Chapter 3 is optimum with a different criterion. It finds the optimum estimate of the first data symbol. In its basic form, the Viterbi algorithm assumes that all possible transmitted finite sequences start from one common state and end in another common state. The decision about the most likely transmitted sequence is delayed at the receiver until the whole sequence is received. The metrics of all candidate state paths are successively updated at each trellis section; all possible state transitions are extended and all paths are deleted at the next trellis section except the path with highest likelihood entering each node. When the whole signal sequence is received, all candidate state paths terminate in the same common node at the far end of the trellis, and the most likely of these is the MLSE output.

The performance of the Viterbi detector is the same as that of the MLRT-based derived receiver in the sense they are both optimum. This is being said, the MLRT-based receiver performance would meet the Viterbi receiver performance as $n \to \infty$ in both cases. Where it is mathematically complex and hard to implement the MLRT-based receiver, the Viterbi receiver offers a solution by dividing the detection problem into its corresponding bit intervals, at the expanse of having delays. Using the upper bound distance criteria D_B^2 for both CPFSK and CPCK, the upper bounds on performance of the Viterbi receiver for CPFSK and CPCK are shown in Figure 4.6. Matching the conclusion from Chapter 3, CPCK provides superior BER performance to that of CPFSK due to CPCK's design flexibility. From this Figure, it is noted that CPCK has SNR advantage of nearly 1 dB and 2 dB over CPFSK and BPSK, respectively.

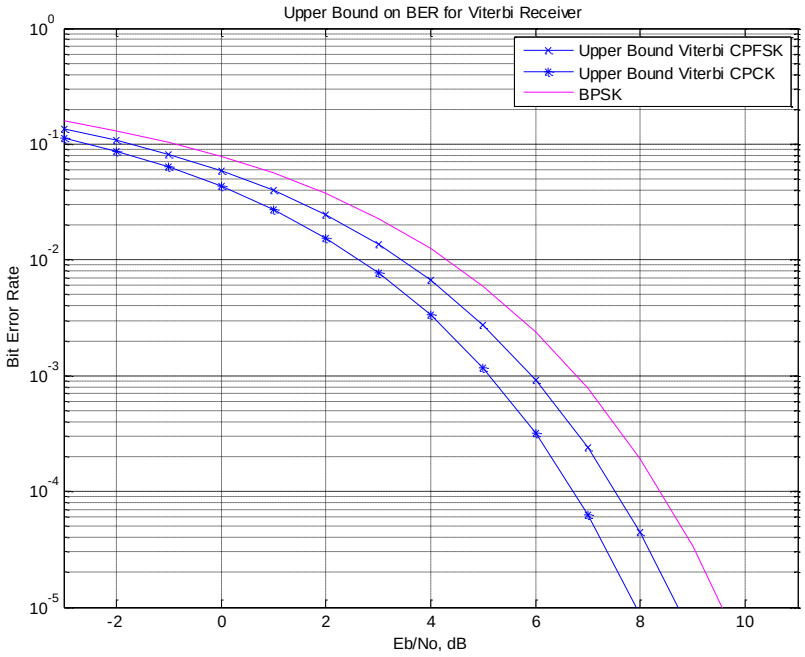

Figure 4.6: Upper Bounds on Viterbi Receiver for CPFSK and CPCK

4.3 Summary and Results

In this Chapter, we studied the minimum distance properties for both signaling schemes, CPFSK and CPCK, and values of optimum operation were provided. Advantages in term of SNR of these optimum systems were highlighted relative to that of PSK. For CPFSK, it was shown that the maximum minimum distance between two transmitted sequences, $\max\{D_n^2\} = {D_B}^2 = 2.434$ is attained at $h = 0.715$, and thus, the upper bound on the SNR gain G_n is limited to about 0.85 dB. Since the upper bound is associated with a certain constraint on the sequence transmitted, the actual $\max\{D_n^2\} \leq {D_B}^2$ is attained at $h = 0.71$, close to the optimum upper bound h. Moreover, it was illustrated that no significant SNR gain is attainable for CPFSK with $n > 3$. So $n = 3$ can be called the optimum observation interval, where further observations don't add benefits to the system and only causes exponential growth in the receiver's complexity. For CPCK, it was shown that the maximum minimum distance between two transmitted sequences, $\max\{D_n^2\} = {D_B}^2 = 2.93$ is attained at $(q, w) = (0.2.4)$, and thus, the upper bound on the SNR gain G_n is limited to about 1.66 dB. ${D_B}^2(q, w)$ has many local maxima for integer values of q and the global maxima reported previously at $(q, w) = (0.2.4)$. ${D_B}^2(q, 0)$ is the CPFSK case,

reported previously as $D_B{}^2(h)$. By manipulating q and restricting the values assigned to it, one can arrive at simpler expressions for the $D_n{}^2(q,w)$. The actual $D_n{}^2$ will always be smaller than the global maxima of its bound. For some $q \neq 0, \pm 1, \pm 2, ...$, however, a $D_n{}^2$ close to the global maxima may be obtained. Computer simulations were carried out in order to find the parameters maximizing $D_n{}^2$ and G_n for different n, q and w. It was noticed that SNR gain increase is not as major from $n = 3$ to $n = 4$ and we are approaching the upper bound value for SNR gain of 1.66 dB. So, $n = 4$ was taken as the optimum observation interval, where further observations didn't add major benefits to the system. SNR gains for CPFSK and CPCK were reported at the corresponding sections.

Studying the distance properties for CPFSK and CPCK was necessary in order to prepare for the discussion of the other type of CPM signals receiver, which is the Viterbi receiver. The Viterbi receiver is based on the maximum-likelihood sequence estimation (MLSE) theory, which searches for the minimum Euclidean distance path through the trellis that characterizes the memory in the transmitted signal. Upper bounds results using Viterbi receiver were reported for CPFSK and CPCK. Matching the conclusion from Chapter 3, CPCK provides superior BER performance to that of CPFSK due to CPCK's design flexibility. Using the upper bound distance criteria D_B^2 for both CPFSK and CPCK, the upper bounds on performance of the Viterbi receiver for optimum CPFSK; $h = 0.715$, and CPCK; $(q,w) = (0,2.4)$, were found. It showed that CPCK provides superior BER performance to that of CPFSK due to CPCK's design flexibility. It was noted that CPCK has SNR advantage of nearly 1 dB and 2 dB over CPFSK and BPSK, respectively.

To demonstrate the complexity reduction by the Viterbi receiver, we take a simple example. In an n-long sequence, for the MLRT-based receiver, there are M^n possibilities, where M is the modulation order, that needs to correlate the received signal with. And it is noticed that the growth in complexity is exponential. Where in the Viterbi receiver, the correlation process is taken down to the bit-interval level instead of the full sequence duration-level, as in the case of MLRT-based receiver. At each bit duration, there are pM correlations, where $h = 2v/p$. So the total number of correlations is n-multiple of pM. These correlations constitute the distance metric, in which the Viterbi algorithm looks for

the path with the minimum distance. For example, if $n = 10$, in the case of binary modulation, MLRT-based receiver needs to perform $2^{10} = 1024$ correlations, where in the Viterbi, with $h = 1/2$, it is only $10 \times 4 \times 2 = 80$. Nevertheless, this comes at the expense of delaying the outputs and the fact that the Viterbi is only optimum as $n \to \infty$. It is also noticed that the value of h does effect the number of computations performed by the Viterbi detector, which has been emphasized in finding the upper bound of Viterbi BER. Viterbi's superiority over MLRT-based receiver in terms of the number of correlations is only true for a certain threshold, $n \geq n_{TH}$. For $n < n_{TH}$, the MLRT-based receiver has the edge in terms of the number of correlations over the Viterbi receiver. Viterbi detector is the practical implementation of Maximum Likelihood Detection for CPFSK and CPCK signals. Figure 4.7 shows a comparison between the MLRT-based receiver and the Viterbi receiver in terms of the number of required correlations, and how the h affects the Viterbi's number of computations.

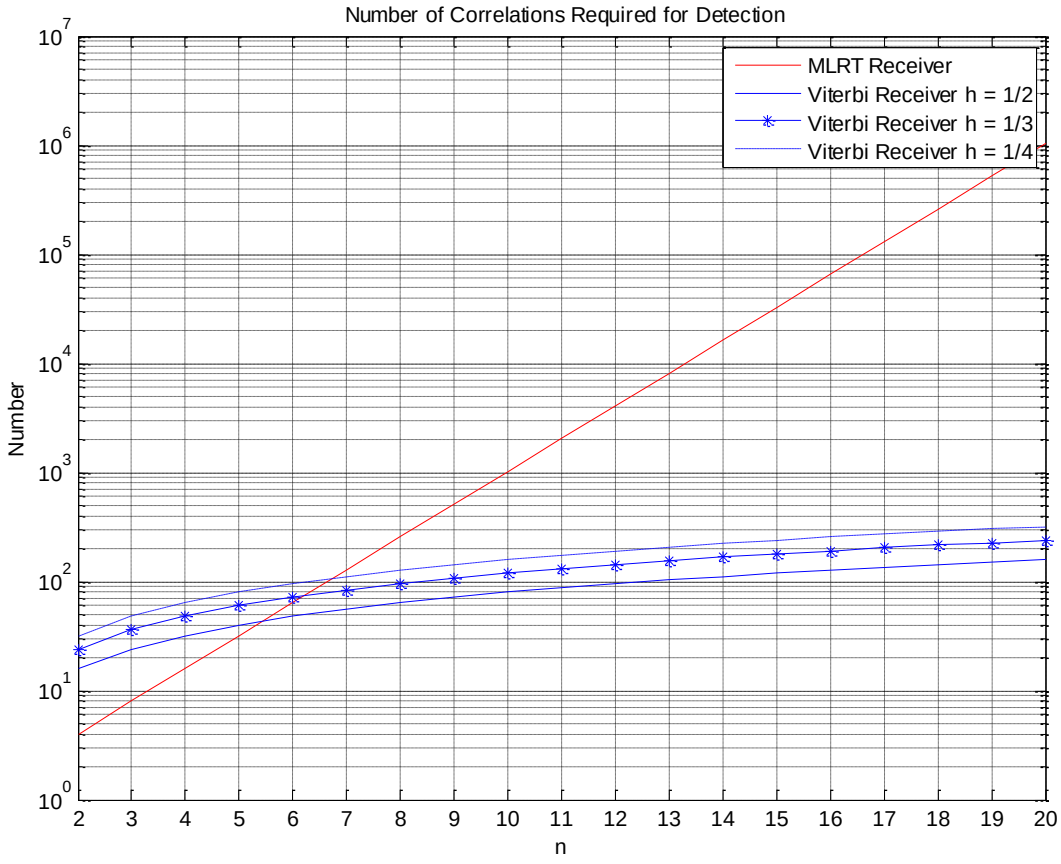

Figure 4.7: Number of Correlations vs. n

Chapter 5

Decision Aided Detection of CPFSK and CPCK

The successful application of CPFSK and CPCK signaling techniques for reliable transmission of digital data over communication channels requires complex signal processing techniques. Both CPFSK and CPCK offer tradeoffs among power, bandwidth and signal processing complexity. It is evident from Chapters 3 and 4 that receivers for these signaling techniques are quite complex and the complexity grows exponentially with the number of observed symbols in the detection process. Therefore, it is of interest to explore alternative receivers that are less complex and yet perform close to that of the optimum. Thus, the intent of this Chapter is to present a Decision Aided Receiver (DAR) based on heuristics as an alternative for the AMF receiver that is optimum at low values of SNR. Decision aided detection strategy is presented and explicit expressions for computation of BER are developed for AWGN environment.

5.1 DAR Structure and Detection Strategy

The received signal over n-bit interval contaminated with AWGN with one-sided spectral density of N_o watts/Hz can be modeled as:

$$r(t) = s(t, \boldsymbol{a}) + n(t), \qquad 0 \le t \le nT \tag{5.1}$$

Where $n(t)$ is the noise process and during the interval $0 \le t \le T$, the signal $s(t, \boldsymbol{a})$ is given by

$$s(t, \boldsymbol{a}) = \begin{Bmatrix} \sqrt{2s}\cos\left(2\pi f_c t + \dfrac{a_1 \pi h t}{T}\right) & ; \quad CPFSK \\ \sqrt{2s}\cos\left(2\pi f_c t + a_1 \pi \left\{\dfrac{ht}{T} - w\left(\dfrac{t}{T}\right)^2\right\}\right); & \quad CPCK \end{Bmatrix} \tag{5.2}$$

where s is the signal power, f_c is the carrier frequency, $a_1 = \pm 1$ is the data in the first bit interval and h and w represent the modulation parameters and are defined in Chapter 2. In Equation 5.1, $\boldsymbol{a}$ is an n-bit binary data sequence given by $\boldsymbol{a} = (a_1, a_2, a_3 \ldots, a_n)$. The signal during the i^{th} bit interval is given by

$$s(t, \boldsymbol{a})$$

$$= \begin{Bmatrix} \sqrt{2s}\cos\left(2\pi f_c t + \dfrac{a_i \pi h (t - (i-1)T)}{T} + \pi h \sum_{j=1}^{i-1} a_j\right) & ; \ CPFSK \\ \sqrt{2s}\cos\left(2\pi f_c t + a_1 \pi \left\{\dfrac{h(t-(i-1)T)}{T} - w\left(\dfrac{(t-(i-1)T)}{T}\right)^2\right\} + \pi h \sum_{j=1}^{i-1} a_j\right); & CPCK \end{Bmatrix}$$

(5.3)

The detection strategy consists of observing the received waveforms given in Equation 5.1 and to produce an estimate of the data transmitted during the first bit interval using the algorithm given in Table 5.1.

Table 5.1: DAR Detection Algorithm

Step 1
$1 \rightarrow i, 1 \rightarrow j$ Observe $r(t)$ during $0 \leq t \leq T$ using the receiver shown in Figure 5.2 and obtain estimate of transmitted data a_1, i.e. $\hat{a}_{ij}$. Determine $P_e(\hat{a}_{ij})$; $j + 1 \rightarrow j$
Step 2
Use estimates $\hat{a}_{ip}$, $p = 1,2, \dots, (j-1)$, observe $r(t)$ over $(j-1)T \leq t \leq jT$ using receiver in Figure 5.2; obtain estimate of data a_j, i.e. $\hat{a}_{ij}$ $j + 1 \rightarrow j$ If $(j \leq n)$, go to step 2;
Step 3
$i \rightarrow k, i + 1 \rightarrow i$ Use $\hat{a}_{kp}$, $p = 2,3, \dots, n$, observe $r(t)$ over $0 \leq t \leq nT$ using the receiver in Figure 5.3. Obtain refined estimate of data a_1, i.e. $\hat{a}_{i1}$. Determine $P_e(\hat{a}_{ik})$; If $P_e(\hat{a}_{k1}) < P_e(\hat{a}_{i1})$; go to step 4 $j \rightarrow 2$ Go to step 2;
Step 4
Stop

The detection strategy given above is also captured using a flow chart shown in Figure 5.1. The DAR strategy consists of observing the received waveform ($r(t) = s(t, \boldsymbol{a}) + n(t)$) during $0 \leq t \leq T$ and obtain an estimate $\hat{a}_{11}$, of data a_1. Using $\hat{a}_{11}$ and observing $r(t)$ over $T \leq t \leq 2T$, we obtain $\hat{a}_{12}$ of data a_2. Next, using $(\hat{a}_{11}, \hat{a}_{12})$, we obtain $\hat{a}_{13}$ of data a_3 during the third bit interval. This process is continued until we obtain $(\hat{a}_{11}, \hat{a}_{12}, \dots, \hat{a}_{1n})$. Using the last $n-1$ of these estimates $(\hat{a}_{12}, \hat{a}_{13}, \dots, \hat{a}_{1n})$ and observing the received waveform over $0 \leq t \leq nT$, a refined estimate of data a_1, i.e. $\hat{a}_{21}$ is obtained. The detection process is stopped or continued depending on whether or not an improvement in the estimate of the first bit data is obtained relative to the previous estimate of the first bit data. In the next section, we present the performance analysis of the algorithm for CPFSK and CPCK signaling techniques.

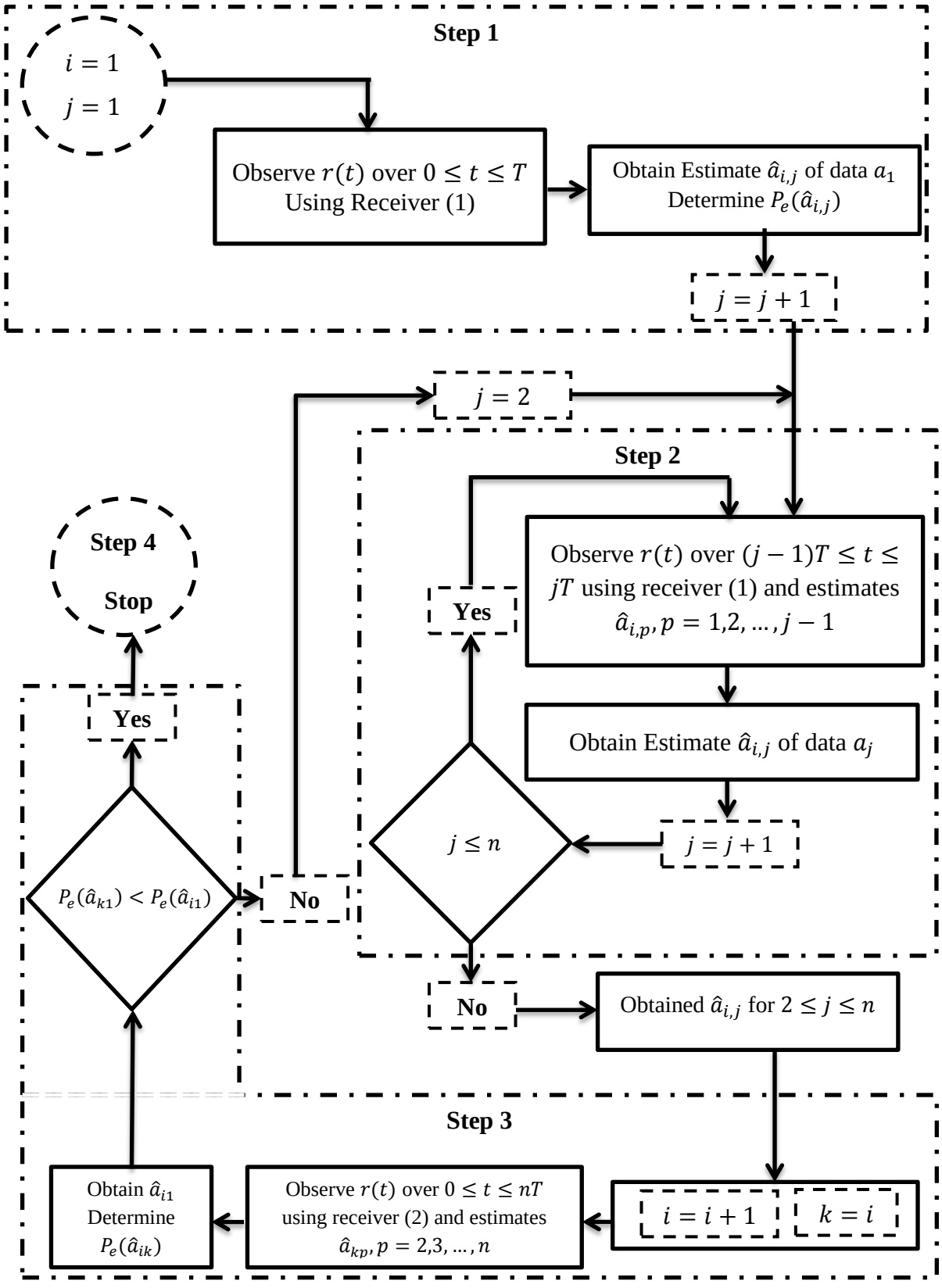

Figure 5.1: DAR Detection Strategy Flow Chart

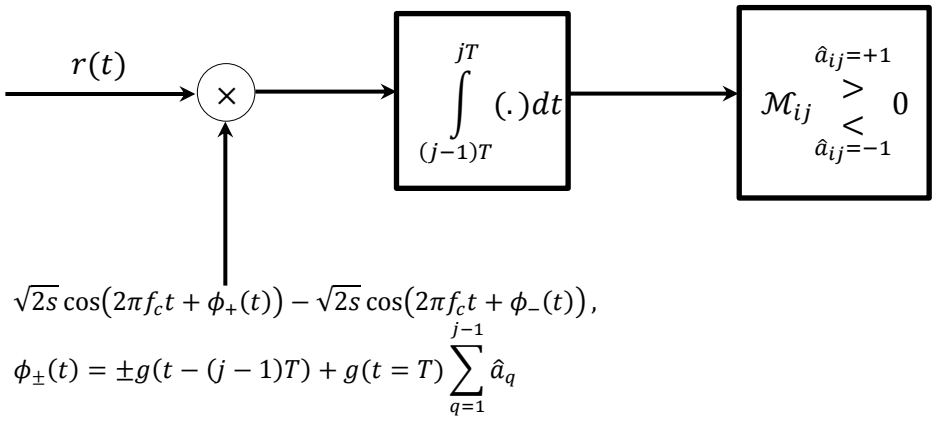

Figure 5.2: DAR for Obtaining Estimates $\hat{a}_{ij}$, $i = 1, 2, \ldots$; and $j = 1, 2, \ldots n$

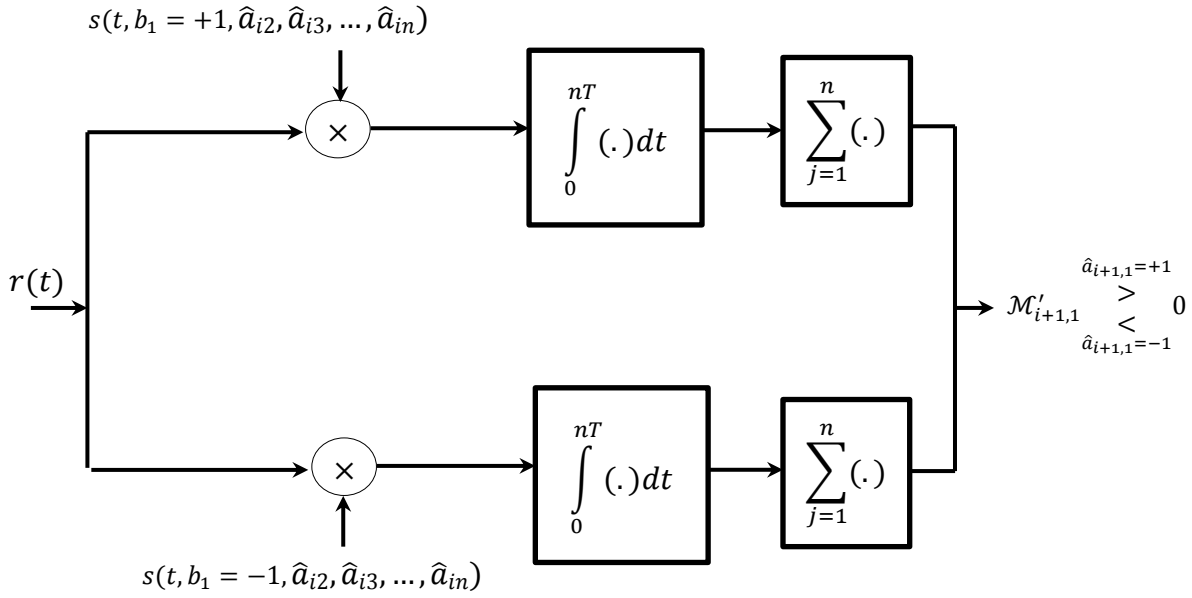

Figure 5.3: DAR for Obtaining Refined Estimates $\hat{a}_{i+1,1}$; $i = 1, 2, \ldots$

5.2 Performance Analysis of DAR

The receiver shown in Figure 5.2 is used to obtain the first set of n estimates. The received waveform during the first bit interval is correlated with the reference signal $y_{i1}(t)$, ($i = 1$ for the first bit interval) to generate $\mathcal{M}_{i,1}$, which is given by

$$\mathcal{M}_{i,1} = \int_0^T r(t) y_{i1}(t) dt \tag{5.4}$$

where

$$y_{i1}(t) = s_1(t, b_1 = +1) - s_1(t, b_1 = -1) \tag{5.5}$$

It is noted that the n-bit length reference signal is represented by $s(t, \boldsymbol{b})$, where $s_j\left(t, \hat{a}_{i,1}, \hat{a}_{i,2}, \dots, \hat{a}_{i,j-1}, b_j = +1\right)$ is used to denote the j^{th} bit reference waveform. The receiver depending upon whether $\mathcal{M}_{i,1}$ is greater or less than 0, produces an estimate of a_1 denoted by $\hat{a}_{i,1}$ to be either a $+1$ or a -1. Using $\hat{a}_{i,1}$ and observing the received waveform during the second bit interval, the receiver generates $\mathcal{M}_{i,2}$, which is given by

$$\mathcal{M}_{i,2} = \int_T^{2T} r(t) y_{i2}(t) dt \tag{5.6}$$

where

$$y_{i2}(t) = s_2\left(t, \hat{a}_{1,1}, b_2 = +1\right) - s_2\left(t, \hat{a}_{1,1}, b_2 = -1\right) \tag{5.7}$$

$\mathcal{M}_{i,2}$ is compared with 0 to produce $\hat{a}_{1,2}$ of transmitted data a_2. Likewise, during the j^{th} bit interval, the receiver generates

$$\mathcal{M}_{i,j} = \int_{(j-1)T}^{jT} r(t) y_{ij}(t) dt \tag{5.8}$$

where

$$y_{ij}(t) = s_j\left(t, \hat{a}_{i,1}, \hat{a}_{i,2}, \dots, b_j = +1\right) - s_j\left(t, \hat{a}_{i,1}, \hat{a}_{i,2}, \dots, b_j = -1\right) \tag{5.9}$$

$\mathcal{M}_{i,j}$ is compared with 0 to produce an estimate $\hat{a}_{i,j}$ of transmitted data a_j. Expanding Equation 5.8 and using Equations 5.1, 5.2 and 5.3, we obtain,

$$\mathcal{M}_{i,j} = A_{i,j} + N_{i,j} \tag{5.10}$$

where $A_{i,j}$ is the signal term and $N_{i,\boldsymbol{j}}$ is the noise term. These are given by

$$A_{i,j} = \int_{(j-1)T}^{jT} s_j\left(t, a_1, a_2, \dots, a_j, a_{j+1}, \dots, a_n\right)\left[s_j\left(t, \hat{a}_{i,1}, \hat{a}_{i,2}, \dots, b_j = +1\right)\right.$$
$$\left. - s_j\left(t, \hat{a}_{i,1}, \hat{a}_{i,2}, \dots, b_j = -1\right)\right] dt \quad (5.11)$$

$$N_{i,j} = \int_{(j-1)T}^{jT} n(t)\left[s_j\left(t, \hat{a}_{i,1}, \hat{a}_{i,2}, \dots, b_j = +1\right)\right.$$
$$\left. - s_j\left(t, \hat{a}_{i,1}, \hat{a}_{i,2}, \dots, b_j = -1\right)\right] dt \quad (5.12)$$

Once estimates $(\hat{a}_{i1}, \hat{a}_{i2}, \dots, \hat{a}_{in})$ are obtained of data $(a_1, a_2, \dots, a_n)$, the receiver shown in Figure 5.3 is used along with $(n-1)$ estimates $(\hat{a}_{i2}, \hat{a}_{i3}, \dots, \hat{a}_{in})$ and $r(t)$ over $0 \le t \le nT$ to obtain a refined estimate $\hat{a}_{i+1,1}$. The receiver in Figure 5.3 computes,

$$\mathcal{M}'_{i+1,1} = \int_0^{nT} r(t)[s(t, b_1 = +1, \hat{a}_{i2}, \hat{a}_{i3}, \dots, \hat{a}_{in}) - s(t, b_1 = -1, \hat{a}_{i2}, \hat{a}_{i3}, \dots, \hat{a}_{in})]dt$$

$$= A'_{i+1,1} + N'_{i+1,1} \quad (5.13)$$

where

$$A'_{i+1,1} = \int_0^{nT} s(t, a)[s(t, b_1 = +1, \hat{a}_{i2}, \hat{a}_{i3}, \dots, \hat{a}_{in})$$
$$- s(t, b_1 = -1, \hat{a}_{i2}, \hat{a}_{i3}, \dots, \hat{a}_{in})]dt \quad (5.14)$$

$$N'_{i+1,1} = \int_0^{nT} n(t)[s(t, b_1 = +1, \hat{a}_{i2}, \hat{a}_{i3}, \dots, \hat{a}_{in})$$
$$- s(t, b_1 = -1, \hat{a}_{i2}, \hat{a}_{i3}, \dots, \hat{a}_{in})]dt \quad (5.15)$$

The estimate is $\hat{a}_{i+1,1} = +1$ if $\mathcal{M}'_{i+1,1} \ge 0$ and $\hat{a}_{i+1,1} = -1$ if $\mathcal{M}'_{i+1,1} < 0$. Using $\hat{a}_{i+1,1}$ and the receiver in Figure 5.2, the detection process is continued to obtain the remaining $(n-1)$ refined estimates $(\hat{a}_{i+1,2}, \hat{a}_{i+1,3}, \dots, \hat{a}_{i+1,n})$. The detection process is stopped or continued by checking at every refinement $\hat{a}_{i,1}$ of a_1 whether or not the probability of error in refinement has improved or not. That is $P_e\left(\hat{a}_{i+1,1}\right) < P_e(\hat{a}_{i1})$. Since $\mathcal{M}_{i,j}$ and $\mathcal{M}'_{i,j}$ are Gaussian random variables, we need to find their mean and variance is order to

estimate the performance of the DAR. Denoting the transmitted data sequence by $\boldsymbol{a} = (a_1, A_k)$ and the n estimates by $C_q = (\hat{a}_{i1}, \hat{a}_{i2}, \dots, \hat{a}_{in})$, the conditional probability that $\hat{a}_{21}$is in error ($i = 2$, second iteration) is given by

$$P_e\left(\hat{a}_{2,1}\middle|A_k, C_q\right) = \Pr[\mathcal{M}'_{2,1} < 0\middle|a_1 = +1, A_k, C_q]P\left(a_1 = +1, A_k, C_q\right)$$

$$+ \Pr[\mathcal{M}'_{2,1} > 0\middle|a_1 = -1, A_k, C_q]P\left(a_1 = -1, A_k, C_q\right)$$

$$= \Pr[\mathcal{M}'_{2,1} < 0\middle|a_1 = +1, A_k, C_q]P\left(a_1 = +1, A_k, C_q\right) \qquad (5.16)$$

Averaging over all possible $A_k = (a_2, a_3, \dots, a_n)$ and C_q, we obtain,

$$P_e\left(\hat{a}_{2,1}\right) = \sum_{A_k}\sum_{C_q} P\left(A_k, C_q|a_1 = +1\right) \times \Pr[\mathcal{M}'_{2,1} < 0\middle|a_1 = +1, A_k, C_q] \qquad (5.17)$$

where

$$P\left(A_k, C_q|a_1 = +1\right) = P(a_2, a_3, \dots, a_n;\ \hat{a}_{11}, \hat{a}_{12}, \dots, \hat{a}_{1n}|a_1 = +1) \qquad (5.18)$$

which upon simplification yields,

$$P\left(A_k, C_q|a_1 = +1\right) =$$
$$P\left(\hat{a}_{1n}\middle|a_1 = +1, a_2, a_3, \dots, a_n, \hat{a}_{11}, \hat{a}_{12}, \dots, \hat{a}_{1,n-1}\right) \times$$
$$P\left(\hat{a}_{1,n-1}\middle|a_1 = +1, a_2, a_3, \dots, a_n, \hat{a}_{11}, \hat{a}_{12}, \dots, \hat{a}_{1,n-2}\right) \times$$
$$\dots \dots \dots \dots \dots \dots \dots \dots \dots \dots \dots \dots \dots \dots \dots \dots \dots \dots \dots \dots \dots \dots \dots .. \times$$
$$P\left(\hat{a}_{1,1}\middle|a_1 = +1\right). P(a_n)P(a_{n-1}) \dots P(a_2) \qquad (5.19)$$

where

$$a_j = +1 \rightarrow P\left(\hat{a}_{1,j}|a_1 = +1, a_2, a_3, \dots, a_j = +1, \hat{a}_{11}, \hat{a}_{12}, \dots, \hat{a}_{1,j-1}\right)$$

$$= \Pr[\mathcal{M}_{1,j} > 0\middle|a_1 = +1, a_2, a_3, \dots, a_j = +1, \hat{a}_{11}, \hat{a}_{12}, \dots, \hat{a}_{1,j-1}]$$

$$Q\left[\frac{E\left[\mathcal{M}_{1,j}|a_1=+1,a_2,a_3,\ldots,a_j=+1,\hat{a}_{11},\hat{a}_{12},\ldots,\hat{a}_{1,j-1}\right]}{\sqrt{Variance\left[\mathcal{M}_{1,j}|a_1=+1,a_2,a_3,\ldots,a_j=+1,\hat{a}_{11},\hat{a}_{12},\ldots,\hat{a}_{1,j-1}\right]}}\right]$$

$$a_j=-1\rightarrow P\left(\hat{a}_{1,j}|a_1=+1,a_2,a_3,\ldots,a_j=-1,\hat{a}_{11},\hat{a}_{12},\ldots,\hat{a}_{1,j-1}\right)$$

$$=\Pr\left[\mathcal{M}_{1,j}<0\middle|a_1=+1,a_2,a_3,\ldots,a_j=-1,\hat{a}_{11},\hat{a}_{12},\ldots,\hat{a}_{1,j-1}\right]$$

$$1-Q\left[\frac{E\left[\mathcal{M}_{1,j}|a_1=+1,a_2,a_3,\ldots,a_j=+1,\hat{a}_{11},\hat{a}_{12},\ldots,\hat{a}_{1,j-1}\right]}{\sqrt{Variance\left[\mathcal{M}_{1,j}|a_1=+1,a_2,a_3,\ldots,a_j=+1,\hat{a}_{11},\hat{a}_{12},\ldots,\hat{a}_{1,j-1}\right]}}\right] \quad (5.20)$$

To compute Equation 5.17, we need to compute

$$\Pr\left[\mathcal{M}'_{2,1}<0\middle|a_1=+1,A_k,C_q\right]=$$

$$Q\left[\frac{E\left[\mathcal{M}'_{2,1}<0\middle|a_1=+1,A_k,C_q\right]}{\sqrt{Variance\left[\mathcal{M}'_{2,1}<0\middle|a_1=+1,A_k,C_q\right]}}\right] \quad (5.21)$$

where

$$Q(x)\triangleq\frac{1}{\sqrt{2\pi}}\int_x^\infty \exp\left(-\frac{t^2}{2}\right)dt \quad (5.22)$$

The mean and the variances required in the evaluation of Equation 5.17 can be computed via Equations 5.10, 5.11 and 5.12 and Equations 5.13, 5.14 and 5.15, respectively. The performance of the DAR given by Equation 5.17, represents the average probability of bit error in deciding data transmitted in the first bit interval. The error probability performance of the DAR, $P_e\left(\hat{a}_{2,1}\right)$, is a function of: i) E_b/N_0, Signal-to-Noise Ratio; ii) modulation parameters (h for CPFSK, q and w for CPCK); and iii) n, observation length of DAR. The set of modulation parameters that should be chosen for a given n and E_b/N_0, is the one that minimizes $P_e\left(\hat{a}_{2,1}\right)$.Closed form expressions for CPFSK and CPCK are given next.

5.2.1 DAR Performance of CPFSK

We start by finding the mean and variance for receiver 1 output $\mathcal{M}_{1,j}$ according to Equation 5.20 and it can be shown that

$$E\left[\mathcal{M}_{1,j}|a_1=+1,a_2,a_3,\dots,a_j,\hat{a}_{11},\hat{a}_{12},\dots,\hat{a}_{1,j-1}\right]$$
$$= E_b\left[\operatorname{sinc}\left[\frac{(a_j-1)h}{2}\right]\cos\left[\pi\frac{(a_j-1)h}{2}+\theta_j\right]\right.$$
$$\left.-\operatorname{sinc}\left[\frac{(a_j+1)h}{2}\right]\cos\left[\pi\frac{(a_j+1)h}{2}+\theta_j\right]\right] \quad (5.23)$$

Variance $\left[\mathcal{M}_{1,j}\middle|a_1=+1,a_2,a_3,\dots,a_j,\hat{a}_{11},\hat{a}_{12},\dots,\hat{a}_{1,j-1}\right]$

$$= E_bN_o[1-\operatorname{sinc}(2h)] \quad (5.24)$$

Now, we need to find the mean and variance for receiver 2 output $\mathcal{M}'_{2,1}$ according to Equation 5.21 and it can be shown that

$$E[\mathcal{M}'_{2,1}|a_1=+1,A_k,C_q]$$
$$= E_b\left[1-\operatorname{sinc}(2h)\right.$$
$$\left.+2\sin(\pi h)\left(\sum_{p=2}^{n}\operatorname{sinc}\left(\frac{(a_p-\hat{a}_{1p})h}{2}\right)\sin\left(\frac{(a_p-\hat{a}_{1p})\pi h}{2}+\vartheta_p\right)\right)\right] \quad (5.25)$$

and

Variance $[\mathcal{M}'_{2,1}|a_1=+1,A_k,C_q]$

$$= E_bN_o[1-\operatorname{sinc}(2h)+2(n-1)\sin^2(\pi h)] \quad (5.26)$$

where

$$\theta_j=\pi h\sum_{p=1}^{j-1}(a_p-\hat{a}_{1p}),\qquad \vartheta_p=\pi h\sum_{r=2}^{p-1}(a_r-\hat{a}_{1r})$$

Figure 5.4 provides graphs for the performance of the DAR in comparison to the BPSK and AMF receiver for CPFSK, for different values of h. It is very hard to describe the behavior of the DAR, since it is based on heuristic considerations. Figure 5.4 (a) shows

that for $h = 0.3$, the 2-bit DAR provides an SNR gain = 1.44 dB relative to that of the 2-bit AMF receiver. For $h = 0.5$, 2-bit AMF receiver outperforms 2-bit DAR by 2.16 dB, and 2-bit DAR provides SNR gain of 1.10 dB relative to 2-bit AMF receiver at $h = 0.8$. This suggested studying the DAR performance at different values of h, which is shown in Figure 5.5. Moreover, the graphs of Figure 5.4 suggest that as h increases, the SNR value at which the DAR performance exceeds that of BPSK increases as well.

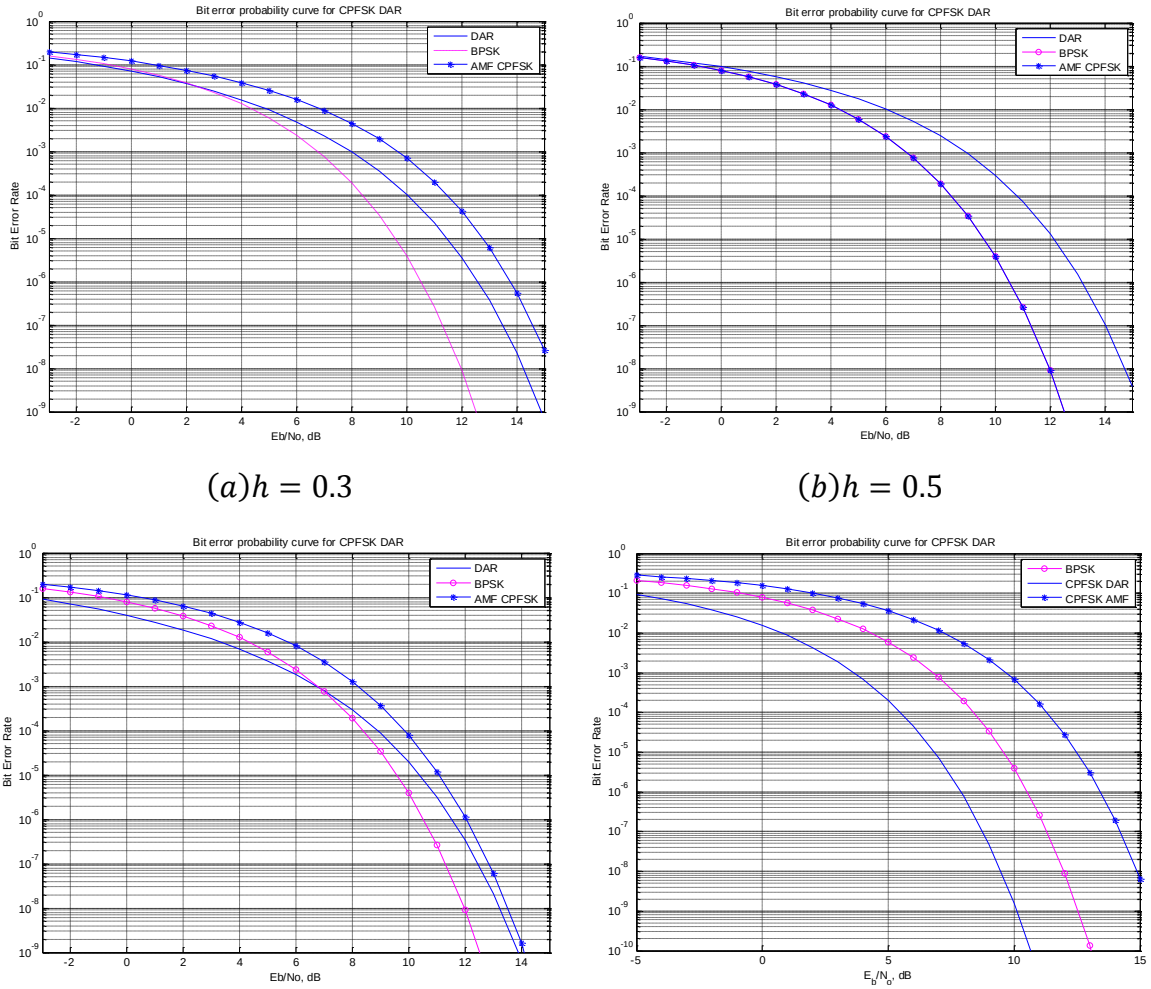

$(a) h = 0.3$ $(b) h = 0.5$

$(c) h = 0.7$ $(d) h = 0.8$

Figure 5.4: Performance, $P_e(\hat{a}_{2,1})$, of DAR for CPFSK for $n = 2$

Figure 5.5 shows the comparison between the AMF receiver and DAR performance $vs.\ h$ for different values of SNR. At each value of SNR, the BER performance $vs.\ h$ behaves differently for the DAR for CPFSK. However, at almost all values of SNR, DAR

dominates the performance, except for a portion on the h axis where AMF receiver outperforms the DAR, which supports the findings of Figure 5.4. From Figure 5.5 (a) and (b), the middle region where AMF receiver performance exceeds that of the DAR is $0.425 \leq h \leq 0.642$ and $0.395 \leq h \leq 0.690$, respectively. That range of the region varies as the SNR varies. From Figure 5.5 graph (c), we observe that for higher values of SNR, the DAR almost meets the performance of the AMF receiver for $h \geq 0.35$. In general, the graphs of Figure 5.5 shows that the DAR performance improves as h increases, where the AMF receiver performance improves up to $h = 0.5$, yielding BPSK performance, and degrades for $h \geq 0.5$.

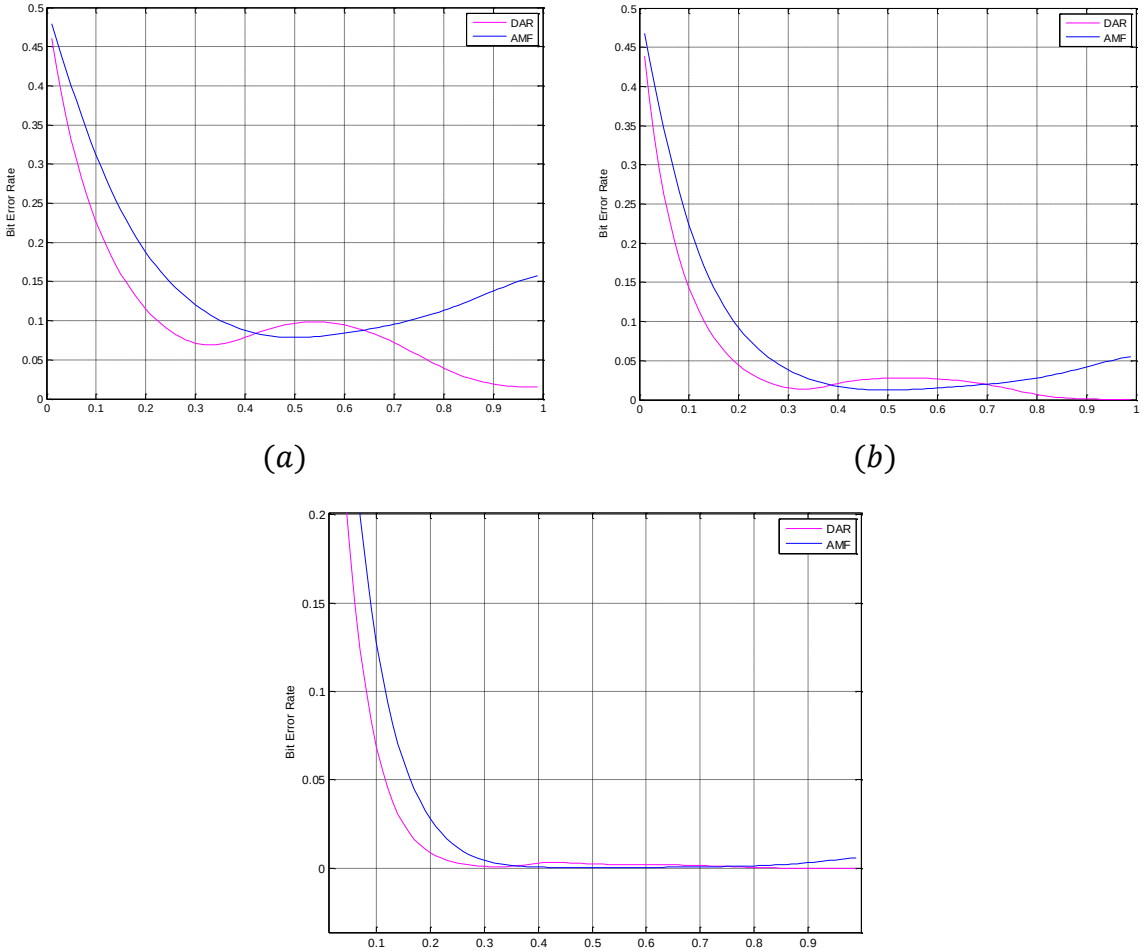

Figure 5.5: Normalized Performance, $P_e(\hat{a}_{2,1})$, of DAR and AMF receiver for CPFSK vs. h, $SNR = (a)$ 0 dB (b) 4 dB (c) 8 dB

Next we investigate the effect of n on the performance of DAR. Figures 5.6 and 5.7 show minimized BER performance of DAR for $0 < h < 1$ for $n = 2,3,4$ and 5.

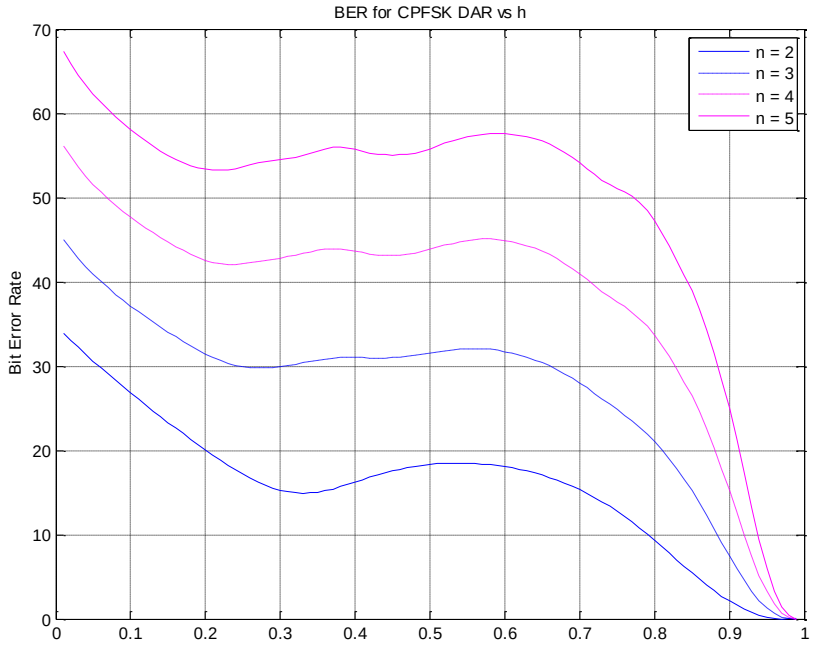

Figure 5.6: Normalized DAR Performance, $P_e(\hat{a}_{2,1})$, vs. h for $SNR = 0$ dB

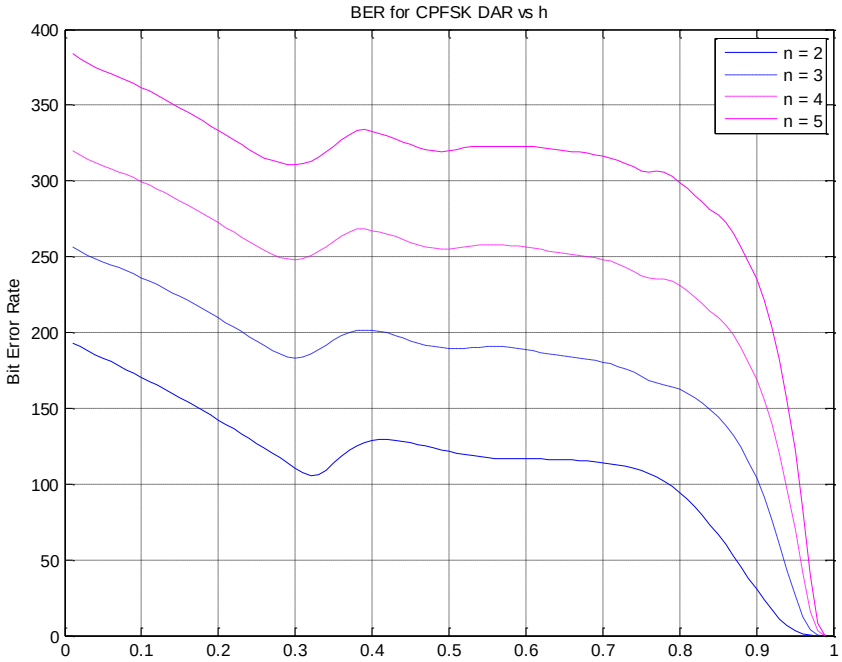

Figure 5.7: Normalized DAR Performance, $P_e(\hat{a}_{2,1})$, vs. h for $SNR = 10$ dB

Figures 5.6 and 5.7 show that as h increases beyond a specific value $h = h_{TH}$, BER drastically decreases; improves. Comparing the Figures 5.6 and 6.7, it is shown that for higher values of SNR, values of h at which the BER starts to drastically decrease, $h = h_{TH}$, becomes higher. For $SNR = 0$ dB at $h_{TH} = 0.6$, the BER starts decreasing and reaches its minimum value. For $SNR = 10$ dB at $h_{TH} = 0.8$, the BER starts decreasing and reaching its minimum value.

Moreover, studying the effect of n through Figures 5.6 and 5.7 showed that as n increases, values of h at which the BER starts to drastically decrease, $h = h_{TH}$, becomes higher. For example, at $SNR = 10$ dB for $n = 2,3,4$ and 5, $h_{TH} = 0.76,0.81,0.82$ and 0.83, respectively. It can be concluded that h_{TH}, after which the BER decreases rapidly, is a function of n and SNR. Also, Figures 5.6 and 5.7 show that as n increases, the performance of DAR degrades for all h. Next we analyze the CPCK DAR performance.

5.2.2 DAR Performance for CPCK

We start by finding the mean and variance for receiver 1 output $\mathcal{M}_{1,j}$ according to Equation 5.20 and it can be shown that

$$E\left[\mathcal{M}_{1,j}|a_1 = +1, a_2, a_3, \dots, a_j, \hat{a}_{11}, \hat{a}_{12}, \dots, \hat{a}_{1,j-1}\right] = \begin{cases} E_b\left(\cos\left(\theta_j\right) - \rho_+\right), & a_j = +1 \\ E_b\left(\rho_- - \cos\left(\theta_j\right)\right), & a_j = -1 \end{cases} \tag{5.27}$$

$$\text{Variance}\left[\mathcal{M}_{1,j}\middle|a_1 = +1, a_2, a_3, \dots, a_j, \hat{a}_{11}, \hat{a}_{12}, \dots, \hat{a}_{1,j-1}\right] = E_b N_o \left[1 - \left[\frac{\cos(\psi)}{2\sqrt{w}}\left[C[u_h] - C[u_l]\right] + \frac{\sin(\psi)}{2\sqrt{w}}\left[S[u_h] - S[u_l]\right]\right]\right] \tag{5.28}$$

where

$$\theta_j = \pi q \sum_{r=1}^{j-1}(a_r - \hat{a}_{1r}), \quad \rho_\pm = \frac{\cos(\psi \pm \theta_j)}{2\sqrt{w}}\left[C[u_h] - C[u_l]\right] + \frac{\sin(\psi \pm \theta_j)}{2\sqrt{w}}\left[S[u_h] - S[u_l]\right]$$

$$\psi = \frac{\pi(q+w)^2}{2w}, \qquad u_h = -\frac{h}{\sqrt{w}}, \qquad u_l = \frac{2w - h}{\sqrt{w}}$$

Now, we need to find the mean and variance for receiver 2 output $\mathcal{M}'_{2,1}$ according to Equation 5.21 and it can be shown that

$$E[\mathcal{M}'_{2,1}|a_1 = +1, A_k, C_q]$$
$$= E_b\left[1 - \frac{\cos(\psi)}{2\sqrt{w}}\left[C[u_h] - C[u_l]\right] + \frac{\sin(\psi)}{2\sqrt{w}}\left[S[u_h] - S[u_l]\right] + 2\sin(\pi q)\,\rho_{\pm}\big|_{i\geq 2}\right] \quad (5.29)$$

and

Variance $[\mathcal{M}'_{2,1}|a_1 = +1, A_k, C_q]$

$= E_b N_o\left[1 - \left[\frac{\cos(\psi)}{2\sqrt{w}}\left[C[u_h] - C[u_l]\right] + \frac{\sin(\psi)}{2\sqrt{w}}\left[S[u_h] - S[u_l]\right]\right] + 2(n-1)\sin^2(\pi q)\right] (5.30)$

where

$$\rho_{\pm}\big|_{i\geq 2} = \frac{1}{T}\sum_{i=2}^{n}\int_{(i-1)T}^{iT}\sin\left((a_i - \hat{a}_{1i})\pi\left[h\frac{t-(i-1)T}{T} - w\left(\frac{t-(i-1)T}{T}\right)^2\right] + \vartheta_i\right).dt$$

$$\vartheta_i = \pi q\sum_{k=2}^{i-1} a_{jk} - a_{uk}$$

$$\begin{Bmatrix}\rho_+, & a_i > \hat{a}_{1i}\\ \rho_-, & a_i < \hat{a}_{1i}\\ \rho = \sin\vartheta_i, & a_i = \hat{a}_{1i}\end{Bmatrix}$$

$$\rho_{\pm}\big|_{i\geq 2} = \frac{\cos(\psi \pm \vartheta_i)}{2\sqrt{w}}\left[S[u_h] - S[u_l]\right] - \frac{\sin(\psi \pm \vartheta_i)}{2\sqrt{w}}\left[C[u_h] - C[u_l]\right]$$

$$\psi = \frac{\pi(q+w)^2}{2w}, \qquad u_h = -\frac{h}{\sqrt{w}}, \qquad u_l = \frac{2w-h}{\sqrt{w}}$$

In all cases, $C(x)$ and $S(x)$ are the Fresnel integrals, which require numerical evaluation, and are given by

$$C(x) = \int_0^x \cos\left(\frac{\pi u^2}{2}\right)du, \qquad S(x) = \int_0^x \sin\left(\frac{\pi u^2}{2}\right)du$$

The performance of the DAR for observation lengths $2T$, $3T$ and $4T$ sec are shown in Figure 5.8(a), (b) and (c), respectively, for optimum CPCK systems. Also, in the same figure are shown performances of corresponding AMF receiver for these optimum CPCK systems. From Fig. 3(a), it is observed that 2-bit DAR provides an SNR gain of 4.57 dB relative to that of the 2-bit AMF receiver, for optimum CPCK ($(q, w) = (0.98, 4.15)$). However, with the latter receiver, decision about the data a_1 is available after $2T$ secs,

whereas with DAR decision is available only after $3T$ secs. SNR gains of nearly 6.1 and 7.4 dB are observed for $n = 3$ and $n = 4$, respectively, when optimum CPCK systems are employed. By going to $3T$ and $4T$ observations from $2T$, the performance of the DAR becomes better, for optimum CPCK systems.

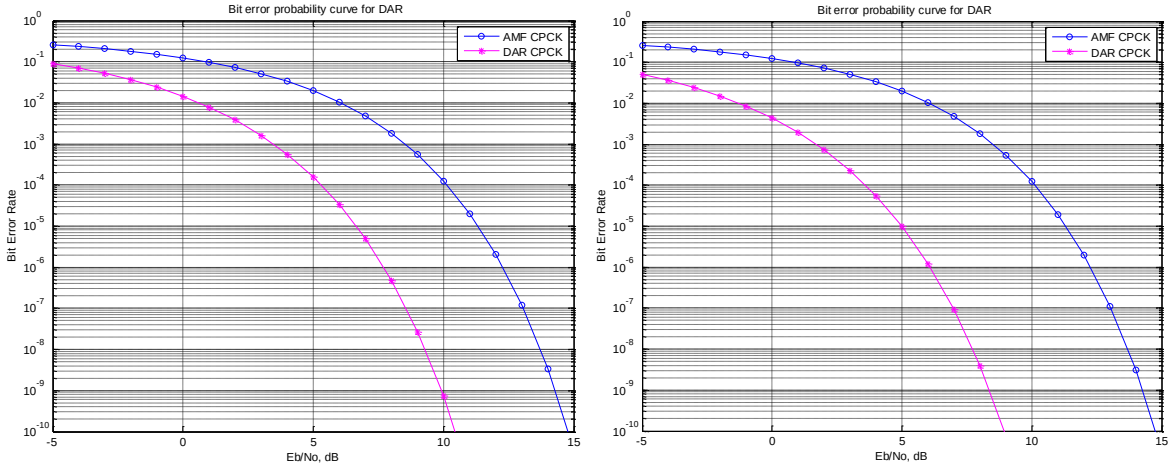

(a) (b)

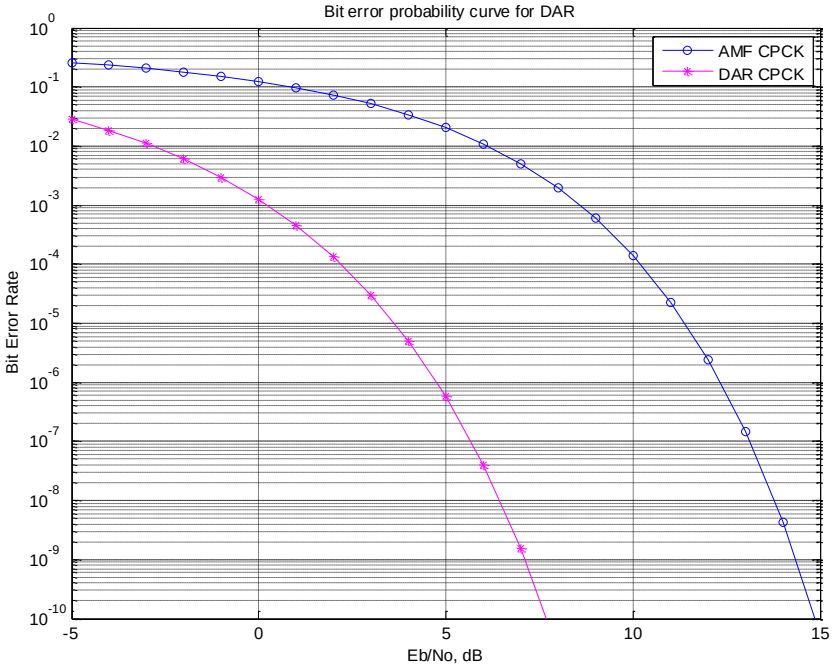

(c)

Figure 5.8: Performance, $P_e(\hat{a}_{2,1})$, of DAR for optimum CPCK systems, for (a) $n = 2$, (b) $n = 3$ and (c) $n = 4$

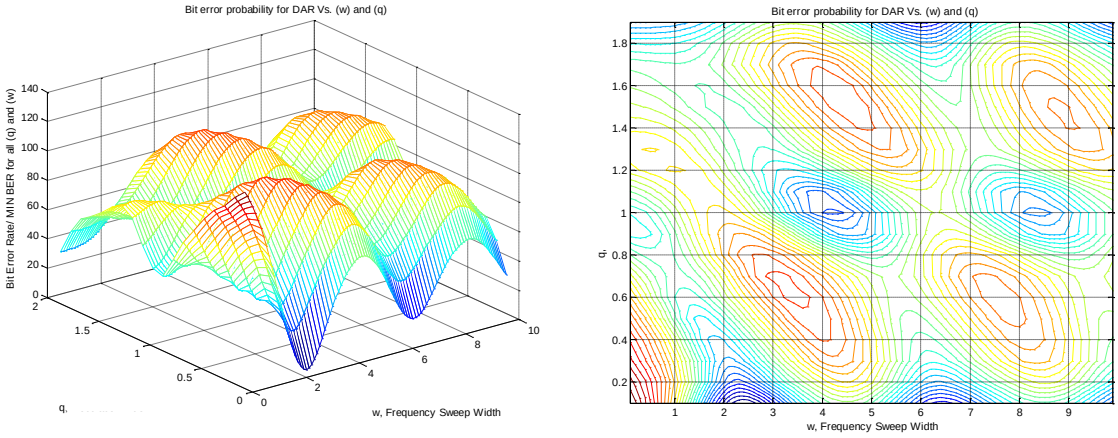

(a)

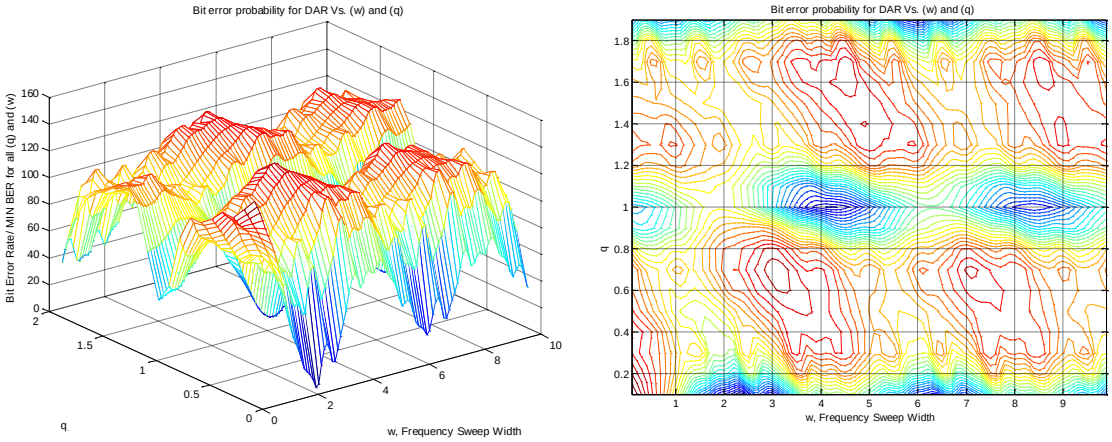

(b)

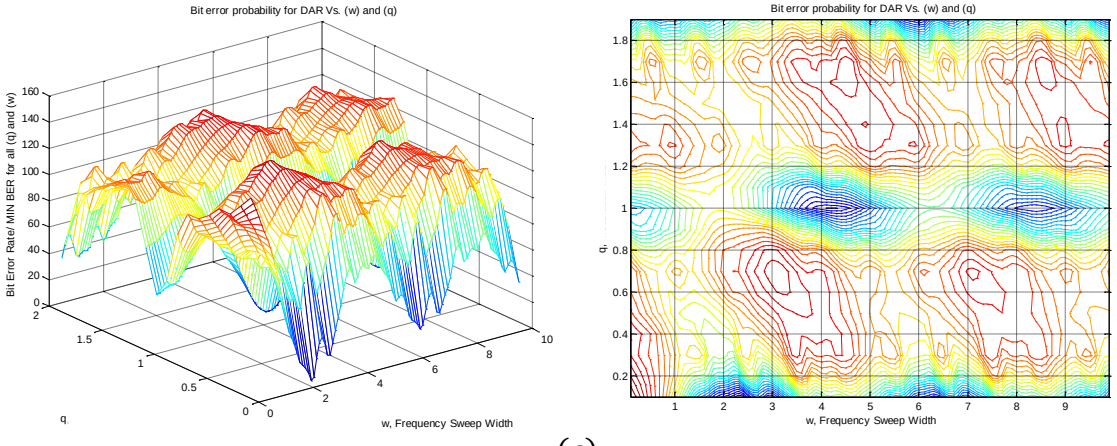

(c)

Figure 5.9: $10\log_{10}(P_e(\hat{a}_{2,1})/\min\{P_e(\hat{a}_{2,1})\})$ Contours of DAR for CPCK at $SNR = 6$ dB for (a) $n = 2$, (b) $n = 3$ and (c) $n = 4$

Table 5.2: CPCK DAR min$\{BER\}$ Parameters for $SNR = 6$ dB

n	(q, w)	min{BER}
2	$(0.98, 4.15)$	3.341×10^{-5}
3	$(0.99, 4.36)$	1.149×10^{-6}
4	$(1.01, 4.50)$	4.044×10^{-8}

In Figure 5.9, $10\log_{10}(P_e(\hat{a}_{2,1})/\min\{P_e(\hat{a}_{2,1})\})$ contours of DAR receiver as a function of (q, w) at $SNR = 6$ dB are shown for $n = 2,3,$ and 4. It is noted from this Figure that there exist multiple sets of (q, w) that result in optimum CPCK system. In other words, there are several sets of (q, w) that result in minimum BER. In Table 5.2 is shown example sets of (q, w) for $n = 2,3$ and 4 and corresponding minimum BER for DAR. The contour plots can be effectively used in the CPCK system design using DAR to accommodate the different power, bandwidth and receiver complexity requirements.

5.3 CPFSK vs. CPCK DAR Performance

In order to compare the performance of CPFSK and CPCK, we have plotted BER performance vs. SNR in Figure 5.10 for both modulations. In this Figure, performance of DAR and AMF receiver for 2-bit optimum CPCK system is shown. In the same Figure, the performance of BPSK, DAR and AMF receiver for 2-bit optimum CPFSK system ($h = 0.8$) are shown. It is noted that CPCK system is superior to CPFSK system when corresponding optimum modulation parameters are used with DAR. Also, we observed that CPCK system offers more flexibility in terms of the choice of modulation parameters in the overall system design using DAR.

5.3 Summary and Results

CPFSK and CPCK signaling techniques are regarded as reliable for transmission of digital data over communication channels, and have been used in many practical applications. However, these techniques come at the expense of complex signal processing techniques, as discussed in Chapters 3 and 4. Thus, in this Chapter, we presented a novel Decision Aided Receiver (DAR) based on heuristics for CPFSK and CPCK coherent detection, as an alternative for the AMF receiver that is optimum at low values of SNR. Decision aided detection strategy was presented and explicit expressions

for computation of BER were developed for AWGN environment, for both CPFSK and CPCK for the first refinement.

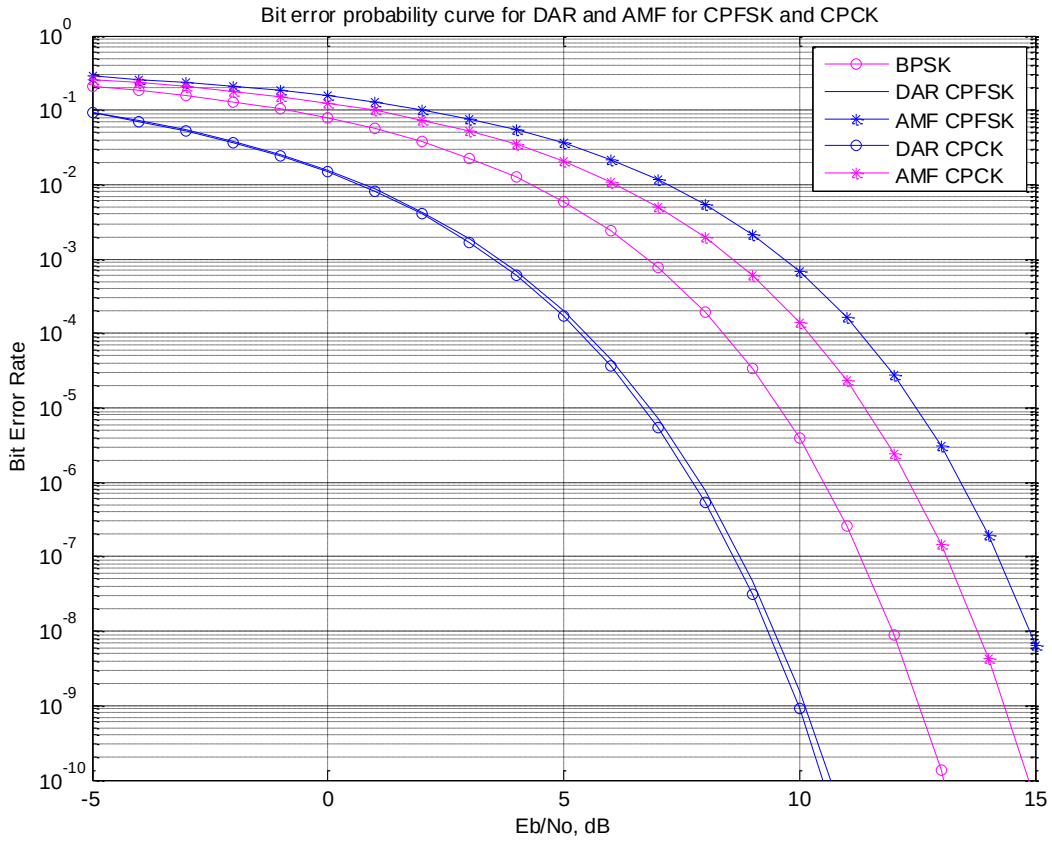

Figure 5.10: Performance of DAR and AMF Receiver for 2-bit Optimum CPCK and CPFSK system

It turned out that it is very hard to describe the behavior of the DAR, since it is based on heuristic considerations. However, we have tried to examine all possible situations in order to describe the behavior of DAR. It was shown that the error probability performance of the DAR, $P_e(\hat{a}_{2,1})$, is a function of: i) E_b/N_0, Signal-to-Noise Ratio; ii) modulation parameters (h for CPFSK, q and w for CPCK); and iii) n, observation length of DAR. The set of modulation parameters that should be chosen for a given n and E_b/N_0, is the one that minimizes $P_e(\hat{a}_{2,1})$.

From the performance analysis carried out, it is clear that the DAR has certain interesting features. The performance of CPFSK using DAR is highly dependent on the operating

value of SNR and also is sensitive to the value of h. However, at most values of SNR, DAR outperforms the corresponding AMF receiver, except for a small range of h for which AMF receiver outperforms DAR. For example, at $SNR = 0$ dB the middle region where AMF receiver performance exceeds that of the DAR is $0.425 \leq h \leq 0.642$, and $0.395 \leq h \leq 0.690$ for $SNR = 4$ dB. That range of the region varies as the SNR varies. Moreover, it was observed that for higher values of SNR, the DAR almost meets the performance of the AMF receiver for $h \geq 0.35$. In general, the DAR performance improves as h increases, where the AMF receiver performance improves up to $h = 0.5$, yielding BPSK performance, and degrades for $h \geq 0.5$.

In addition, it was illustrated that as h increases beyond a specific value $h = h_{TH}$, BER drastically decreases. It was shown that for higher values of SNR, values of h at which the BER starts to drastically decrease, $h = h_{TH}$, becomes higher. For example, the BER starts decreasing drastically at $SNR = 0$ dB for $h \geq h_{TH} = 0.6$, and for $h \geq h_{TH} = 0.8$ at $SNR = 10$ dB.

Moreover, studying the effect of n on the BER performance showed that as n increases, values of h at which the BER starts to drastically decrease, $h = h_{TH}$, becomes higher. For example, at $SNR = 10$ dB for $n = 2,3,4$ and 5, $h_{TH} = 0.76,0.81,0.82$ and 0.83, respectively. So, it was concluded that h_{TH}, after which the BER decreases rapidly, is a function of n and SNR.

Analyzing optimum CPFSK system using DAR showed that 2-bit DAR provides an SNR gain of 5.63 dB relative to that of the 2-bit AMF receiver, for optimum CPFSK ($h = 0.8$). SNR gains of nearly 6.9 and 7.7 dB are observed for $n = 3$ and $n = 4$, respectively, when optimum CPFSK systems are employed. By going to $3T$ and $4T$ observations from $2T$, the performance of the DAR becomes better, for optimum CPFSK systems.

Analyzing optimum CPCK system using DAR showed that 2-bit DAR provides an SNR gain of 4.57 dB relative to that of the 2-bit AMF receiver, for optimum CPCK ($(q, w) = (0.98, 4.15)$). However, with the latter receiver, decision about the data a_1 is available after $2T$ secs, whereas with DAR decision is available only after $3T$ secs. SNR gains of

nearly 6.1 and 7.4 dB are observed for $n = 3$ and $n = 4$, respectively, when optimum CPCK systems are employed. By going to $3T$ and $4T$ observations from $2T$, the performance of the DAR becomes better, for optimum CPCK systems.

Contours of DAR receiver as a function of (q, w) at $SNR = 6$ dB for $n = 2,3,$ and 4 showed that there exist multiple sets of (q, w) that result in optimum CPCK system. In other words, there are several sets of (q, w) that result in minimum BER. These contour plots can be effectively used in the CPCK system design using DAR to accommodate the different power, bandwidth and receiver complexity requirements.

Finally, the Chapter was concluded with a comparison between optimum CPFSK and CPCK systems. It was noted that CPCK system is superior to CPFSK system when corresponding optimum modulation parameters are used with DAR. Also, we observed that CPCK system offers more flexibility in terms of the choice of modulation parameters in the overall system design using DAR.

In general, it can be concluded that DAR outperforms the corresponding AMF receiver for both CPFSK and CPCK, but with certain restrictions on the modulation parameters used.

Chapter 6

Conclusions

In this thesis, we investigated the detection strategies, receivers and their performance of two subclasses of CPM modulation called Continuous Phase Frequency Shift Keying (CPFSK) and Continuous Phase Chirp Keying (CPCK) for data communication. This chapter summarizes the contributions made in this thesis and the conclusions from the results obtained. It also discusses some important issues and the scope for future research as determined by projected demands of DCS.

6.1 Summary of Contributions

In Chapter 2, the concept, mathematical descriptions and properties of CPM signals were presented in detail. Moreover, the mathematical frame work required for the development of Continuous Phase Chirp Keying (CPCK) and Continuous Phase Frequency Shift Keying (CPFSK) signaling techniques was provided. It has been demonstrated that the main difference between CPFSK and CPCK is the way the frequency changes within the bit interval, which is due to the properties associated

with the different phase functions used by each signaling technique. Phase functions, frequency functions, phase trees and trellises, baseband and passband waveforms for CPFSK and CPCK with different modulation parameters have been illustrated and verified using MATLAB. CPFSK is considered as a special case of CPCK when the frequency sweep width, $w = 0$.

In Chapter 3, we have examined one of the two main Maximum Likelihood Detectors for CPM. Optimum CPM MLRT-based receiver was derived, and block diagram for receiver implementation has been provided. Also, we have discussed the computational complexity involved in analyzing and simulating the optimum receiver for CPFSK and CPCK. Since the optimum receiver is very complex to be mathematically analyzed, two approximations have been used to arrive at sub-optimum receivers for low- and high-SNR values. At low-SNR, sub-optimum AMF receiver is thoroughly examined for CPFSK and CPCK. It was shown that the AMF performance of CPFSK with $h = 0.5$ matches that of BPSK for all n. Moreover, it was shown that as n increases, the next nearest BER performance to that of BPSK occurs at $h = 0.646$. For CPCK, it was found that $min\{BER\}$ occurs at $q = 0.5$ and $q = 1.5$ independent of SNR value, w and n, yielding BPSK performance. The q values yielding BPSK performance for CPCK were found by searching the region $0 \leq q \leq 2$. Other values for q can exist outside these boundaries.

Using high-SNR approximation, sub-optimum high-SNR receiver has been provided for CPFSK and CPCK. This receiver has provided two bounds for CPFSK and CPCK optimum receiver, an upper union bound and a lower bound. Different plots and graphs have been provided in both cases in order to study the relationships between BER and the different modulation parameters for both CPFSK and CPCK, such as: E_b/N_0 vs. h, E_b/N_0 vs. h and n, E_b/N_0 vs. q and n, E_b/N_0 vs. w and n…etc. In general, for CPFSK and CPCK, the BER performance improved as the length of the observation interval n increased. However, that amount of improvement decreased with each increment of the observation interval length. This indicated that increasing the length of the observation interval beyond a certain limit provided only marginal BER improvement and higher receiver complexity. Moreover, for CPFSK, it has been noted that optimum performance

is achieved at $h = 0.715$ for all n, and near optimum performance is achieved at $h = 0.5$. In addition, the difference in performance between the upper bound and the lower bound at low-SNR was relatively big, which means that these bounds are not tight at low-SNR; however, the performance corresponding to both bounds would meet at high-SNR values. For CPCK, 3D plots were used in order to study the relation between BER and the combinations of modulation parameters. Wherein CPFSK high-SNR receiver the minimum BER occurred at $h = 0.715$ for all n and SNR values, for CPCK high-SNR receiver, the minimum BER occurs at different points for different n for all SNR values. Using the 3D plots and their corresponding contours, the set of points (q, w) where $\min\{BER\}$ occurs were found.

The different graphs for AMF receiver and high-SNR receiver provided in Chapter 3 helps system designers by giving multiple options, in terms of values of n and h, in order to meet a certain BER, subject to different bandwidth and receiver complexity constraints. It is noted that the choice of h, q and w decides the bandwidth and n decides the complexity of the receiver.

Moreover, in order to answer the question of "What threshold that separates high-SNR from low-SNR when studying the effect of the different parameters on BER?", plots of the composite bounds, derived from the performance of the AMF and high-SNR receivers for both CPFSK and CPCK were provided. The optimum performance for CPFSK and CPCK will be bounded by these composite bounds. It was noticed that at a certain SNR value, the upper bound is decided using the high-SNR upper bound instead of the AMF. Thus, the point at which the optimum receiver performance gets upper bounded by the upper bound of the high-SNR receiver instead of the AMF, can be considered as the SNR value that separates high- and low-SNR for any set of modulation parameters and n. This SNR value can be thought of as a function of n, the modulation scheme in use and its modulation parameters. Comparing optimum CPFSK and CPCK using high-SNR receiver showed that CPCK has SNR advantage of 0.65 dB and 1.50 dB relative to CPFSK and BPSK, respectively. Computer Simulations verified the mathematical analysis provided for the different receivers. In addition, CPCK has been found more flexible than CPFSK, from a design point of view, in the sense that CPCK allowed for the manipulation of more parameters, which gave better control on the

modulation scheme. In general, CPCK can achieve superior BER performances to that of CPFSK.

Chapter 3 suggested that tradeoffs between BER, power, bandwidth and receiver complexity can be further explained through studying the minimum distance properties for both signaling schemes, CPFSK and CPCK. In Chapter 4, we studied the minimum distance properties for both signaling schemes, CPFSK and CPCK, and values of optimum operation were provided. Advantages in term of SNR of these optimum systems were highlighted relative to that of PSK. For CPFSK, it was shown that the maximum minimum distance between two transmitted sequences, $\max\{D_n^2\} = {D_B}^2 = 2.434$ is attained at $h = 0.715$, and thus, the upper bound on the SNR gain G_n is limited to about 0.85 dB. Moreover, it was illustrated that no significant SNR gain is attainable for CPFSK with $n > 3$. So $n = 3$ can be called the optimum observation interval, where further observations don't add benefits to the system and only causes exponential growth in the receiver's complexity. For CPCK, it was shown that the maximum minimum distance between two transmitted sequences, $\max\{D_n^2\} = {D_B}^2 = 2.93$ is attained at $(q, w) = (0.2.4)$, and thus, the upper bound on the SNR gain G_n is limited to about 1.66 dB. ${D_B}^2(q, w)$ has many local maxima for integer values of q and the global maxima reported previously at $(q, w) = (0.2.4)$. ${D_B}^2(q, 0)$ is the CPFSK case, reported previously as ${D_B}^2(h)$. Computer simulations were carried out in order to find the parameters maximizing ${D_n}^2$ and G_n for different n, q and w. It was noticed that SNR gain increase is not as major from $n = 3$ to $n = 4$ and we are approaching the upper bound value for SNR gain of 1.66 dB. So, $n = 4$ was taken as the optimum observation interval, where further observations didn't add major benefits to the system. SNR gains for CPFSK and CPCK were reported at the corresponding sections.

Studying the distance properties for CPFSK and CPCK led to the discussion of the other type of CPM signals receiver, which is the Viterbi receiver. The Viterbi receiver is based on the maximum-likelihood sequence estimation (MLSE) theory, which searches for the minimum Euclidean distance path through the trellis that characterizes the memory in the transmitted signal. Upper bounds results using Viterbi receiver were reported for CPFSK

and CPCK. Matching the conclusion from Chapter 3, CPCK provides superior BER performance to that of CPFSK due to CPCK's design flexibility. Using the upper bound distance criteria D_B^2 for both CPFSK and CPCK, the upper bounds on performance of the Viterbi receiver for optimum CPFSK; $h = 0.715$, and CPCK; $(q, w) = (0,2.4)$, were found. It showed that CPCK provides superior BER performance to that of CPFSK due to CPCK's design flexibility. It was noted that CPCK has SNR advantage of nearly 1 dB and 2 dB over CPFSK and BPSK, respectively. The complexity reduction introduced by the Viterbi receiver was illustrated through examples and graphs.

In Chapter 5, we presented a novel Decision Aided Receiver (DAR) based on heuristics for CPFSK and CPCK coherent detection, as an alternative for the AMF receiver that is optimum at low values of SNR. Decision aided detection strategy was presented and explicit expressions for computation of BER were developed for AWGN environment, for both CPFSK and CPCK for the first refinement.

It turned out that it is very hard to describe the behavior of the DAR, since it is based on heuristic considerations. However, we have tried to examine all possible situations in order to describe the behavior of DAR. It was shown that the error probability performance of the DAR for the first refinement, $P_e(\hat{a}_{2,1})$, is a function of: i) E_b/N_0, Signal-to-Noise Ratio; ii) modulation parameters (h for CPFSK, q and w for CPCK); and iii) n, observation length of DAR. The set of modulation parameters that should be chosen for a given n and E_b/N_0, is the one that minimizes $P_e(\hat{a}_{2,1})$.

From the performance analysis carried out, it is clear that the DAR has certain interesting features. The performance of CPFSK using DAR is highly dependent on the operating value of SNR and also is sensitive to the value of h. However, at most values of SNR, DAR outperforms the corresponding AMF receiver, except for a small range of h for which AMF receiver outperforms DAR. For example, at $SNR = 0$ dB the middle region where AMF receiver performance exceeds that of the DAR is $0.425 \leq h \leq 0.642$, and $0.395 \leq h \leq 0.690$ for $SNR = 4$ dB. That range of the region varies as the SNR varies. Moreover, it was observed that for higher values of SNR, the DAR almost meets the performance of the AMF receiver for $h \geq 0.35$. In general, the DAR performance

improves as h increases, where the AMF receiver performance improves up to $h = 0.5$, yielding BPSK performance, and degrades for $h \geq 0.5$.

In addition, it was illustrated that as h increases beyond a specific value $h = h_{TH}$, BER drastically decreases. It was shown that for higher values of SNR, values of h at which the BER starts to drastically decrease, $h = h_{TH}$, becomes higher. For example, the BER starts decreasing drastically at $SNR = 0$ dB for $h \geq h_{TH} = 0.6$, and for $h \geq h_{TH} = 0.8$ at $SNR = 10$ dB.

Moreover, studying the effect of n on the BER performance showed that as n increases, values of h at which the BER starts to drastically decrease, $h = h_{TH}$, becomes higher. For example, at $SNR = 10$ dB for $n = 2,3,4$ and 5, $h_{TH} = 0.76,0.81,0.82$ and 0.83, respectively. So, it was concluded that h_{TH}, after which the BER decreases rapidly, is a function of n and SNR.

Analyzing optimum CPFSK system using DAR showed that 2-bit DAR provides an SNR gain of 5.63 dB relative to that of the 2-bit AMF receiver, for optimum CPFSK ($h = 0.8$). SNR gains of nearly 6.9 and 7.7 dB are observed for $n = 3$ and $n = 4$, respectively, when optimum CPFSK systems are employed. By going to $3T$ and $4T$ observations from $2T$, the performance of the DAR becomes better, for optimum CPFSK systems.

Analyzing optimum CPCK system using DAR showed that 2-bit DAR provides an SNR gain of 4.57 dB relative to that of the 2-bit AMF receiver, for optimum CPCK ($(q, w) = (0.98, 4.15)$). However, with the latter receiver, decision about the data a_1 is available after $2T$ secs, whereas with DAR decision is available only after $3T$ secs. SNR gains of nearly 6.1 and 7.4 dB are observed for $n = 3$ and $n = 4$, respectively, when optimum CPCK systems are employed. By going to $3T$ and $4T$ observations from $2T$, the performance of the DAR becomes better, for optimum CPCK systems.

Contours of DAR receiver as a function of (q, w) at $SNR = 6$ dB for $n = 2,3,$ and 4 showed that there exist multiple sets of (q, w) that result in optimum CPCK system. In other words, there are several sets of (q, w) that result in minimum BER. These contour

plots can be effectively used in the CPCK system design using DAR to accommodate the different power, bandwidth and receiver complexity requirements.

Finally, the Chapter was concluded with a comparison between optimum CPFSK and CPCK systems. It was noted that CPCK system is superior to CPFSK system when corresponding optimum modulation parameters are used with DAR. Also, we observed that CPCK system offers more flexibility in terms of the choice of modulation parameters in the overall system design using DAR. In general, it can be concluded that DAR outperforms the corresponding AMF receiver for both CPFSK and CPCK, but with certain restrictions on the modulation parameters used.

6.2 Recommendations for Future Work

In light of the work presented in this thesis, there exists a number of areas for further research and examination. They are as follows:

6.2.1 MIMO-CPCK Systems

With the combination of Internet and multimedia application in next generation wireless communication, the demand for wide-band high data rate communication services is increasing. Usually more bandwidth is required for higher data-rate transmission. Due to spectral limitations, it is often unfeasible or very expensive to increase the bandwidth. Moreover, another major pitfall of wireless communication systems (WCS) is fading and multipath propagation.

Most recent developments in information technology proved that spectrally efficient transmission over wireless channels is realizable with Multiple Input Multiple Output (MIMO) systems. A key feature of MIMO systems is its ability to turn multipath propagation, which is usually a hindrance for WCS, into an advantage for the user. MIMO systems effectively take advantage of random fading [51] and multipath delay spread [54], for increasing transfer rates. A general block diagram for MIMO systems is shown in Figure 6.1. The challenge in implementing a MIMO system lies in the efficient realization of a detector that can separate the spatially multiplexed signals.

In the literature, multipath fading in multi-antenna wireless systems was mostly dealt by other diversity schemes, such as time diversity, frequency diversity and receiver diversity, with the last scheme being the most widely applied one. However, it is hard to efficiently employ receiver diversity at remote locations, since these locations need to remain relatively simple, inexpensive and small. Moreover, In Mobile communication systems, it may be difficult to put many antennas in the mobile unit. Therefore, multiple transmit antennas are preferred at the base stations. Thus, Space-Time Coding schemes are gaining growing interest as they offer high data rate transmission over wireless fading channels while putting the diversity burden on the base station.

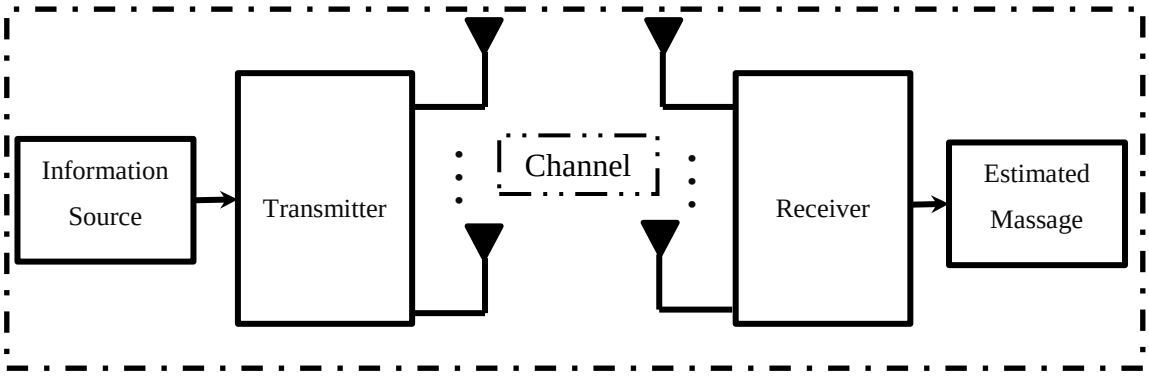

Figure 6.1: General MIMO System Block Diagram

Space-Time Coded (STC) Systems are one of the most recent technical advances that has the potential of solving the traffic bottleneck in future internet demanding wireless networks. The key idea in space-time systems is that the signal's natural and conventional dimension, time, is complemented with the spatial dimension. In just a few years, STC has penetrated large-scale commercial-driven standards such as Wireless Local Area Networks (WLANs) and 3G networks with a potential for greater implementation in 4G technology.

Due to the advantages offered by MIMO, STC and CPM systems, a main area of research is combining STC with CPM in what is called, STC-CPM system. Actually, our next research direction would be the evaluation of STC-CPCK systems performance. Since both of them offers various advantages each on its own, it is expected that combining them would enhance the total performance of the system.

6.2.2 Signaling Format

The information carrying phase of CPM signals can be generally viewed as

$$\phi = f\big(t, a, h, g(t)\big) \tag{6.1}$$

In our work with the DAR, we have considered single-h CPM, yet, this work can be extended to multi-h CPM. Moreover, we have employed two distinct pulse shapes i.e. REC and Chirp, however, same work can be done employing other pulse shapes such as Raised cosine (RC), Spectrally Raised Cosine (SRC), Gaussian Minimum Shift Keying (GMSK) and Half-Cycle Sinusoid (HCS). Another area of future work could be the extension of DAR algorithm to partial response CPFSK, CPCK and CPM signaling in general, which usually gives better distance properties relative to full response CPM.

6.2.3 Detection Problem

The DAR receiver we evaluated, assumes ideal conditions such as 100% synchronization, ideal coherent detection and pure AWGN channel model, however, it is not practically true, hence, another area of future work could be in testing the proposed CPCK DAR in non-Gaussian noise. In addition, generalizing the DAR strategy to M-ary CPM is an interesting area of research. Moreover, the MLRT-based optimum receiver still requires more analysis, in an attempt to find a closed-form expression describing the BER performance. It is also desirable to simulate the actual optimum receiver in order to verify the mathematical analysis and performance of the sub-optimum receivers.

References

[1] FEHER, K., 1995. *Wireless digital communications :modulation and spread spectrum applications.* Upper Saddle River, N.J.: Prentice-Hall PTR.

[2] MAGILL, D.T., NATALI, F.D. and EDWARDS, G.P., 1994. Spread-spectrum technology for commercial applications. *Proceedings of the IEEE,* **82**(4), pp. 572-584.

[3] JUNG, P., BAIER, P.W. and STEIL, A., 1993. Advantages of CDMA and spread spectrum techniques over FDMA and TDMA in cellular mobile radio applications. *Vehicular Technology, IEEE Transactions on,* **42**(3), pp. 357-364.

[4] MATTHEWS, H., 1977. *Surface wave filters :design, construction, and use.* New York: Wiley.

[5] HUEMER, M., KOPPLER, A., RUPPEL, C.C.W., REINDL, L., SPRINGER, A. and WEIGEL, R., 1999. SAW based chirp Fourier transform for OFDM systems, *Ultrasonics Symposium, 1999. Proceedings. 1999 IEEE* 1999, pp. 373-376 vol.1.

[6] BHARGAVA, V.K., 1981. *Digital Communications by Satellite: Modulation, Multiple Access and Coding.* New York; Toronto: Wiley.

[7] ANDERSON, J. B., AULIN, T. and SUNDBERG, C.-E., 1986. *Digital Phase Modulation.* New York: Plenum Press.

[8] AULIN, T. and SUNDBERG, C.-E., 1981. Continuous Phase Modulation-Part I: Full Response Signalling. *Communications, IEEE Transactions on,* **29**(3), pp. 196-209.

[9] SKLAR, B., 1988. *Digital communications: fundamentals and applications.* Englewood Cliffs, N.J.: Prentice-Hall.

[10] OSBORNE, W. and LUNTZ, M., 1974. Coherent and Noncoherent Detection CPFSK. *Communications, IEEE Transactions on,* **22**(8), pp. 1023-1036.

[11] SCHONHOFF, T., 1976. Symbol Error Probabilities for M-ary CPFSK: Coherent and Noncoherent Detection. *Communications, IEEE Transactions on,* **24**(6), pp. 644-652.

[12] AULIN, T., RYDBECK, N. and SUNDBERG, C.-E., 1981. Continuous Phase Modulation--Part II: Partial Response Signaling. *Communications, IEEE Transactions on,* **29**(3), pp. 210-225.

[13] MIYAKAWA, H., HARASHIMA, H., TATSUI, N. and TANAKA, Y., 1975. DIGITAL PHASE-MODULATION SCHEME USING PHASE-CONTINUOUS WAVEFORM. *Electronics and Communications in Japan (English translation of Denshi Tsushin Gakkai Zasshi),* **58**(12), pp. 35-42.

[14] ANDERSON, J.B. and TAYLOR, D.P., 1978. A bandwidth-efficient class of signal-space codes. *Information Theory, IEEE Transactions on,* **24**(6), pp. 703-712.

[15] AULIN, T. and SUNDBERG, C.-E., 1982. On the minimum Euclidean distance for a class of signal space codes. *Information Theory, IEEE Transactions on,* **28**(1), pp. 43-55.

[16] RAVEENDRA, K.R. and SRINIVASAN, R., 1987. Coherent detection of binary multi-h CPM. *Communications, Radar and Signal Processing, IEE Proceedings F,* **134**(4), pp. 416-426.

[17] HWANG, H.-K., LEE, L.-S. and CHEN, S.-H., 1989. Multi-H phase-coded modulations with asymmetric modulation indexes. *Selected Areas in Communications, IEEE Journal on,* **7**(9), pp. 1450-1461.

[18] FONSEKA, J.P. and MAO, R., 1994. Nonlinear continuous phase modulation. *Communications, IEEE Transactions on,* **42**(9), pp. 2661-2663.

[19] FONSEKA, J.P., 1990. Adaptive CPFSK signaling, *Communications, 1990. ICC '90, Including Supercomm Technical Sessions. SUPERCOMM/ICC '90. Conference Record., IEEE International Conference on* 1990, pp. 626-630 vol.2.

[20] FONSEKA, J.P., 1991. Nonlinear continuous phase frequency shift keying. *Communications, IEEE Transactions on,* **39**(10), pp. 1473-1481.

[21] FONSEKA, J.P. and RONGQIANG MAO, 1995. Generalized nonlinear continuous phase modulation. *Communications, IEEE Transactions on,* **43**(5), pp. 1868-1871.

[22] RONGQIANG MAO and FONSEKA, J.P., 1995. Nonlinear multi-h phase codes for CPFSK signaling. *Communications, IEEE Transactions on,* **43**(8), pp. 2350-2359.

[23] RAVEENDRA, K.R. and SRINIVASAN, R., 1991. A novel decision-directed receiver for detection of CPM signals, *TENCON '91.1991 IEEE Region 10 International Conference on EC3-Energy, Computer, Communication and Control Systems* 1991, pp. 72-76.

[24] ZAITSEV, D.L. and ZHURAVLEV, V.I., 1968. Noise immunity of digital data transmission system using linearly frequency-modulated signals. *Elektrosvyaz,* **22**(4), pp. 17-23.

[25] SHEN, H., MACHINENI, S., GUPTA, C. and PAPANDREOU-SUPPAPPOLA, A., 2004. Time-varying multichirp rate modulation for multiple access systems. *Signal Processing Letters, IEEE,* **11**(5), pp. 497-500.

[26] DIXON, R.C., 1976. *Spread spectrum systems.* New York: Wiley.

[27] GOTT, G.F. and NEWSOME, J.P., 1971. H.F. data transmission using chirp signals. *Electrical Engineers, Proceedings of the Institution of,* **118**(9), pp. 1162-1166.

[28] GUGLER, W., SPRINGER, A. and WEIGEL, R., 2000. A chirp-based wideband spread spectrum modulation technique for WLAN applications, *Spread Spectrum Techniques and Applications, 2000 IEEE Sixth International Symposium on* 2000, pp. 83-87 vol.1.

[29] BERNI, A.J. and GREGG, W.D., 1973. On the Utility of Chirp Modulation for Digital Signaling. *Communications, IEEE Transactions on*, **21**(6), pp. 748-751.

[30] PEEBLES, P.Z., 1998. *Radar principles.* New York: Wiley.

[31] COOK, C.E. and BERNFELD, M., 1967. *Radar signals ;;an introduction to theory and application.* New York: Academic Press.

[32] Winkler, M. R., 1962. Chirp signals for communications, *IEEE WESCON Convention Record, Tech. Rep.*

[33] HIRT, W. and PASUPATHY, S., 1981. Continuous Phase Chirp (CPC) Signals for Binary Data Communication-Part I: Coherent Detection. *Communications, IEEE Transactions on*, **29**(6), pp. 836-847.

[34] HIRT, W. and PASUPATHY, S., 1981. Continuous Phase Chirp (CPC) Signals for Binary Data Communication--Part II: Noncoherent Detection. *Communications, IEEE Transactions on*, **29**(6), pp. 848-858.

[35] SUNDBERG, C.-E., 1986. Continuous phase modulation. *Communications Magazine, IEEE*, **24**(4), pp. 25-38.

[36] Raveendra, K. R., 1987. Continuous phase chirp signals for M-ary data communications. *Tel Aviv, Israel: Proceedings of the XXIInd General Assembly of the URSI, August 1987*.

[37] RAVEENDRA, K.R., 1996. Digital transmission using multimode phase-continuous chirp signals. *Communications, IEE Proceedings-*, **143**(2), pp. 87.

[38] FONSEKA, J.P., 1999. Partial response continuous phase chirp modulation. *Electronics Letters*, **35**(6), pp. 448-449.

[39] DAVE, B.A. and RAO, R.K., 2005. Data transmission using digital asymmetric phase continuous chirp signals, *Proceedings - 6th World Wireless Congress, WWC, May 25, 2005 - May 27*, 2005 2005, Delson Group Inc, pp. 283-288.

[40] XIAOWEI WANG, MINRUI FEI and XIN LI, 2008. Performance of chirp spread spectrum in wireless communication systems, *Communication Systems, 2008. ICCS 2008. 11th IEEE Singapore International Conference on* 2008, pp. 466-469.

[41] HENGSTLER, S., KASILINGAM, D.P. and COSTA, A.H., 2002. A novel chirp modulation spread spectrum technique for multiple access, *Spread Spectrum Techniques and Applications, 2002 IEEE Seventh International Symposium on* 2002, pp. 73-77 vol.1.

[42] SPRINGER, A., GUGLER, W., HUEMER, M., KOLLER, R. and WEIGEL, R., 2001. A wireless spread-spectrum communication system using SAW chirped delay lines. *Microwave Theory and Techniques, IEEE Transactions on,* **49**(4), pp. 754-760.

[43] HUAPING LIU, 2005. Multi-code ultra-wideband signaling using chirp waveforms, *Military Communications Conference, 2005. MILCOM 2005. IEEE* 2005, pp. 1219-1224 Vol. 2.

[44] FANYU, M. and XUEMAI, G., 2011. A combined chirp signal modulation technique for multiple access system. *Information Technology Journal,* **10**(2), pp. 416-421.

[45] KADRI, A., RAO, R.K. and JIANG, J., 2009. Low-power chirp spread spectrum signals for wireless communication within nuclear power plants. *Nuclear Technology,* **166**(2), pp. 156-169.

[46] KADRI, A. and UNIVERSITY OF WESTERN ONTARIO, 2010. *Low-power chirp signals for wireless data communication in industrial environments.* PhD Dissertation

[47] VAN TREES, H.L., 1968. *Detection, estimation, and modulation theory.* New York: Wiley.

[48] SKLAR, B., 1993. Defining, designing, and evaluating digital communication systems. *Communications Magazine, IEEE,* **31**(11), pp. 91-101.

[49] XIONG, F., 2000. *Digital modulation techniques.* Boston: Artech House.

[50] PROAKIS, J.G. and SALEHI, M., 2008. *Digital communications.* 5th edn. Boston: McGraw-Hill Higher Education.

[51] FOSCHINI, G.J. and GANS, M.J., 1998. On Limits of Wireless Communications in a Fading Environment when Using Multiple Antennas. *Wireless Personal Communications,* **6**(3), pp. 311-335.

[52] TELATAR, E., 1999. Capacity of multi-antenna Gaussian channels. *European Transactions on Telecommunications,* **10**(6), pp. 585-596.

[53] ALAMOUTI, S., 1998. A simple transmit diversity technique for wireless communications. *Selected Areas in Communications, IEEE Journal on,* **16**(8), pp. 1451-1458.

[54] PAULRAJ, A.J., 1997. Space-time processing for wireless communications, *Acoustics, Speech, and Signal Processing, 1997. ICASSP-97., 1997 IEEE International Conference on* 1997, pp. 1-4 vol.1.

Curriculum Vitae

Name:	Mohammed Omar Zourob
Place of Birth:	Al Fijaira, United Arab Emirates
Post-secondary Education and Degrees:	American University of Sharjah (AUS) Sharjah, United Arab Emirates 2007-2011 B.E.Sc. Western University London, Ontario, Canada 2011-2013 M.E.Sc.
Professional Affiliation:	IEEE Student Member
Honours and Awards:	AUS Merit Scholarship 2007-2011 Shikha Salama Scholarship for Academic Excellence 2007-2011 AUS Dean's and Chancellor's List 2007-2011 Ranked 1^{st} among 610 AUS Fall 2010 graduates 2007-2011 Western University Graduate Research Scholarship 2011-2013 Queen Elizabeth II Graduate Scholarship 2012-2013
Related Work Experience	Teaching & Research Assistant American University of Sharjah 2008-2010 Teaching & Research Assistant Western University 2011-2013

Publications:

K. Assaleh, T. Shanableh, M. Zourob, "Low Complexity Classification System for Glove-based Arabic Sign Language Recognition", *Lecture Notes in Computer Science (LNCS) 7665, Part III*, pp. 262-268 (2012) Doha, Qatar.

R. K. Rao, M. Zourob, "Decision-Aided Receiver for Continuous Phase Chirp Keying" Submitted for presentation in the *International Symposium on Performance Evaluation of Computer and Telecommunication Systems(ISPECTS 2013),* Toronto, Ontario, Canada.

Publications in Preparation:

R. K. Rao, M. Zourob, "Continuous Phase Chirp Keying based Multiple-Input-Multiple-Output Communication System: Design, Detection and Performance" Under preparation.